AD-A032 127 SOUTHWEST RESEARCH INST SAN ANTONIO TEX F/G 11/4
STRENGTH BEHAVIOR OF GRAPHITE/EPOXY COMPOSITE LAMINATES UNDER B--ETC(U)
JUL 76 P H FRANCIS, D E WALRATH, D N WEED F33615-75-C-5115
UNCLASSIFIED AFML-TR-76-86 NL

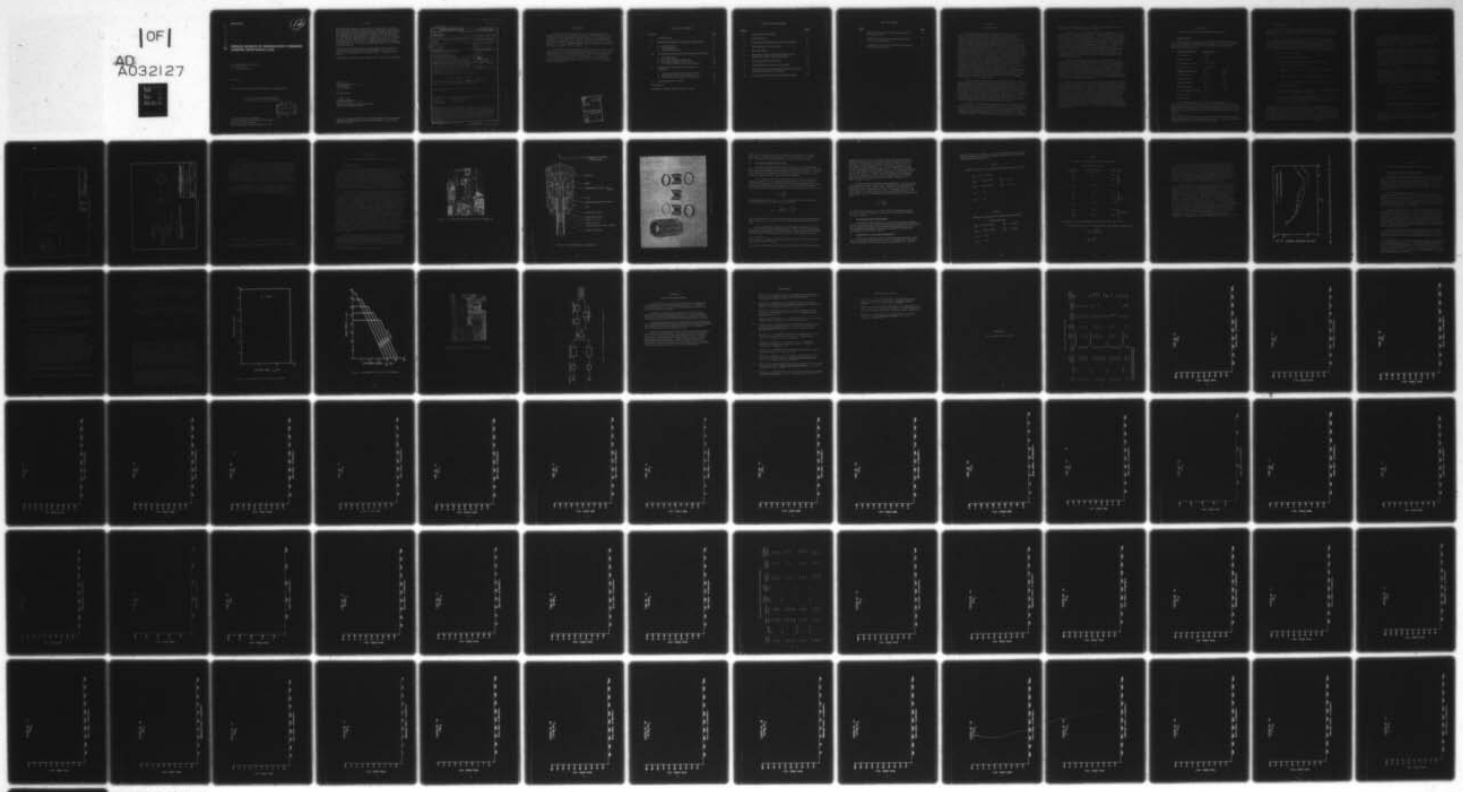

END
DATE FILMED
4-77

AFML-TR-76-86

(12)

P. 3.

STRENGTH BEHAVIOR OF GRAPHITE/EPOXY COMPOSITE LAMINATES UNDER BIAXIAL LOAD

SOUTHWEST RESEARCH INSTITUTE
P. O. DRAWER 28510
SAN ANTONIO, TEXAS 78284

JULY 1976

ANNUAL REPORT FOR PERIOD 15 FEBRUARY 1975 - 15 FEBRUARY 1976

AIR FORCE MATERIALS LABORATORY
AIR FORCE WRIGHT AERONAUTICAL LABORATORIES
AIR FORCE SYSTEMS COMMAND
WRIGHT-PATTERSON AIR FORCE BASE, OHIO 45433

NOTICE

When Government drawings, specifications, or other data are used for any purpose other than in connection with a definitely related Government procurement operation, the United States Government thereby incurs no responsibility nor any obligation whatsoever; and the fact that the Government may have formulated, furnished, or in any way supplied the said drawings, specifications, or other data, is not to be regarded by implication or otherwise as in any manner licensing the holder or any other person or corporation, or conveying any rights or permission to manufacture, use, or sell any patented invention that may be related in any way thereto.

This report has been reviewed by the Information Office (IO) and is releasable to the National Technical Information Service (NTIS). At NTIS, it will be available to the general public, including foreign nations.

This technical report has been reviewed and is approved for publication.

N. J. PAGANO
Project Engineer

FOR THE DIRECTOR

S. W. TSAI, Chief
Mechanics and Surface Interactions Branch
Nonmetallic Materials Division

Copies of this report should not be returned unless return is required by security considerations, contractual obligations, or notice on a specific document.

(9) Annual rept. 15 Feb 75 - 15 feb 76,

UNCLASSIFIED

SECURITY CLASSIFICATION OF THIS PAGE (When Data Entered)

REPORT DOCUMENTATION PAGE	READ INSTRUCTIONS BEFORE COMPLETING FORM
1. REPORT NUMBER: AFML-TR-76-86	2. GOVT ACCESSION NO. / 3. RECIPIENT'S CATALOG NUMBER
4. TITLE (and Subtitle): STRENGTH BEHAVIOR OF GRAPHITE/EPOXY COMPOSITE LAMINATES UNDER BIAXIAL LOAD	5. TYPE OF REPORT & PERIOD COVERED: Annual Rpt. February 15, 1975-February 15, 1976
	6. PERFORMING ORG. REPORT NUMBER
7. AUTHOR(s): P. H. Francis, D. E. Walrath, D. N. Weed	8. CONTRACT OR GRANT NUMBER(s): F33615-75-C-5115
9. PERFORMING ORGANIZATION NAME AND ADDRESS: Southwest Research Institute, P. O. Drawer 28510, San Antonio, Texas 78284	10. PROGRAM ELEMENT, PROJECT, TASK AREA & WORK UNIT NUMBERS: 73420214
11. CONTROLLING OFFICE NAME AND ADDRESS: Air Force Materials Laboratory (AFML/MBM), Air Force Wright Aeronautical Laboratories, Wright-Patterson Air Force Base, OH 45433	12. REPORT DATE: July 1976
	13. NUMBER OF PAGES: 85 (12) 83p.
14. MONITORING AGENCY NAME & ADDRESS (if different from Controlling Office): Air Force Materials Laboratory (AFML/MBM), Air Force Wright Aeronautical Laboratories, Wright-Patterson Air Force Base, Ohio 45433	15. SECURITY CLASS. (of this report): Unclassified
	15a. DECLASSIFICATION/DOWNGRADING SCHEDULE

16. DISTRIBUTION STATEMENT (of this Report)

Approved for public release; distribution unlimited

(16) 7342 (17) 02

17. DISTRIBUTION STATEMENT (of the abstract entered in Block 20, if different from Report)

Approved for public release; distribution unlimited

18. SUPPLEMENTARY NOTES

19. KEY WORDS (Continue on reverse side if necessary and identify by block number)

composites
biaxial loading
first ply failure
tubular specimens
graphite epoxy

20. ABSTRACT (Continue on reverse side if necessary and identify by block number)

The room temperature mechanical ply properties of Fiberite hy-E 1034C graphite/epoxy composite material were characterized using unidirectional thin wall tubes and flat coupons. Four ply laminated tubes having $[0/90]_s$ and $[\pm 45]_s$ stacking sequences were fabricated in preparation for biaxial experiments to determine first ply failure (FPF) thresholds. Initial results using acoustic emission techniques to detect FPF on $[0/90]_s$ tubes are reported.

DD FORM 1 JAN 73 1473 EDITION OF 1 NOV 65 IS OBSOLETE

UNCLASSIFIED

SECURITY CLASSIFICATION OF THIS PAGE (When Data Entered)

$[0/90]_S$

$[\pm 45]_S$

328200

FOREWORD

This Annual Report presents the work accomplished during the period February 15, 1975 through February 15, 1976 under USAF Contract F33615-75-C-5115 by Southwest Research Institute, P. O. Drawer 28510, San Antonio, Texas 78284. Dr. James M. Whitney (AFML/MBM) served as Project Engineer from project initiation through August 28, 1975, whereupon Dr. N. J. Pagano (AFML/MBM) was appointed to replace Dr. Whitney and assume cognizance over this contract.

Dr. Philip H. Francis was the SwRI project manager. He was closely assisted by D. E. Walrath in the experimental work, and D. N. Weed, who was responsible for all specimen fabrication. Others who made important contribution to the success of the program include F. S. Campbell and Mr. D. Tanneberger who provided consultation and services regarding acoustic emission instrumentation. Mrs. Cindy Pierson was responsible for the data reduction.

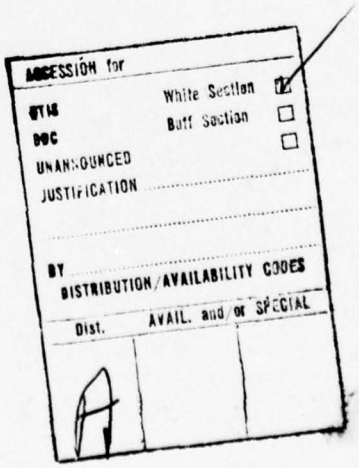

TABLE OF CONTENTS

SECTION		Page
I.	INTRODUCTION	1
II.	MATERIAL SYSTEM AND SPECIMEN FABRICATION	3
	1. Prepreg System	3
	2. Tube Fabrication	4
	3. Flat Panel Fabrication	8
III.	PLY CHARACTERIZATION WITH TUBES AND COUPONS	9
	1. Test Methodology	9
	2. Ply Characterization Using Tubes	13
	3. Ply Characterization Using Coupons	14
	4. Discussion of Unidirectional Ply Properties	14
IV.	EXPLORATORY DETECTION OF FIRST PLY FAILURE	19
	1. Theoretical Estimates of Damage Envelopes	19
	2. FPF Detection Using Acoustic Emission	20
	3. Preliminary Test Results on $[0/90]_s$ Tubes	21
V.	RESULTS AND CONCLUSIONS	26
REFERENCES		27
APPENDIX: STRESS-STRAIN CURVES: TUBES		

LIST OF ILLUSTRATIONS

Figure		Page
1	Tab Mold Mount Assembly	6
2	Tab Mold Insert	7
3	Tabular Specimen Mounted in the Test Apparatus	10
4	Upper Hydraulic Grip Assembly	11
5	Inner Grip Sleeve	12
6	Theoretical Torsional Buckling Strength of Unidirection [0°] Tube, After Reference 6.	18
7	Estimated FPF Loci for $[0/90]_s$	22
8	Estimated FPF Loci for $[\pm 45]_s$ Laminate	23
9	Closeup View of Tube Instrumented With Strain Gages and Acoustic Emission Transducers	24
10	Block Diagram of the Acoustic Emission System	25

LIST OF TABLES

Table		Page
1	Summary of Average Ply Properties Measured Using $[0]_4$ Tubes	15
2	Summary of Average Ply Properties Measured Using Coupon Specimens	15
3	Comparison of Average Ply Properties Measured Using Tubes and Coupons	16

SECTION I

INTRODUCTION

Recent developments in materials and structures technology have begun to push advanced filamentary composites out of the exclusive domain of research studies and into secondary structural hardware in aerospace systems and other usage. Hand-in-hand with these developments there is a growing need for reliable methods for strength and failure prediction under complex loading environments. Until recently, the general subject of material integrity of filamentary composites has been approached by either one of two general directions.[1] On the one hand there have been micromechanical descriptions of failure processes. Numerous studies, both experimental and analytical, have been directed at describing single, independent failure mechanisms such as matrix/fiber debonding, fiber rupture, matrix decohesion, fiber crippling, ply delamination and laminate edge effects. These investigations have been successful in providing useful design tools for predicting failure when caused by a single mechanism of the type just mentioned. The practical limitation of this approach, however, lies in our inability to combine two or more of these mechanisms into an analytical framework suitable for describing more complex--and realistic--failure processes. The mechanism or mechanisms which govern failure depend strongly on the state of stress (strain) in a ply or laminate, and no general physically-based theory has yet emerged which subsumes these several isolated mechanisms. Thus, micromechanical failure descriptions appear to be limited in principle to circumstances where a single mechanism is known a priori to dominate failure for a given stress state.

The second general method which has been used has been to construct abstract mathematical models based on the concept of limit surfaces, borrowed originally from classical metal plasticity theory.[1] The approach here is to define failure as the vanishing of some polynomial stress (or strain) functional, most commonly of quadratic form. Symmetry restrictions are imposed upon the functional, and the coefficients are defined in terms of familiar tension, compression, and shear strengths. In this way, a tensorially correct mathematical model can be constructed which permits strength predictions to be made for general stress (strain) states. This approach suffers, however, in the respect that the mechanics of the failure processes are sidestepped, with the result that predicted failure loci only approximate true values.

Recently[2] a somewhat different approach to failure prediction has been proposed. It has been recognized that what is needed is a physically detectable event or phenomenon which foreshadows final failure in a laminated filamentary composite. Such a phenomenon might be likened to the yield point in polycrystalline metals; deformation within the yield point is ideally reversible with no permanent damage. Once the yield point is exceeded, however, permanant

deformation and damage are done to the material, regardless of the stress (strain) state causing the yield point exceedance.

In filamentary composite laminates it has been suggested that first ply failure (FPF) might form the basis for a physical theory of irreversible damage valid for all stress (strain) states. The FPF theory says, in effect, that any combination of stresses sufficient to cause local failure of some ply in a laminate constitutes a critical stress state. Stress states insufficient to create FPF cause no permanent damage of the laminate. Computationally, FPF is predicted by using a laminated plate type of theory to compute the stress (strain) state within each ply, and then applying one or more empirical failure criteria to the plies. This approach has the advantages of a) being tensorially consistent in applying to complex stress states, b) borrowing from the well-developed body of laminated plate theory, and c) allowing from one to several micromechanical ply failure modes to be applicable simultaneously.

The FPF hypothesis has yet to be tested comprehensively. Little experimental data are available on the failure characteristics of laminated composites under static multiaxial loads. In the case of multiaxial fatigue loads, data are almost non-existent. Thus, in order to test the validity of the FPF approach, what is needed first is a reliable method of subjecting a laminate to a controlled multiaxial loading state. Beyond this, however, an experimental technique is needed which will enable the FPF event to be detected. Such a technique should be sensitive to detecting a local ply failure event when the ply is within the laminate thickness, for the FPF event will not always occur on an observable surface ply.

The objective of this on-going research study is to develop experimental procedures and a data base to assess the validity of FPF as a criterion for initial laminate degradation or "failure". The research has involved characterizing simple laminates under biaxial loads, and developing an experimental methodology for detecting FPF, first under monotonic, and later under cyclic loading. This is being done by subjecting tubular laminated specimens to various known stress states. The stress level is gradually increased until FPF can be detected. An experimental technique, based upon the use of acoustic emission instrumentation, was developed and is reported herein. Since this technique did not prove fruitful, the investigators are developing alternative methodologies based upon the application of dye penetrants and by replication techniques in connection with hysteresis records of the specimen at successively higher stress levels. The results of these investigations will be reported later.

SECTION II

MATERIAL SYSTEM AND SPECIMEN FABRICATION

1. Prepreg System

The material system chosen for this research study was Fiberite hy-E 1034C high-temperature graphite/epoxy prepreg tape. This prepreg system uses Union Carbide's T-300 fiber, and is certified to meet the following Fiberite property specifications:

Prepreg Specifications	Nominal Values	
Resin Content	40%	
Volatile Content	0.5%	
Ply Thickness (cured)	.005 inches	
Gel Time at 340°F	11 minutes	
Composite Properties*	75°F	350°F
Tensile Strength	235.0	200.0
Tensile Modulus	23.5	23.5
Flexural Strength	270.0	220.0
Flexural Modulus	23.0	23.0
Short Beam Shear Strength	16.0	9.5
Specific Gravity	1.60	
Fiber Volume	65%	

This material system is in wide use at the present time. It is currently being used by Rockwell International in the Fabrication of the Space Shuttle payload bay doors, McDonnell Douglas Astronautics in the Space Shuttle aft propulsion system structure, and by Lockheed Missiles and Space Division in the C4 Trident interstage structure, as well as other hardware and research projects.

---

*These data were obtained from composites which were fabricated by standard autoclave techniques using 100 psi augmented pressure. All strength values are reported in X 10^3 psi units, all moduli are X 10^6 psi.

2. Tube Fabrication

Four-ply laminated tubes were fabricated, in three different layup orientations, having a nominal outer diameter of 1.013 inches, and a trimmed length of 10.0 inches. The three layups chosen for fabrication and test were: $[0]_4$, $[0/90]_s$, and $[\pm 45]_s$.

Processing details have been given elsewhere.[3] The procedure involves fitting a hollow, perforated mandrel with an elastomeric bladder, and then wrapping the prepreg tape, together with appropriate vent and bleeder materials, around the mandrel. This assembly is then placed inside a split female mold, and the mandrel pressurized from within during the cure cycle. The details of this procedure are described by the following steps:

1) Prepare template for layup.

2) Layup prepreg to desired orientation.

3) Prepare mandrel by applying a release coat of MS-136.

4) Spiral wrap vent cloth over mandrel.

   a. Wrap a teflon film perforated on 2-inch center over vent cloth.

   b. Spiral wrap one ply of Mochburg paper bleeder over vent film.

   c. Wrap one ply of TX1040 separator cloth over bleeder.

5) Roll layup onto mandrel.

6) Tape both ends of layup to prevent resin loss allowing approximately 2-inches of vent to extend beyond layup.

7) Place layup in female mold. Place mold in oven and proceed with cure cycle according to Fiberite specification:
   350° F (specimen temperature) for 2 hours at 90 psig; then cool to 150° F under above pressure.

Up to now, about 30 tubes have been fabricated. Due to the extremely fragile nature of the 4-ply, 0° tubes, seven were damaged during removal of the bleeder and vent cloth from inside the specimens. This problem, however, has been solved by replacing the nylon vent film with a teflon flurocarbon film. The teflon film ensures a better release between the vent cloth and bleeder ply thus making it possible to remove the vent cloth and bleeder as separate units, which then places less transverse peel stress on the specimen.

One other problem area concerning tube fabrication was encountered in achieving a clean butt joint in the 90° plies of the $[0/90]_s$ tubes. Three $[0/90]_s$ tubes were rejected due to the variable wall thickness in the area of the overlaps in the two 90° plies. This problem was eliminated by wrapping the 90° plies in one continuous piece with the overlap being in a 360° spiral wrap from end to end of the specimen.

After the tubes are fabricated and trimmed to size, they must be tabbed inside and outside at either end for insertion into the hydraulic grip system. The tubes have a finished length of 10.0 inches, and 2.5 inch long tabs are placed at either end, leaving about 5.0 inches of gage length. Initial efforts at tabbing involved placing a wet layup of glass or Mochburg paper* in the tab areas, curing, and machining to tolerance. This procedure proved time-consuming and expensive, as well as providing a tab that was too stiff in the hoop direction to permit the compensating feature of the hydraulic grip system to function effectively. Therefore, efforts were made to develop an improved tabbing technique.

The procedure currently being used results in a cast tab of neat resin Epon 815, using curing agent U. Figures 1 and 2 show diagrams of the tab molding apparatus. Basically, the tube is guided downward through a split, close-fitting outer sleeve, until the tube seats and is accurately aligned concentrically between the outer sleeve and a mandrel insert; these concentric cylinders form the mold for the neat resin. The resin is then introduced, cured, and then the tube removed with both tabs on one specimen end in place, requiring no further work to bring them in tolerance. The specific tab processing details are summarized as follows:

1) Specimen is sanded and wiped clean with M.E.K. in tab area.

2) Mold is preheated to 120° F.

3) Resin is mixed (Epon 815 and 20% of curing agent U.)

4) Mixture is then placed in vacuum and degassed until all air is removed.

5) Mixture is then poured into mold, and tube is placed into mold where it remains until cure is complete.

6) Same steps repeated for opposite end of tube.

---

*Three tab systems were tried using this approach: 7781 dry glass, impregnated with Epon 815 resin; three plies of 1009-36 Scotch ply with [0/90/0] orientation; and three plies of Mochburg paper bleeder, impregnated with Epon 815 resin.

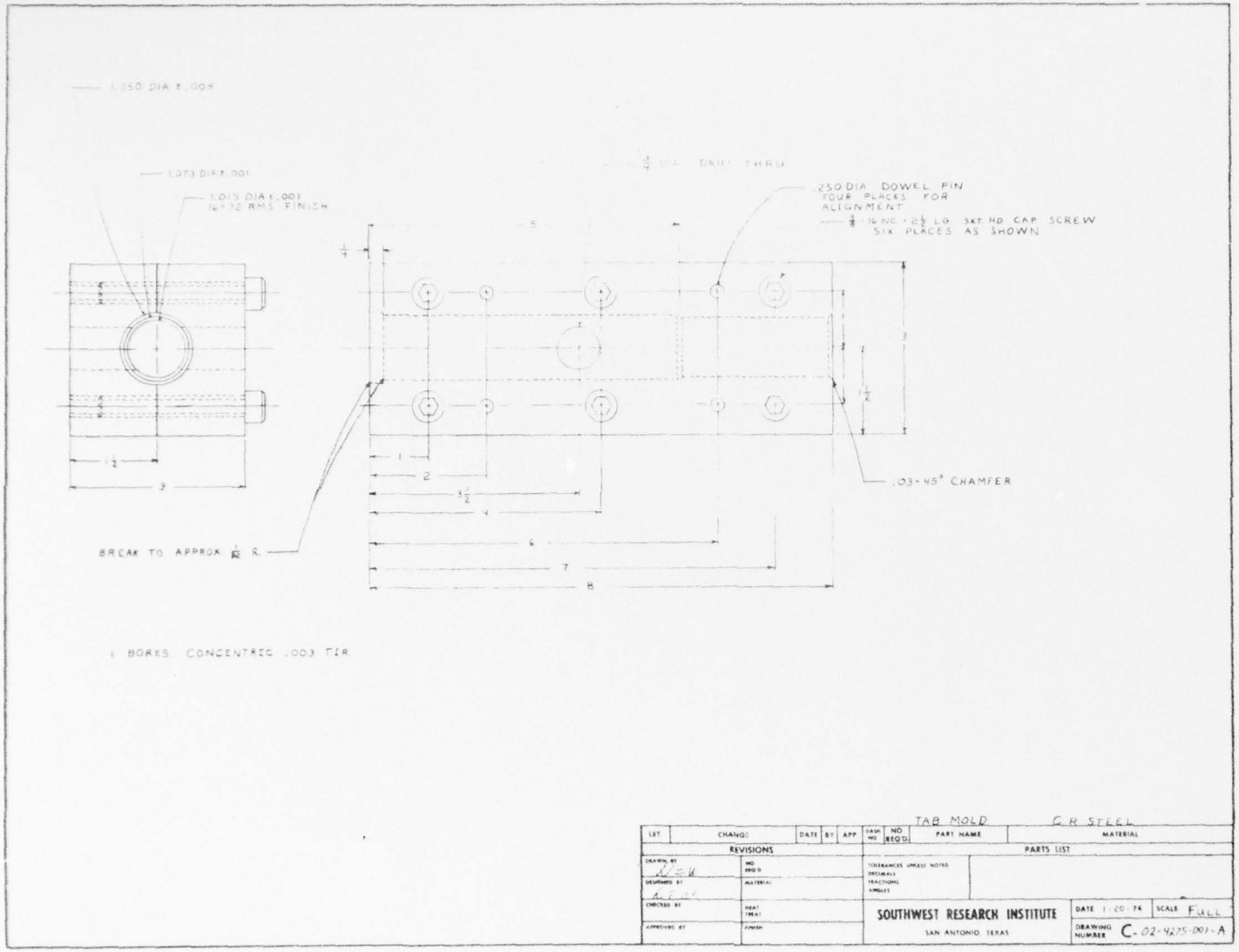

Figure 1. Tab Mold Mount Assembly

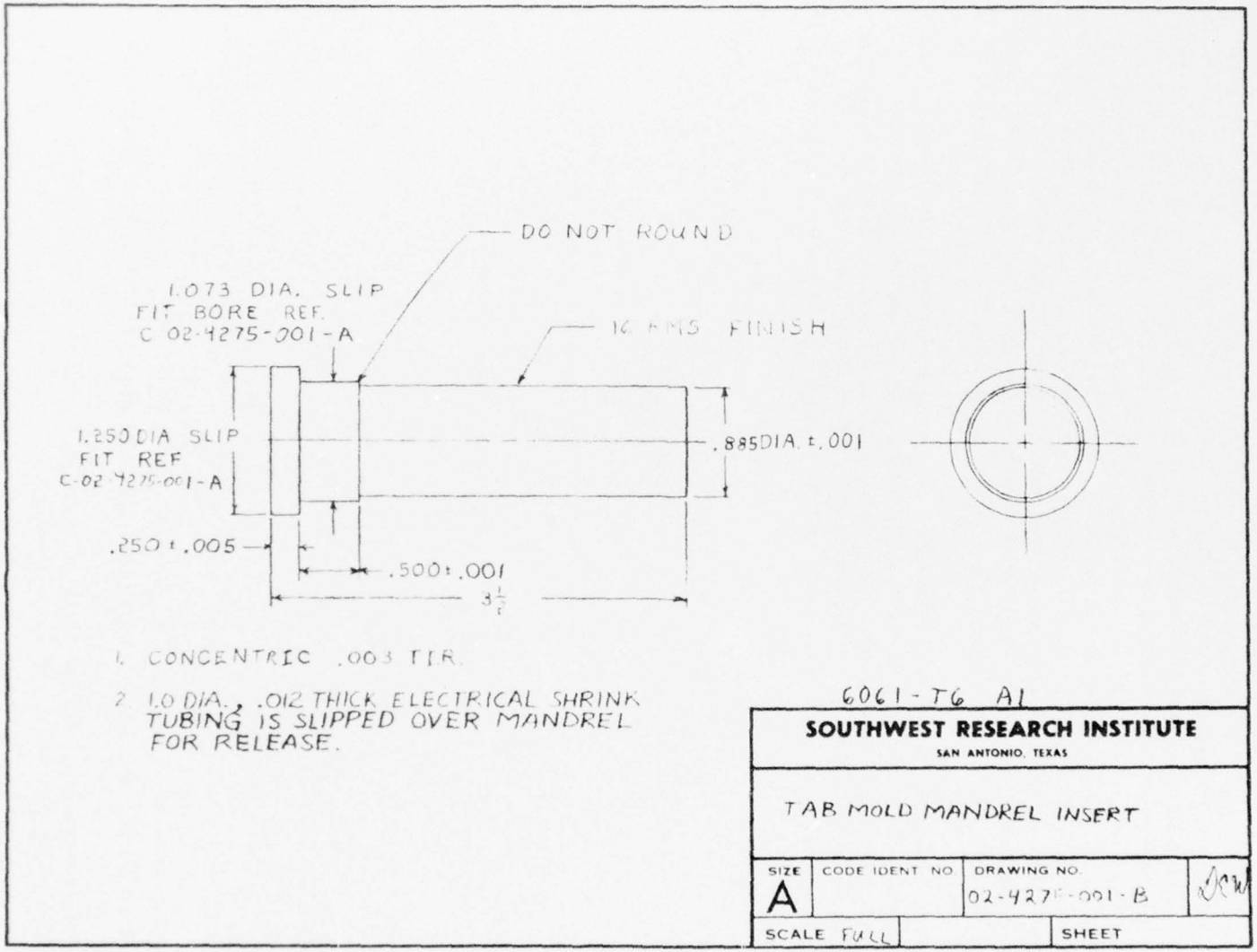

Figure 2. Tab Mold Insert

3. Flat Panel Fabrication

Four panels, each measuring 11 inches by 4 inches, were fabricated for purposes of making coupon-type specimens. The panels were processed in a blanket press using the same cure cycle as was used in tube processing. One ply of vent cloth (perforated on 2-inch centers) and one bleeder ply were used on either side of the layup during cure. The four layups that were prepared were $[0]_6$, $[90]_8$, $[0/90_2/0]_2$, and $[\pm\mp 45]_s$. After fabrication the laminate plate was trimmed and squared, and areas to be tabbed were sanded with 120 grit sandpaper and wiped clean with MEK or acetone. A liquid adhesive* was then applied to bond the tabs onto the panel. The panel was cut into 3/4-inch wide tensile specimens using a diamond slitting blade.**

The tabs, which are bonded to the laminated panel before cutting the specimens from the panel, were fabricated of unidirectional glass tape (Scotch Ply 1009-36 E Glass, 3M Company). The tape was laminated into a 7-ply strip [(0/90)/0] 0.055-inch thick. After cure, the strip was machined into a 1-1/2 - inch wide tab strip with a 35° chamber along one side.

---

*Epoxi-Patch, manufactured by the Hysol Division of the Dexter Corporation.

**6-inch diameter, 0.025-inch thick, manufactured by Elgin Diamond Products of 366 Bluff City Blvd., Elgin, Illinois.

SECTION III

PLY CHARACTERIZATION WITH TUBES AND COUPONS

1. Test Methodology

Tubular specimens were instrumented with two 350 ohm strain gage rosettes mounted centrally on the tube, 180 degrees apart. Each rosette consisted of three strain gages oriented at 0, 45, and 90 degrees to the tube axis providing for measurement of axial, hoop, and shear strain. The six gages were wired into a switching circuit with data displayed on a digital voltmeter and recorded in tabular form. Specimens were loaded, under load control, short of failure two times before being broken during the final loading. Testing was done in an SwRI Electro-Hydraulic Biaxial Machine equipped with the servo-hydraulic grip system developed earlier under Air Force sponsorship.[4] The test set up is shown in Figure 3.

Initial testing was delayed by the premature rupture of an inner grip sleeve (see Figure 4). When the replacement sleeve also ruptured, it was decided to modify the grip system. As described in Reference 4, the original procedure for fabricating the inner grip sleeve is a time consuming (and therefore costly) process. Basically, the original procedure required molding the segmented metal-reinforcing sleeve in the Adiprene polymer material, machining a seal-lip in each end, and assembling with an "O" ring-sectional tubing arrangement inside to effect initial sealing (see Figure 5). Even with the "O" ring arrangement, however, the initial seal was often difficult to achieve. To correct this problem, the inner grip sleeve mold was rebuilt to provide grooves inside each end of the finished grip sleeve. These grooves accommodate graphite-filled teflon spring-loaded high pressure seals which are commercially available.* This method completely eliminated the machining operation and the complicated "O" ring-sectional tubing arrangement. The only assembly involved was insertion of the seals into the sleeves, which proved to be a simple operation. The final modification involved grinding the grip assembly stem smaller to accommodate the new seals. When testing was resumed, the new inner sleeve worked very well, eliminating the previously encountered initial sealing problem.

Coupon type specimens were instrumented with two 350 ohm strain gages to measure longitudinal and transverse strain. Longitudinal tensile loading was done with an Instron Model TTC tensile test machine. Load-versus-strain plots were recorded using X-Y plotters. Data from both tubes and coupons were tabulated and typed into a Hewlett-Packard Model

---

*Bal-Seal Engineering Company, Tustin, California.

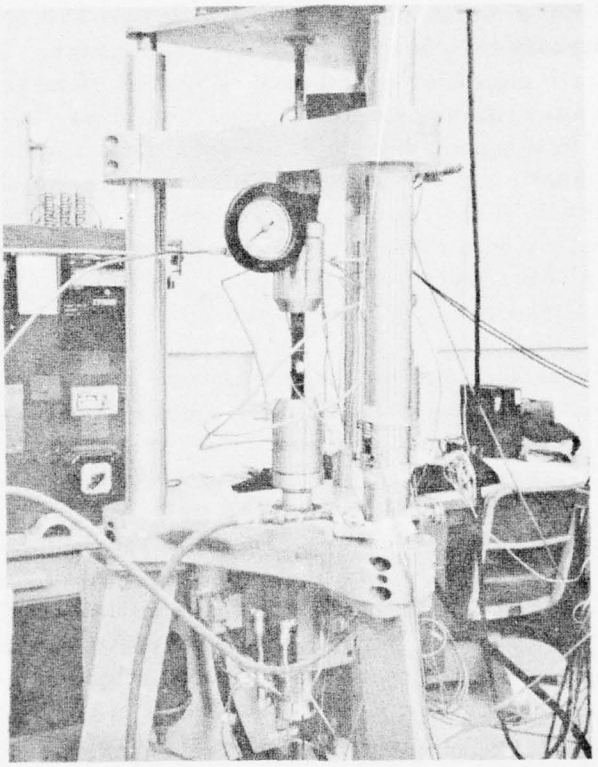

Figure 3. Tubular Specimen Mounted in the Test Apparatus

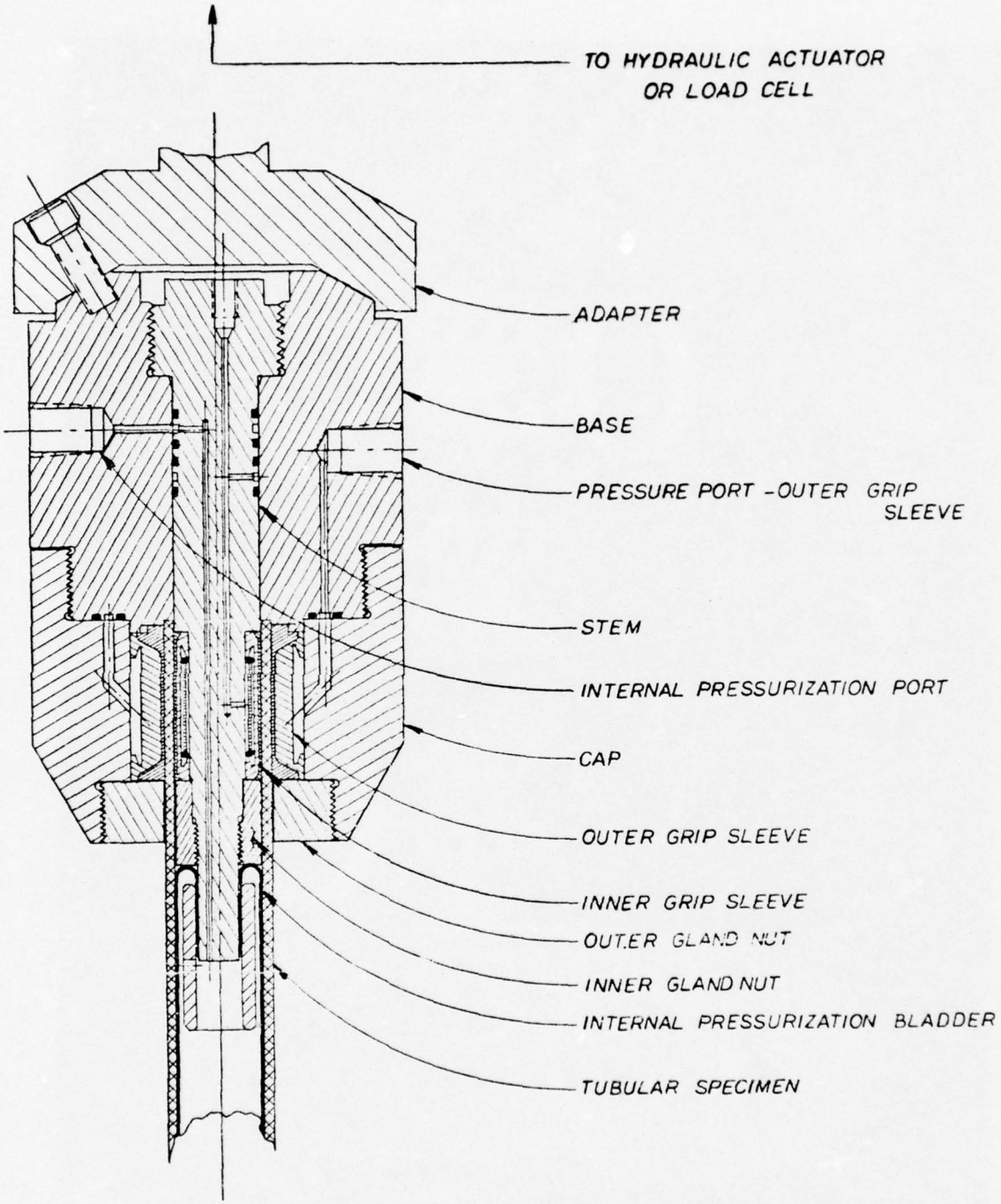

Figure 4. Upper Hydraulic Grip Assembly

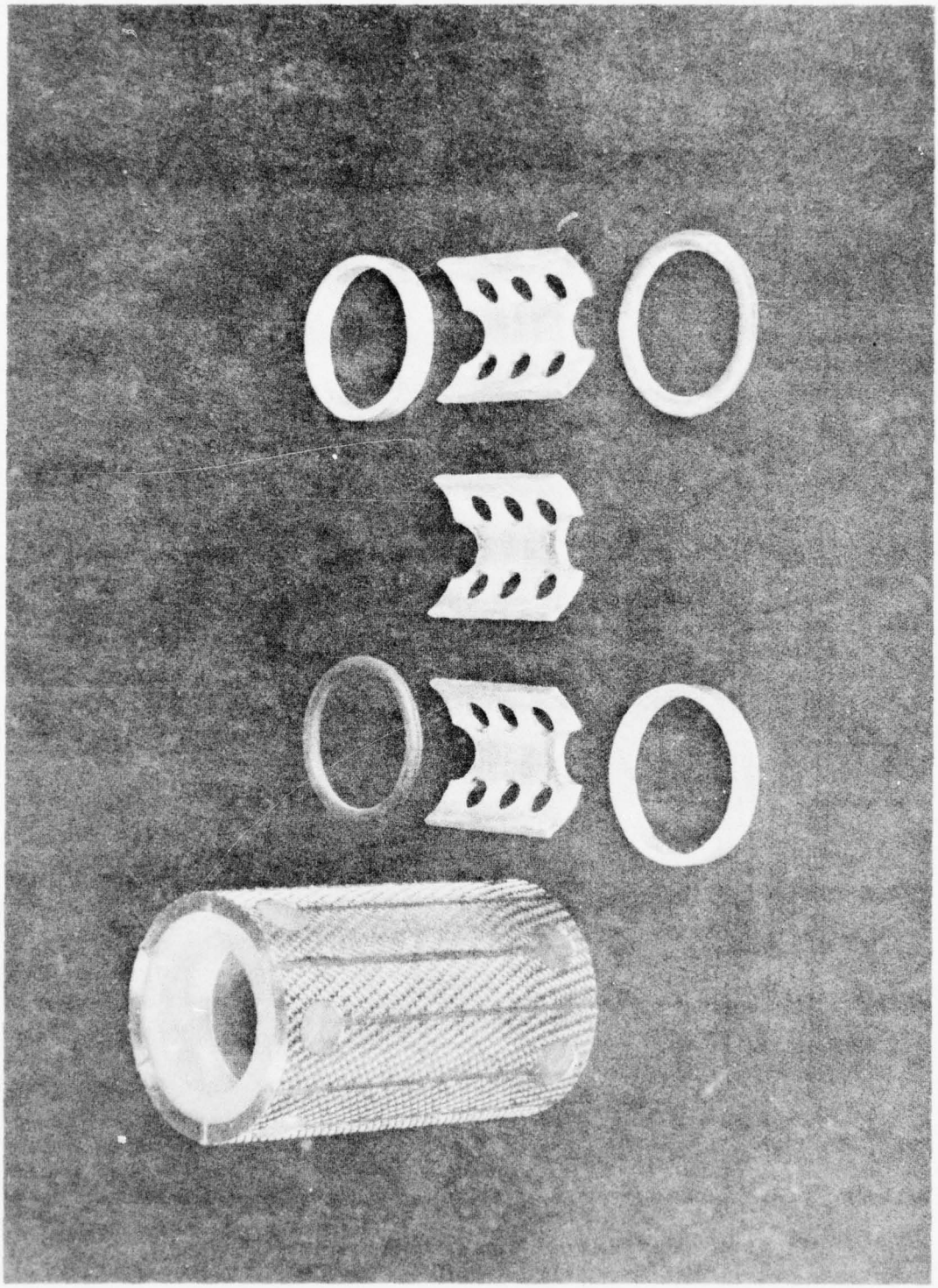

Figure 5. Inner Grip Sleeve

9830A electronic data processor for storage on magnetic tape cassettes, making later retrieval, reduction, and plotting on the plotter, a simple task. The data shown in the Appendix were reduced in this manner.

2. Ply Characterization Using Tubes

In order to predict first ply failure (FPF) by use of laminated plate theory, the ply properties of the material must first be determined. Fourteen $[0]_4$ tubes were tested in uniaxial loading to obtain elastic modulus, Poisson's ratio, and ultimate strength data. A summary of the test results, as well as stress-strain curves, are contained in the Appendix.

Four unidirectional, 4-ply tubes, designated 8, 24, 25, and 31 were loaded in axial tension. No ultimate strength data were obtained, as the 10,000-pound load capacity of the biaxial testing machine would not have been sufficient to cause failure in the specimens. The axial elastic modulus, E_{xx} was calculated as the slope of an axial stress-versus-axial strain curve:*

$$E_{xx} = \frac{\Delta \sigma_x}{\Delta \epsilon_x}$$

The principal Poisson's ratio, ν_{xy}, was calculated from an axial stress-versus-hoop strain curve and the elastic modulus:

$$\nu_{xy} = - \frac{E_{xx}}{\Delta \sigma_x / \Delta \epsilon_y} = - \frac{\Delta \epsilon_y}{\Delta \epsilon_x}$$

The average properties thus obtained from these four tubular specimens were: elastic modulus, E_{xx}, of 19.3×10^3 ksi, and a principal Poissons's ratio of 0.35.

A second set of five unidirectional 4-ply tubes, designated 9, 12, 23, 25+ and 62 were loaded by internal pressure. Tubes 9, 12, 23, and 62 were untabbed; that is, they had no end reinforcement. Tube number 25 was tabbed. Some difference in modulus data was observed. The testing machine was

---

*The subscript x refers to the fiber direction, and y is transverse to the fiber direction in the ply plane.

+Tube number 25 was tested first in axial tension, later by internal pressure.

modified slightly for this series of tests, using low pressure (200 psi) air instead of the high pressure (10,000 psi) hydraulic intensifier to load the specimen. This was done to provide more accurate load control and measurement at low loading pressures. The elastic modulus E_{yy} was calculated in a similar manner as E_{xx}, and the minor Poisson's ratio, ν_{yx} was calculated in the same manner as ν_{xy}. Accurate determination of ν_{xy} was difficult due to inaccuracies in measuring the small values of the induced axial strain ϵ_x. Despite scatter in the data (see the Appendix), however, acceptable values of ν_{yx} were found and were in accord with values calculated from the other orthotropic elastic constants: ν_{yx} = 0.03, and S_y^{ut} = 3.5 ksi.

Five unidirectional 4-ply tubes, designated to as 11, 14, 20, 54, and 55 were tested in torsion. Tubes number 11 and 20 were broken during the first loading cycle. Tube number 11 was inadvertently cracked when an attempt was made to insert it into the grips. Tube number 20 was accidentally crushed in compression due to an error in controller operation. The shear moduli G_{xy} were calculated from the shear stress-versus-shear strain curve.

$$G_{xy} = \frac{\Delta \tau_{xy}}{\Delta \gamma_{xy}}$$

An average shear modulus G_{xy} of 0.94×10^3 ksi and a shear strength S_{xy} of 11.1 ksi were obtained. A summary of the average ply properties is shown in Table 1.

3. Ply Characterization Using Coupons

Thirteen flat coupon specimens, cut from the four different laminate panels, were tested in axial tension to provide data comparable to that measured with the tubular specimens. A data summary and the stress-strain curves are presented in the Appendix. Average ply properties measured using coupon specimens are shown in Table 2.

4. Discussion of Unidirectional Ply Properties

Table 3 is presented in order to compare data generated using coupons with that generated using tubular specimens. Certain tests are, of course, directly comparable, for example, internal pressurization of 0° tubes and

tensile testing of 90° coupons. In order to compare tensile tests of ±45° coupons to data generated with torsionally loaded tubes, the procedure proposed by Rosen was used.[5]

Table 1

Summary of Average Ply Properties Measured Using $[0]_4$ Tubes

$E_{xx} = 19.3 \times 10^3$ ksi

$E_{yy} = 1.44 \times 10^3$ ksi $\qquad S_y^{ut} = 3.5$ ksi

$G_{xy} = 0.94 \times 10^3$ ksi $\qquad S_{xy}^{us} = 11.1$ ksi

$\nu_{xy} = .35$

$\nu_{yx} = .03$

Table 2

Summary of Average Ply Properties Measured Using

Coupon Specimens

$E_{xy} = 23.0 \times 10^3$ ksi $\qquad S_x^{ut} = 214$ ksi

$E_{yy} = 1.6 \times 10^3$ ksi $\qquad S_y^{ut} = 6.8$ ksi

$\nu_{xy} = .34$

$\nu_{yx} = .03$

Table 3

Comparison of Average Ply Properties Measured

Using Tubes and Coupons*

Property	$[0°]_4$ Tube Data	Coupon Data	
E_{xx}	19.3	23.0	$[0°]_6$
S_x^{ut}	--	214	$[0°]_6$
ν_{xy}	0.35	0.34	$[0°]_6$
E_{yy}	1.44	1.6	$[90°]_8$
S_y^{ut}	3.5	6.8	$[90°]_8$
ν_{yx}	0.03	0.03	$[90°]_8$
G_{xy}	0.94	0.87	$[\pm(\mp 45)]_s$
S_{xy}^{us}	11.1	10.8	$[\pm(\mp 45)]_s$

*All strength values are reported in ksi units, all moduli are 10^3 ksi.

Rosen's analysis of $[\pm 45]$ coupons results in the following expressions:

$$G_{xy} = \frac{\sigma_x}{2(\epsilon_x - \epsilon_y)}$$

$$S_{xy}^{us} = \frac{S_x^{ut}}{2}$$

As can be seen from Table 3, the elastic constants measured using tubes, and those measured using coupons are in close agreement. However, some differences in transverse strengths do exist. The variation in transverse strength S_y^{ut} may be the result of the thickness difference between the two specimens; the statistical dispersion in strength values, particularly in unidirectional ply properties, is strongly dependent upon specimen thickness. Reduced strength values may also be attributed to longitudinal cracking during specimen preparation (teflon fluorocarbon film removal from inner surface) or in handling and insertion into the test facility. Thus, satisfactory transverse strenth data on thin, 0° tubes were difficult to obtain.

When testing $[0°]_4$ tubes in torsion, it was noted that coincident with initial longitudinal splitting the tube showed a spiral distortion resembling a torsional buckling mode. In order to determine whether torsional buckling might be expected prior to the onset of failure with this $[0°]_4$ specimen, a buckling analysis was made. The analysis drew from the results of Simitses, (6) who studied the elastic stability of orthotropic elastic shells under general loading. The orthotropic elastic constants given in Table 1 were used to predict the critical torsional shear strength, τ_{cr}, to create instability in a tube with a given length-to-radius ratio L/R. The results of this analysis are shown in Figure 6. The critical buckling stress is given by the envelope of the cusps for each of the mode numbers n = 2, 3, 4, ... used in the analysis. Two curves are given; the upper curve corresponds to the first approximation (Eq. (20) of Reference 6), whereas the lower curve corresponds to the more accurate second approximation (Eq. (21) of Reference 6). As can be seen from Figure 6, the theoretical buckling strength of the $[0°]_4$ tube for L/R = 10 is nearly 15 ksi, well above the approximately 11 ksi torsional shear strength developed by the tubes. These results indicate that torsional buckling does not influence apparent shear strength on these tubular specimens.

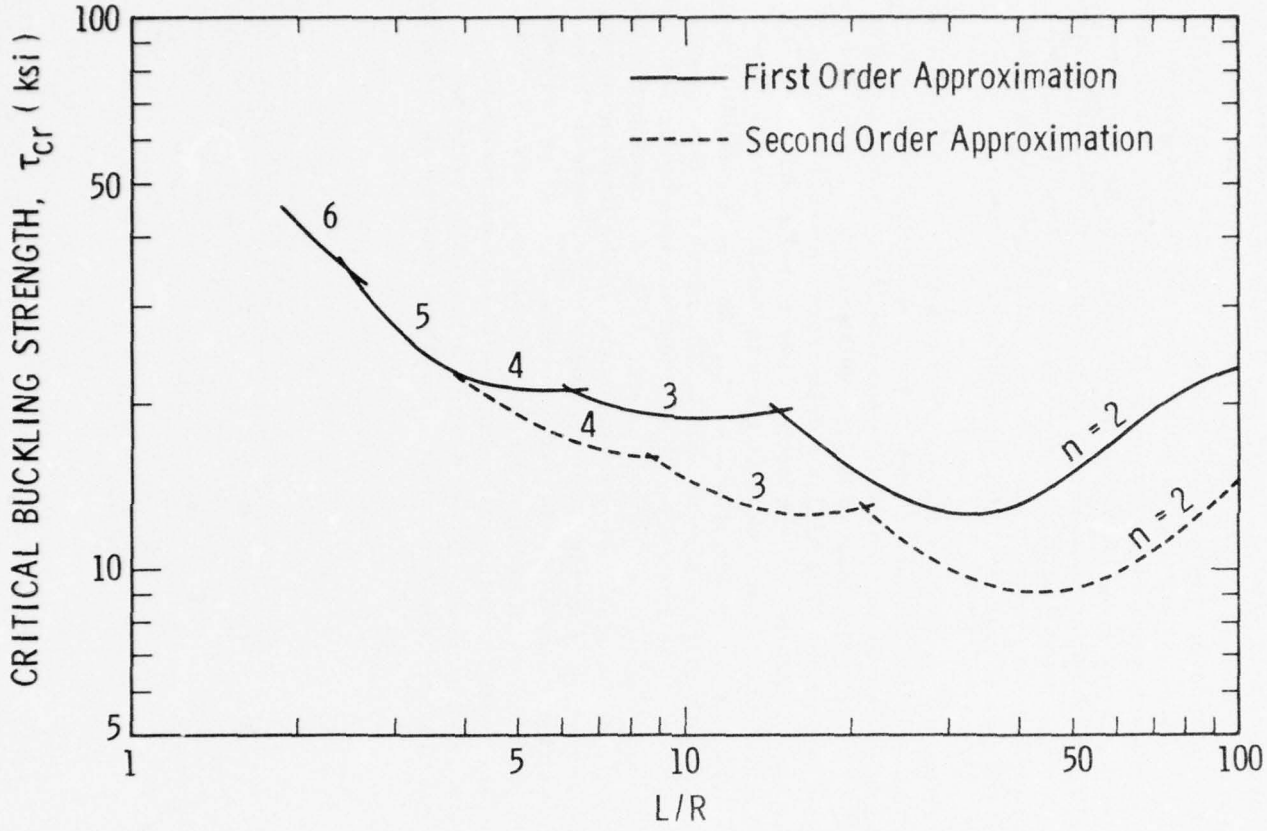

Figure 6. Theoretical Torsional Buckling Strength of Unidirectional [0°] tube, After Reference 6 .

SECTION IV

EXPLORATORY DETECTION OF FIRST PLY FAILURE

1. Theoretical Estimates of Damage Envelopes

In conducting exploratory experiments to detect first ply failure (FPF) it is very useful to have an analytical model that will predict, at least approximately, when FPF can be expected to develop for a particular laminate under a given loading state. The mechanics of the FPF process are not yet well understood and any mathematical model built upon an inadequate base of empirical observation is, at best, speculative. Nevertheless, it is useful to have such a model to help estimate the region of load where FPF may be expected to develop.

Currently, laminated plate theory* provides the most useful and elementary approach to FPF estimation. The basic theory has been well developed[7,8] and widely used, and need not be repeated here. As usually applied, laminate theory provides a linear elastic calculation of the stress states in each ply of an angle ply laminate. Aside from the linear elastic assumption, this approach treats each ply as a homogeneous orthotopic layer, and assumes that all plies deform compatibly under the action of the applied loads so that there is no interlaminar relative displacement.

There are two modifications of conventional laminate theory that have been suggested as being necessary to account more realistically for stresses and deformations in laminated plates. The first of these is the "nonlinear shear" effect. While the extensional stress-strain response of high modulus composites is usually nearly linear to failure, the in-plane shear behavior of a ply is normally strongly nonlinear. This observation has led several investigators[9-12] to modify conventional laminated plate theory to account for this nonlinear shear effect. Experience with practical angle-ply laminates, however, suggests that overall laminate response tends to be surprisingly linear despite ply nonlinearity.[13]

The second respect in which conventional laminate theory has been modified is in the accommodation of initial stresses due to curing. Typical epoxy resin composites have a cure temperature of 300° - 350°F. When the fabricated article is brought from cure temperature down to ambient, the

---

*For thin quasi-isotropic, symmetric angle ply tubes under pure axial pressure, or torsional loading the geometric correction to the laminated plate theory to account for through-thickness stress variations in tubes is of order t/D, where t is the specimen thickness and D is the specimen diameter.[7,8] Since this correction is small (of order 2% for the tubes used in the present program) the terms "plate" and "tube" are used interchangeably in describing the membrane deformation mechanics.

potential exists, due to differing thermal expansion properties in the matrix and in the reinforcement, and due to thermally anisotropic ply properties, for residual stress systems to be established which may affect mechnical behavior. Hahn and Pagano[14] have proposed a total strain theory which estimates these initial stresses, and found that they attain magnitudes of the order of 10 ksi in a $[0/\pm 60]_s$ boron/epoxy laminate.

In the present work the authors have chosen to use the simplest possible analytical model for FPF estimation. Laminate theory has been used without correction for nonlinear shear or residual curing stress effects.* FPF is estimated by applying the maximum strain criterion to each ply in the laminate to determine the laminate stress level at which some ply first reaches its critical fiber, transverse, or in-plane shear strain level. This approach provides a useful initial estimate for the applied load corresponding FPF, and has been used in guiding the experimental detection of FPF by acoustic emission techniques.

Figures 7 and 8 present FPF estimates for the two angle ply stacking sequences used in this research: $[0/90]_s$ and $[\pm 45]_s$. Their correlation with measured FPF levels (if indeed any) has yet to be demonstrated.

2. FPF Detection Using Acoustic Emission

To measure first ply failure (FPF), tubes were each instrumented with two 350-ohm 3-gage rosettes and two acoustic emission transducers (see Figure 9). Each transducer consisted of a disk of piezoelectric ceramic PZT-5 with a silicon rubber housing. The transducers were resonant at the frequency of 200 kHz. Figure 10 is a diagram of the system. The output from each transducer was fed into a high-input impedance, low noise level preamplifier through a short coaxial cable. As a signal conditioner, a bandpass filter, having a response in the frequency range from 100 to 300 kHz was used together with a solid state amplifier to achieve a gain for the overall system which could be varied from 60 to 90 dB. From there, the signal was fed into a band pass filter and into a coincident gate. Signals were then counted by a digital counter, passed to a digital-to-analog converter, and recorded on a 4 channel Biomation wave form recorder. Output from the coincidence gate was also passed to a frequency-to-voltage converter and recorded on a separate channel of the waveform recorder.

This instrumentation system is capable of delivering cumulative count data from acoustic emissions generated in the gage section as defined

---

*At the time of writing this report the model was being modified to account for thermal pre-strain, which has the effect of increasing the predicted FPF stresses.

by the wave speed and the time delay characteristic of the coincidence gate. Ultrasonic resonance tests of $[0]_4$, $[\pm 45]_s$ and $[0/90]_s$ tubes provided wave speeds all very close to 2×10^5 in/sec. During initial experiments with the acoustic emission equipment, the coincidence gate was varied from 10 to 60 microseconds.

3. Preliminary Test Results on $[0/90]_s$ Tubes

Two $[0/90]_s$ tubes, numbered 15 and 16, were instrumented for strain and acoustic emission, and tested by axial tension. Elastic modulus, Poisson's ratio, ultimate strengths, and stress-strain curves for these tubes are shown in the Appendix. The average properties measured during testing are listed in Table 4.

Table 4

Average Properties Measured Using $[0/90]_s$ Tubes

$E_{xx} = 8.9 \times 10^3$ ksi $\qquad S_x^{ut} = 78.3$ ksi

$\gamma_{xy} = .061$

Tube number 15 was tested first, with the acoustic emission sensors spaced 2 inches apart centrally on the tube. The coincidence gate was set at 10 microseconds. Two loadings were made to 2000 pounds load (25.7 ksi stress level). Little acoustic activity was observed. Second, loading was to 54 ksi. A considerable increase in acoustic activity was observed beginning at approximately 50 ksi, indicated by small lights in each sensor circuit which indicate pulses. The pulses were not counted, however, implying that the bursts were not originating between the sensors. When the specimen was loaded to failure, the activity again began at approximately 50 ksi, and increased in intensity until the signal conditioner amplifiers were saturated. Failure in the specimen occurred 1 inch from the end of the tab, or about 1 inch outside the region monitored by the acoustic emission sensors.

To monitor more of the tube gage section for the second test, coincident gate time was increased to 60 microseconds, and the sensors were spaced 4 inches apart on tube number 16. In hope of avoiding saturation, overall sensitivity of the system was reduced by decreasing amplification in the signal conditioner. Test results were about the same, however, with observed, uncounted activity taking place at 50 ksi and above. Tube number 16 failed 1/4-inch from the end tab, again outside the monitored gage section. This would account for activity being picked up by the sensors but not counted.

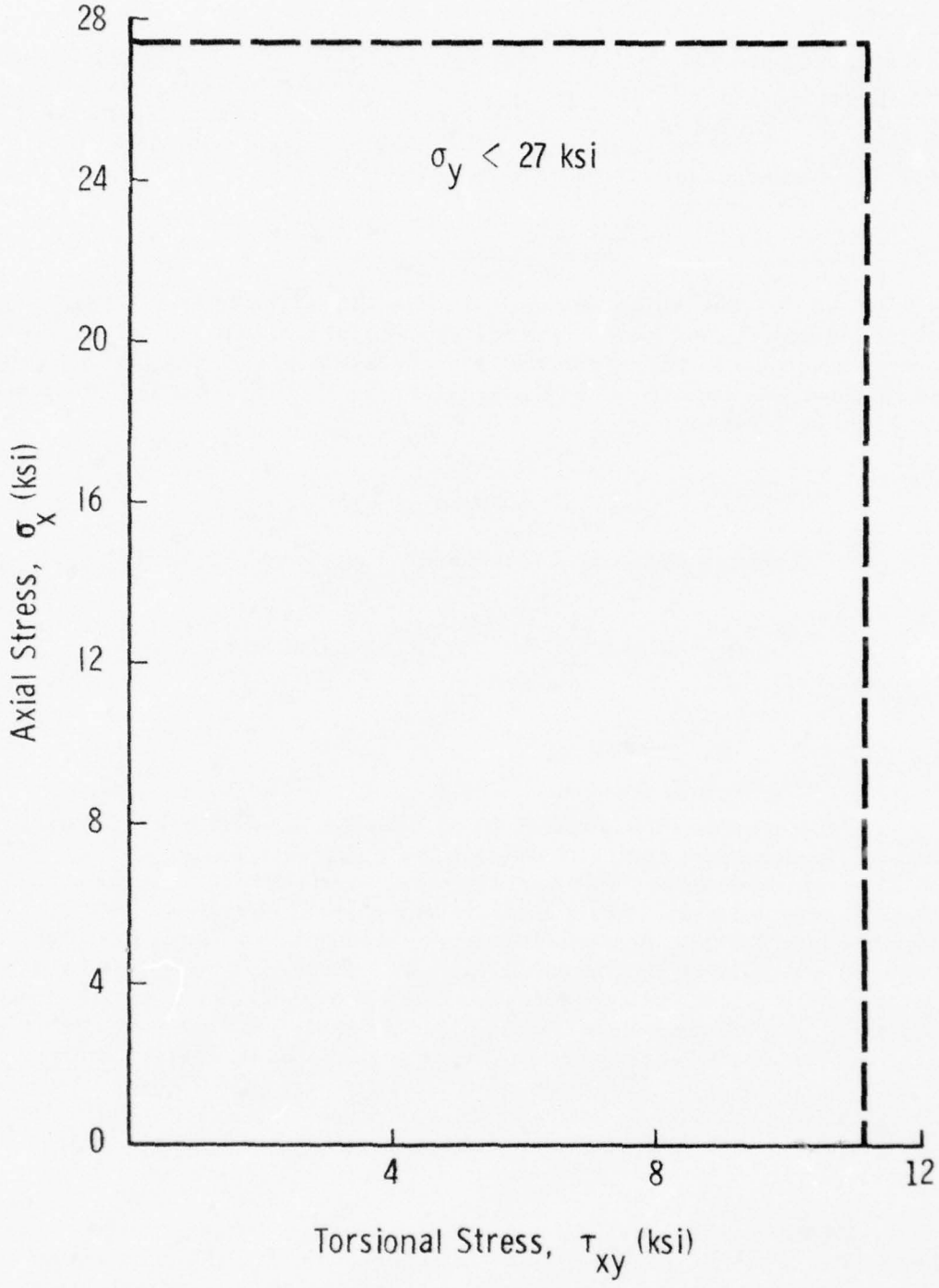

Figure 7. Estimated FPF Loci for $[0/90]_s$ Laminate

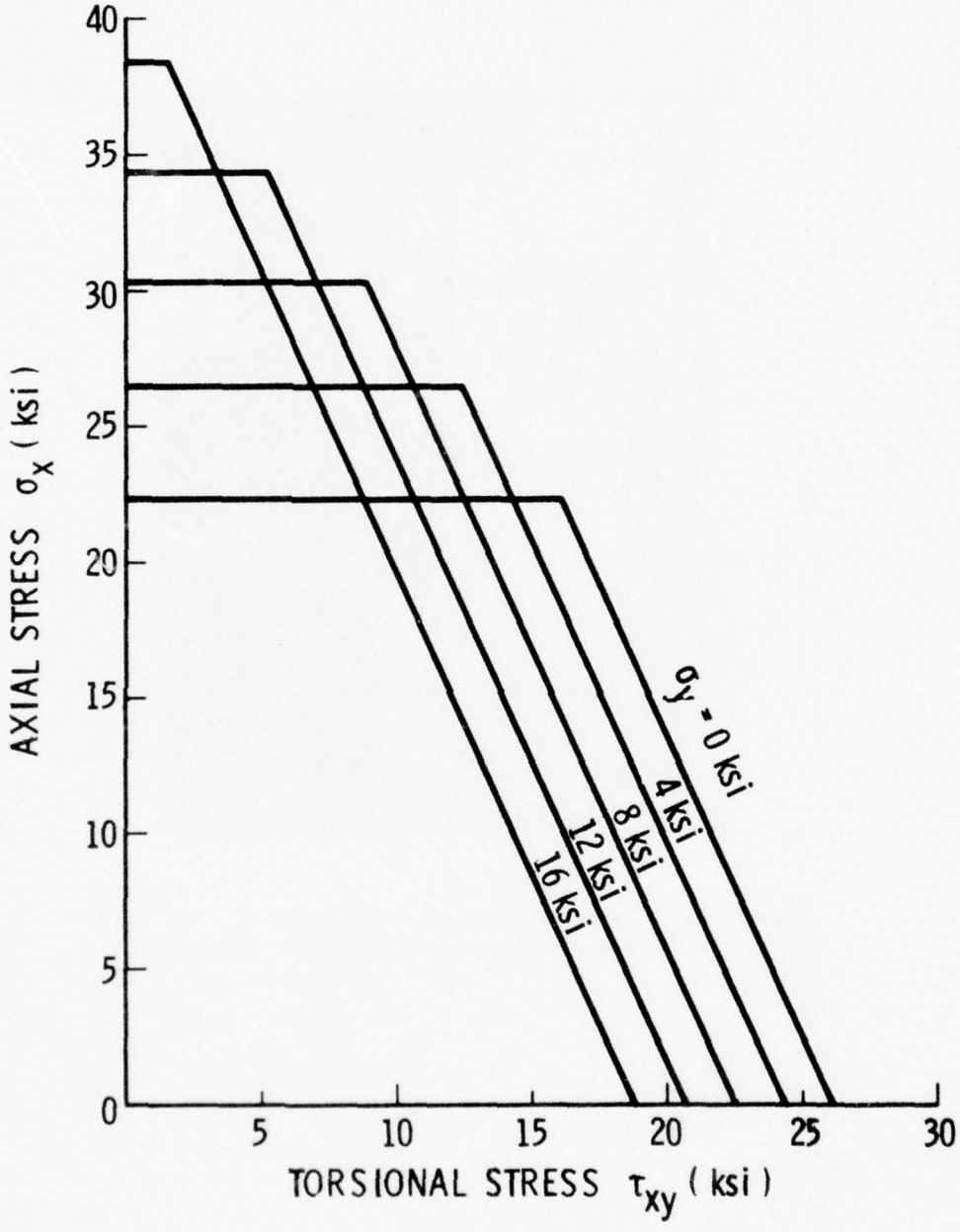

Figure 8. Estimated FPF Loci for [±45] Laminate

Figure 9. Closeup View of Tube Instrumented With Strain Gages and Acoustic Emission Transducers

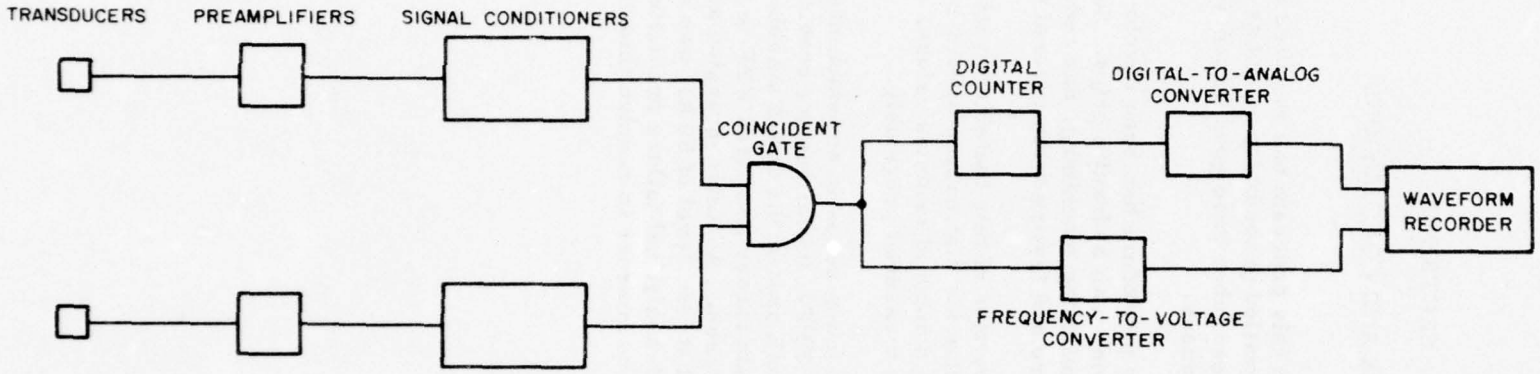

Figure 10. Block Diagram of the Acoustic Emission System

SECTION V

RESULTS AND CONCLUSIONS

Work done thus far on this program has resulted in a capability for routine manufacture of thin-walled graphite/epoxy tubes of controlled high (65 - 70%) fiber volume. These tubes have good dimensional tolerance in both wall thickness and roundness.

A simpler end tabbing procedure has been developed and used for loading these tubular specimens with hydraulic grips. Successful molding of neat epoxy resin tabs, eliminating machining, has reduced the time spent between specimen manufacture and testing from several weeks to a few days.

The physical ply properties of this material system have been measured and correlated with both tubular and flat coupon specimens. Angle ply laminates were tested and verified with computed modulus values, using laminated theory and the ply properties measured previously.

Exploratory research using acoustic emission has shown that this may be a useful tool in predicting FPF. Initial results provided only qualitative results, however, because both specimens failed outside of the monitored gage section. Laminated plate theory predicted FPF in $[0/90]_s$ tubes at approximately 27 ksi axial stress. Acoustic emission activity did not become evident until an axial stress level of 50 ksi was reached. Further work needs to be done on both analytical failure prediction and on the acoustic emission measurement system in order to resolve this difference.

REFERENCES

1. Francis, P. H., and Bert, C. W., "Composite Material Mechanics: Inelasticity and Failure," Fibre Science and Technology, Vol. 8, No. 1 (January 1975), pp. 1-19.

2. Tsai, S. W., and Hahn, H. T., "Failure Analysis of Composite Materials," in: INELASTIC BEHAVIOR OF COMPOSITE MATERIALS, AMD-Vol. 13, ASME, New York, 1975, pp. 73-96.

3. Weed, D. N., and Francis, P. H., "Process Development for the Fabrication of High-Quality Composite Tubes," Fibre Science and Technology (in press).

4. Nagy, A., and Lindholm, U. S., "Hydraulic Grip System for Composite Tube Specimens," AFML-TR-73-239, November 1973.

5. Rosen, B. W., "A Simple Procedure for Experimental Determination of the Longitudinal Shear Modulus of Unidirectional Composites," Journal of Composite Materials, Vol. 6, No. 4 (October 1972), pp. 552-554.

6. Simites, G. J., "Instability of Orthotropic Cylindrical Shells Under Combined Torsion and Hydrostatic Pressure," AIAA Journal, Vol. 5, No. 8 (August 1967), pp. 1463-1469.

7. Ashton, J. E., Halpin, J. C., and Petit, P. H., PRIMER ON COMPOSITE MATERIALS: ANALYSIS, Chapter 3, Technomic Publishing Co., Stamford, 1969.

8. Jones, R. M., MECHANICS OF COMPOSITE MATERIALS, Chapter 4, McGraw-Hill Book Co., New York, 1975.

9. Hahn, H. T., and Tsai, S. W., "Nonlinear Elastic Behavior of Unidirectional Composite Laminae," Journal of Composite Materials, Vol. 7, No. 1 (January 1973), pp. 102-118.

10. Sims, D. F., "In-Plane Shear Stress-Strain Response of Unidirectional Composite Materials," Journal of Composite Materials, Vol. 7, No. 1 (January 1973), pp. 124-128.

11. Hahn, H. T., "Nonlinear Behavior of Laminated Composites," Journal of Composite Materials, Vol. 7, No. 2 (April 1973), pp. 257-271.

REFERENCES (concluded)

12. Hahn, H. T., "A Note on Determination of the Shear Stress-Strain Response of Unidirectional Composites," Journal of Composite Materials, Vol. 7, No. 3 (July 1973), pp. 383-386.

13. Ashton, J. E., "Analysis and Design Methods for Composite Structures: Overly Intimidating!," Design lecture given at 16th AIAA/ASME/SAE Structures, Dynamics and Materials Conference, Denver, May 27, 1975.

14. Hahn, H. T., and Pagano, N. J., "Curing Stresses in Composite Laminates," Journal of Composite Materials, Vol. 9, No. 1 (January 1975), pp. 91-106.

APPENDIX

Stress-Strain Curves: Tubes

TEST DATA FOR TUBULAR SPECIMENS

TUBE No.	LAY-UP	OUTSIDE DIAMETER (in)	THICKNESS (in)	FIBER VOLUME (%)	VOID VOLUME (%)	MODULUS (10^3 ksi)	POISSON'S RATIO	ULTIMATE STRENGTH (ksi)
	$[0]_4$		(longitudinal tension)			E_{xx}	ν_{xy}	S_x^{ut}
8		1.009	.021			19.0	.31	
24		1.010	.021	70.7	2.0	19.9	.33	
25		1.010	.021	70.7	2.0	19.6	.38	
31		1.009	.022	66.3	2.1	18.8	.38	
	$[0]_4$		(internal pressure)			E_{yy}	ν_{yx}	S_y^{ut}
9		1.012	.022	64.6	2.2	1.46	.034	4.136
12		1.013	.021	68.4	2.1	1.42		2.706
23		1.011	.021	70.5	2.0	1.52	.026	4.268
25		1.010	.021	70.7	2.0	1.48		
62		1.012	.022			1.33		3.08
	$[0]_4$		(torsion)			G_{xy}		S_{xy}^{us}
11		1.012	.021	66.2	2.2	.89		*
14		1.012	.022	67.6	2.1	.89		5.12**
20		1.012	.021	65.8	2.2	.905		
54		1.012	.022			.96		10.7
55		1.012	.022			.96		11.4
	$[0/90]_s$		(longitudinal tension)			E_{xx}	ν_{xy}	S_x^{ut}
15		1.014	.025	54.0	2.4	8.6	.061	70.8
16		1.013	.024	58.9	2.3	9.3	0.61	85.8

*split longitudinally on insertion into grips
**not included in averaged strength levels

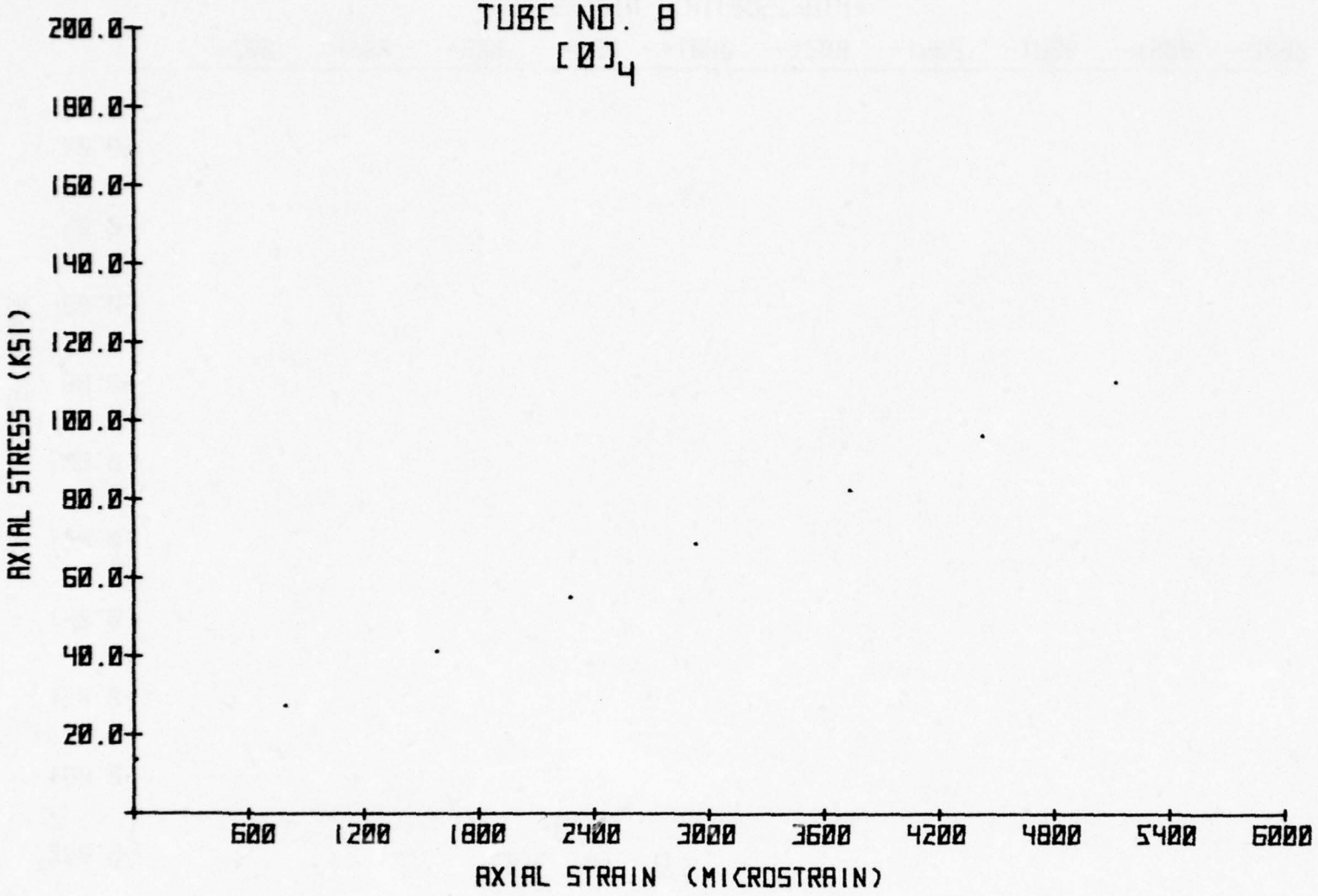
TUBE NO. 8
[0]4
200.0
180.0
160.0
140.0
120.0
100.0
80.0
60.0
40.0
20.0
AXIAL STRESS (KSI)
600
1200
1800
2400
3000
3600
4200
4800
5400
6000
AXIAL STRAIN (MICROSTRAIN)

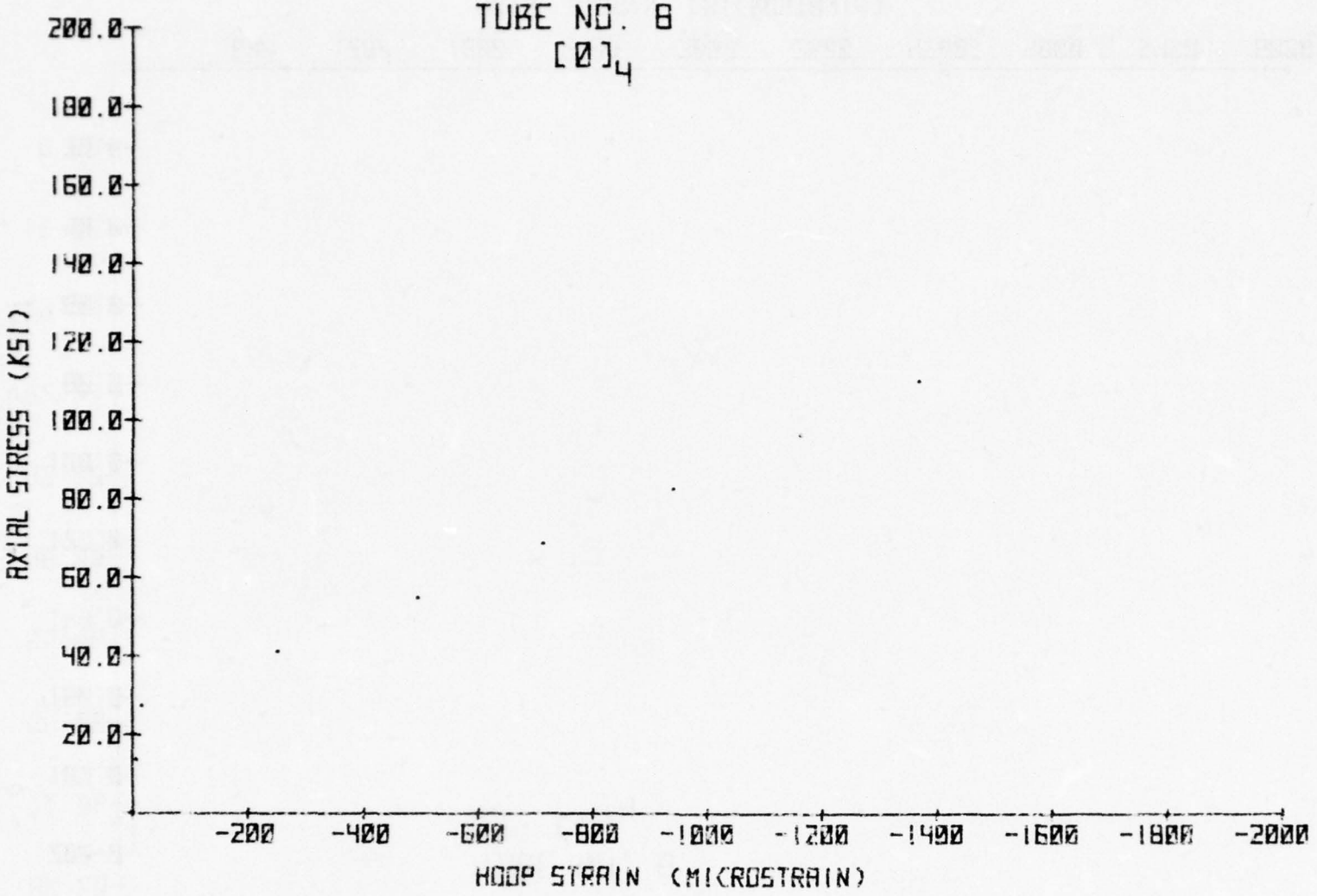
TUBE NO. 8
[0]4
200.0
180.0
160.0
140.0
120.0
100.0
80.0
60.0
40.0
20.0
AXIAL STRESS (KSI)
-200
-400
-600
-800
-1000
-1200
-1400
-1600
-1800
-2000
HOOP STRAIN (MICROSTRAIN)

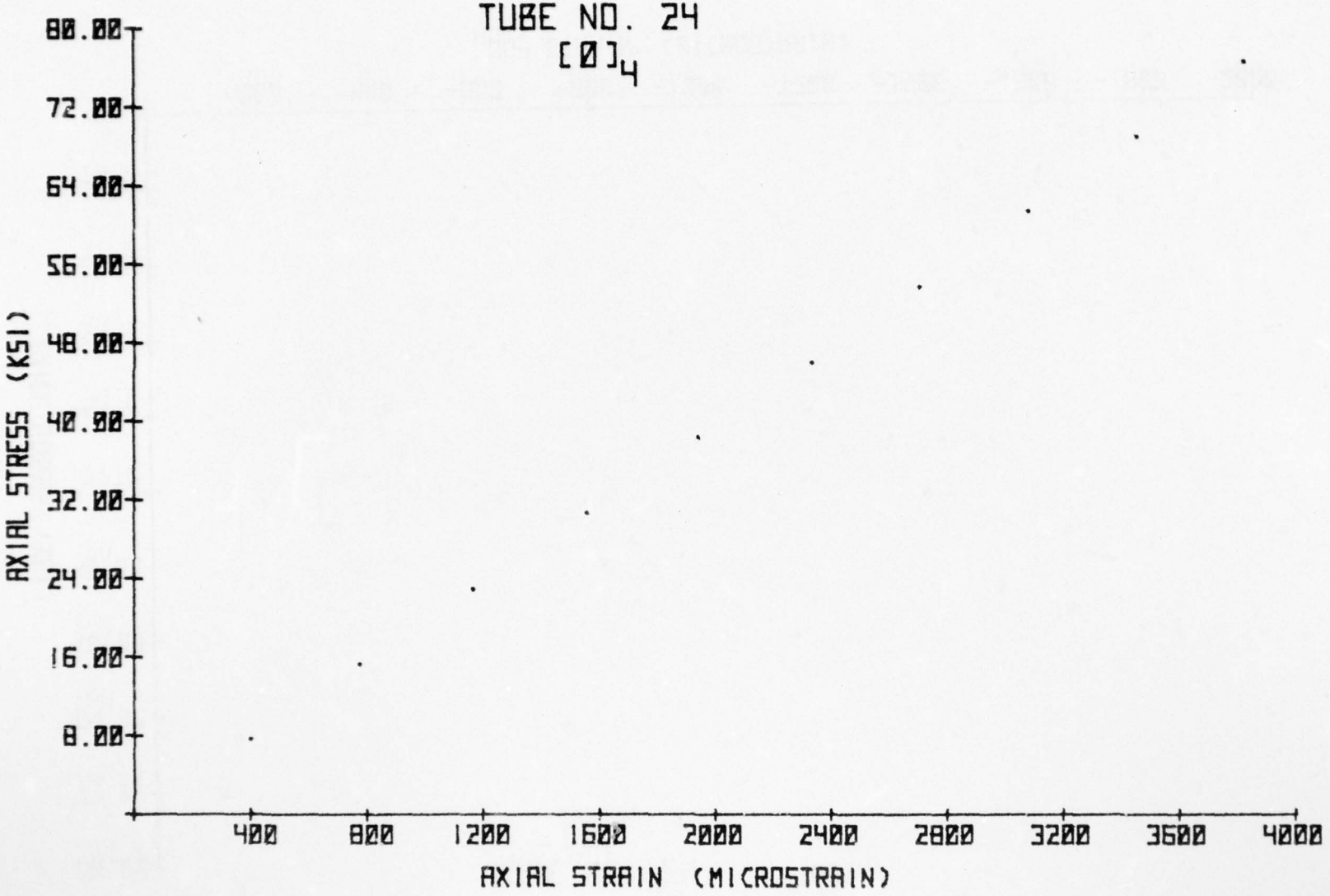
TUBE NO. 24
[0]4
80.00
72.00
64.00
56.00
48.00
40.00
32.00
24.00
16.00
8.00
AXIAL STRESS (KSI)
400
800
1200
1600
2000
2400
2800
3200
3600
4000
AXIAL STRAIN (MICROSTRAIN)

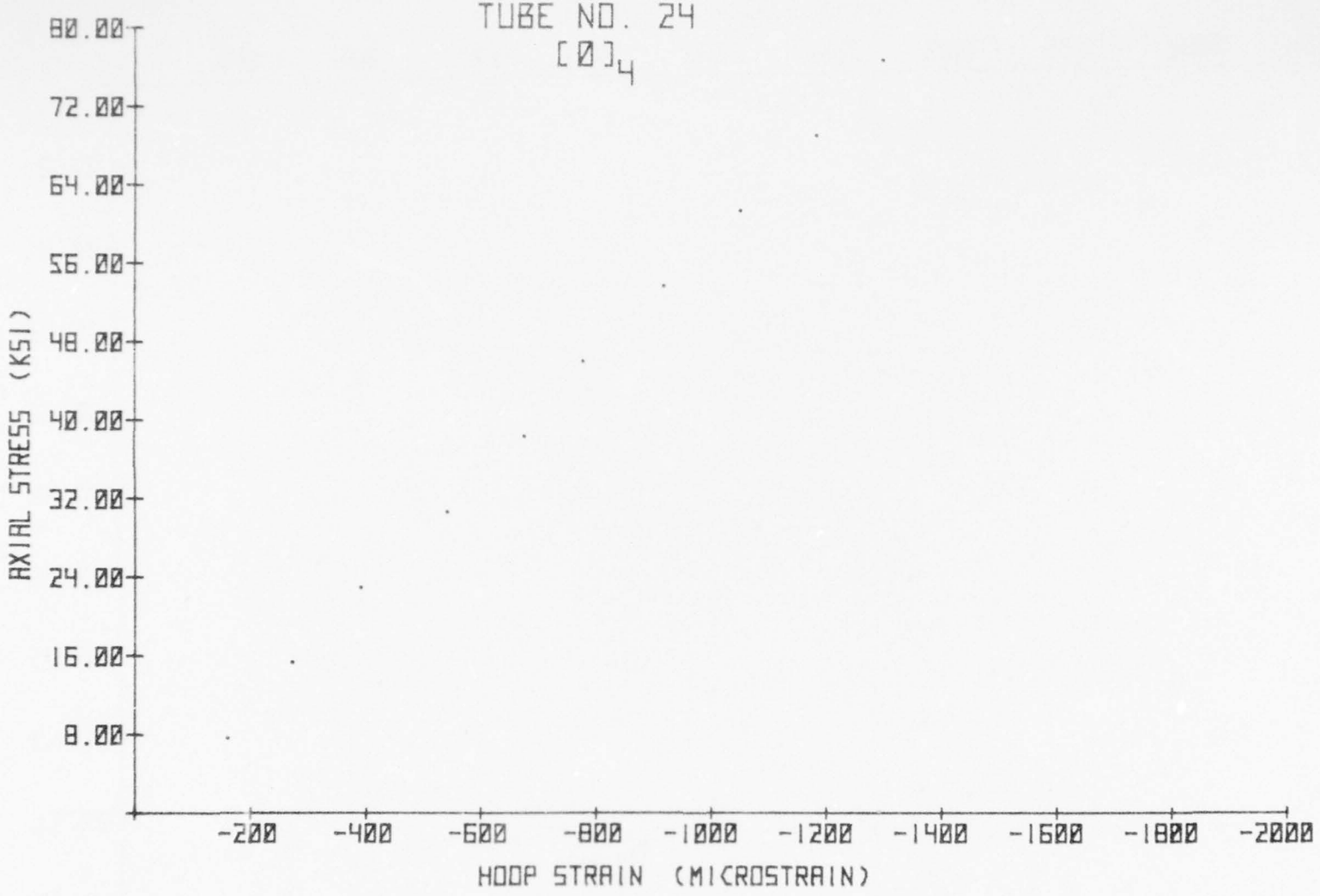
TUBE NO. 24
[0]4
80.00
72.00
64.00
56.00
48.00
40.00
32.00
24.00
16.00
8.00
AXIAL STRESS (KSI)
-200
-400
-600
-800
-1000
-1200
-1400
-1600
-1800
-2000
HOOP STRAIN (MICROSTRAIN)

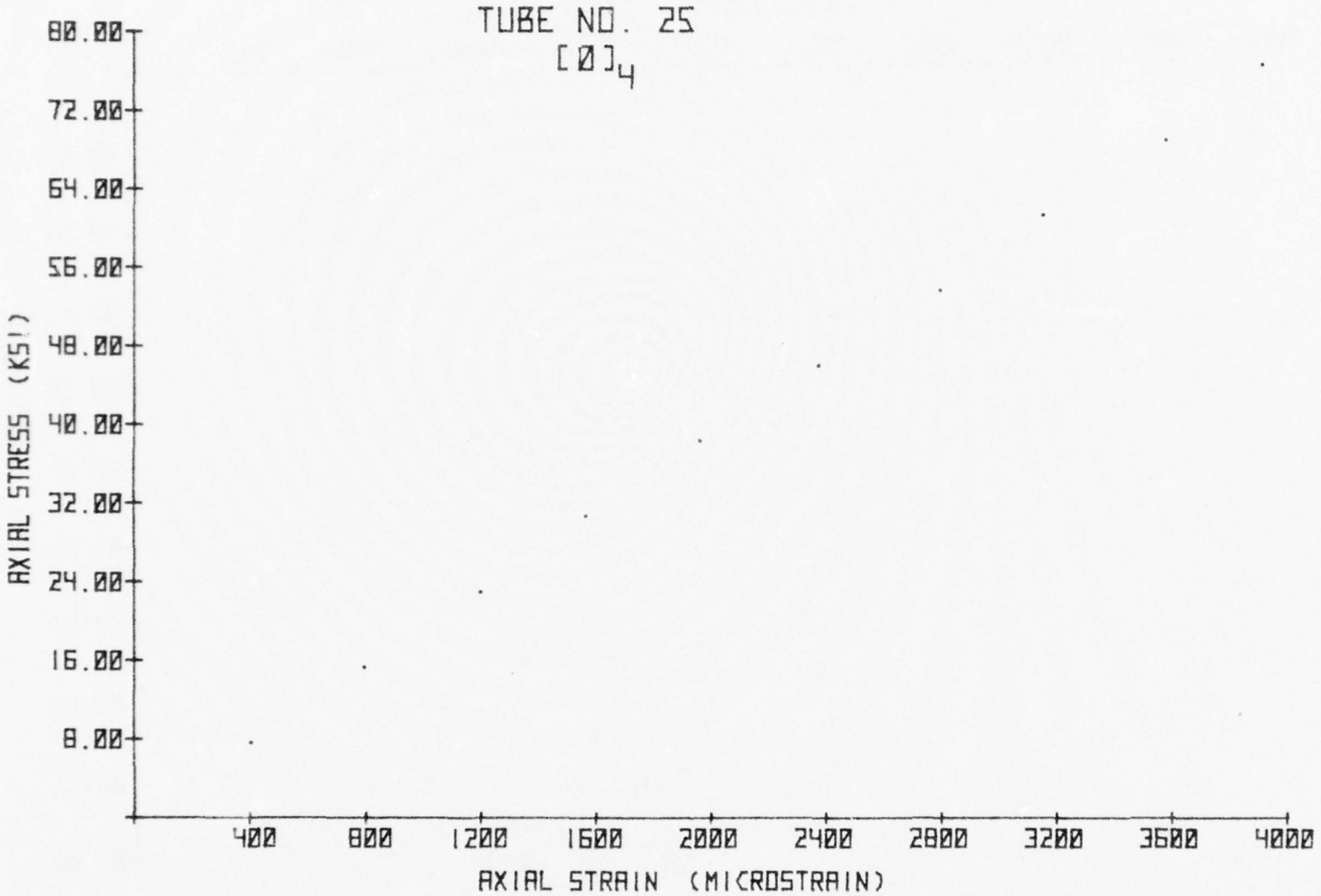
TUBE NO. 25
[0]4
80.00
72.00
64.00
56.00
48.00
40.00
32.00
24.00
16.00
8.00
AXIAL STRESS (KSI)
400
800
1200
1600
2000
2400
2800
3200
3600
4000
AXIAL STRAIN (MICROSTRAIN)

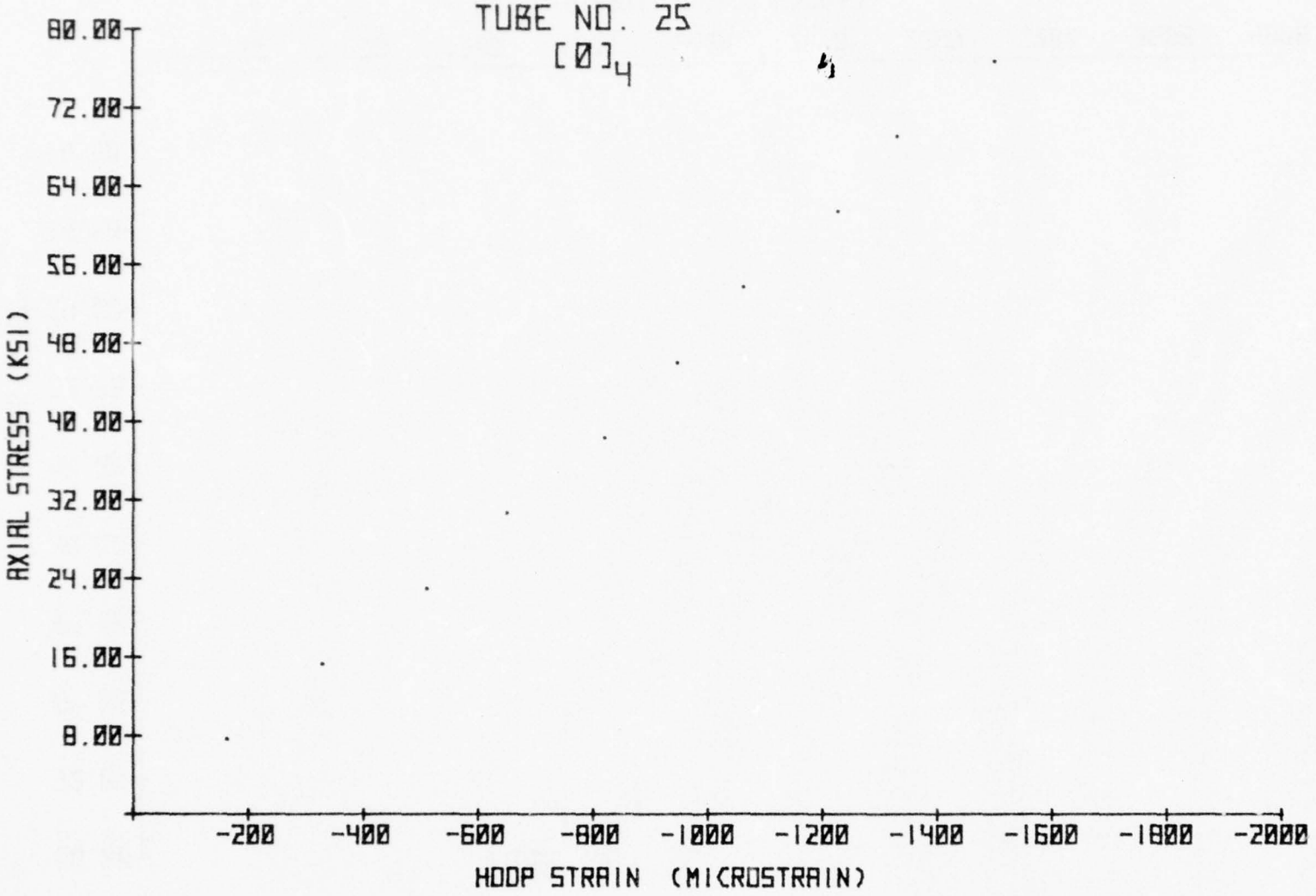
TUBE NO. 25
[0]4
80.00
72.00
64.00
56.00
48.00
40.00
32.00
24.00
16.00
8.00
AXIAL STRESS (KSI)
-200
-400
-600
-800
-1000
-1200
-1400
-1600
-1800
-2000
HOOP STRAIN (MICROSTRAIN)

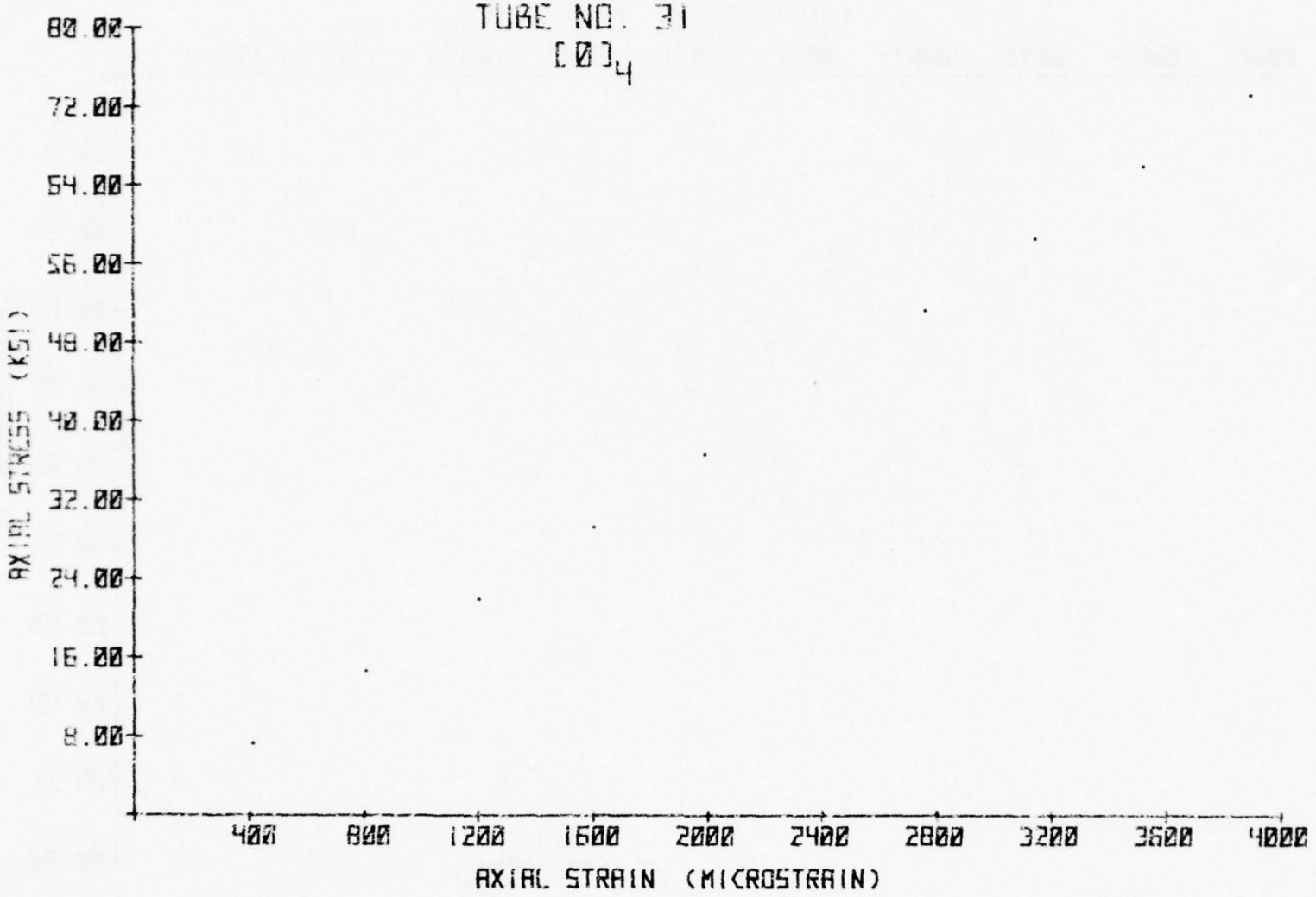
TUBE NO. 31
[0]4
80.00
72.00
64.00
56.00
48.00
40.00
32.00
24.00
16.00
8.00
AXIAL STRESS (KSI)
400
800
1200
1600
2000
2400
2800
3200
3600
4000
AXIAL STRAIN (MICROSTRAIN)

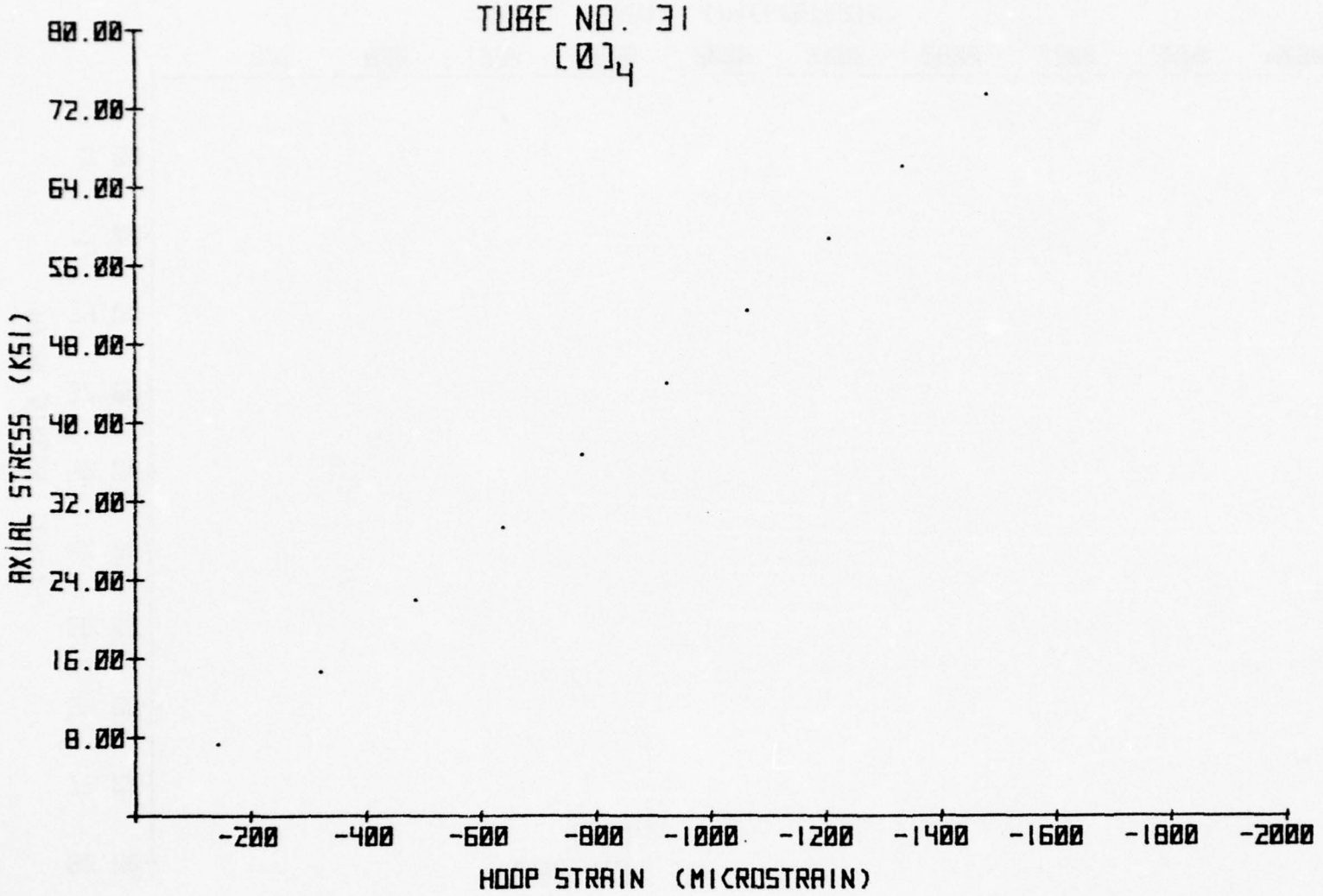
TUBE NO. 31
[0]4
80.00
72.00
64.00
56.00
48.00
40.00
32.00
24.00
16.00
8.00
AXIAL STRESS (KSI)
-200
-400
-600
-800
-1000
-1200
-1400
-1600
-1800
-2000
HOOP STRAIN (MICROSTRAIN)

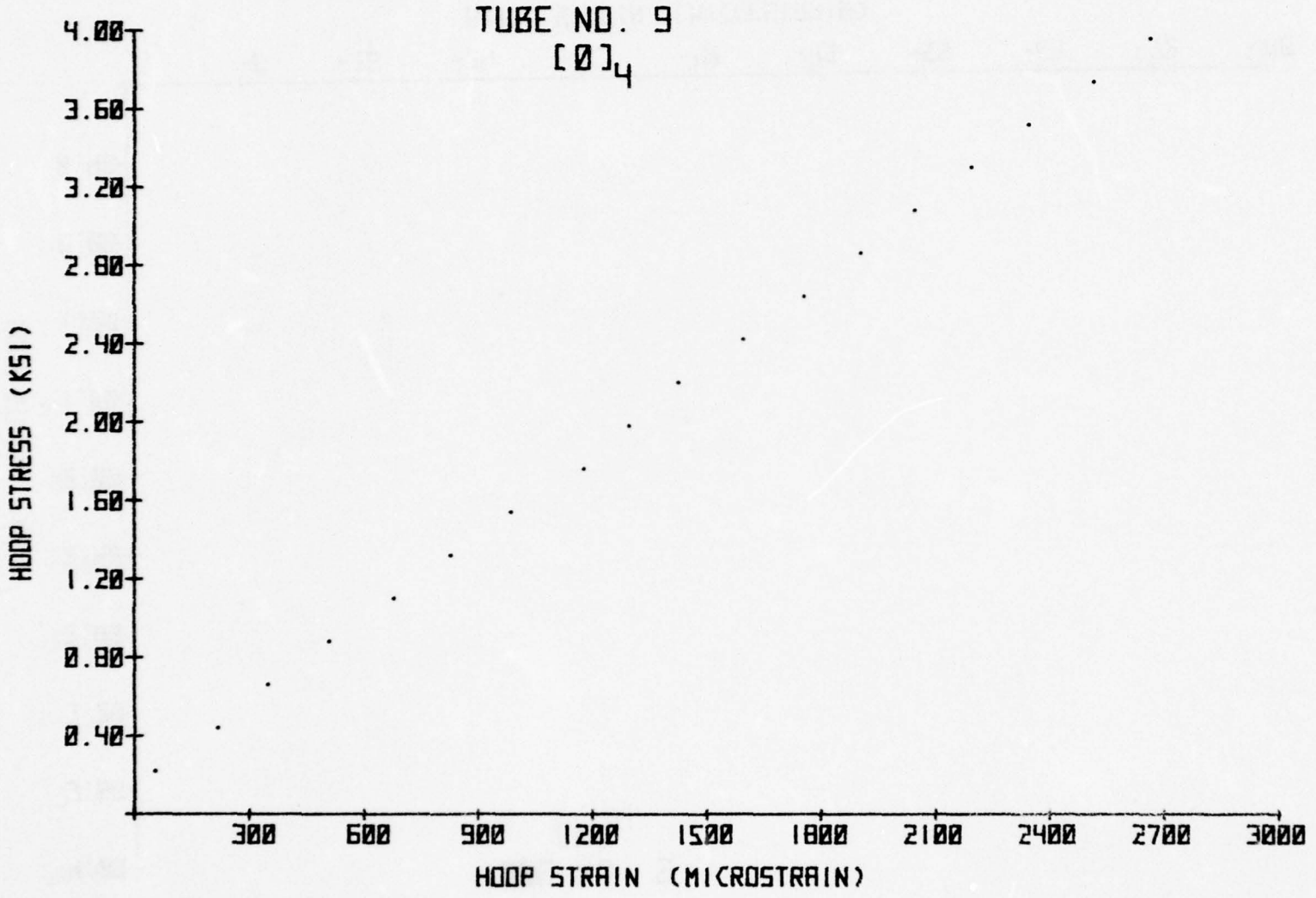
TUBE NO. 9
[0]4
HOOP STRESS (KSI)
4.00
3.60
3.20
2.80
2.40
2.00
1.60
1.20
0.80
0.40
300
600
900
1200
1500
1800
2100
2400
2700
3000
HOOP STRAIN (MICROSTRAIN)

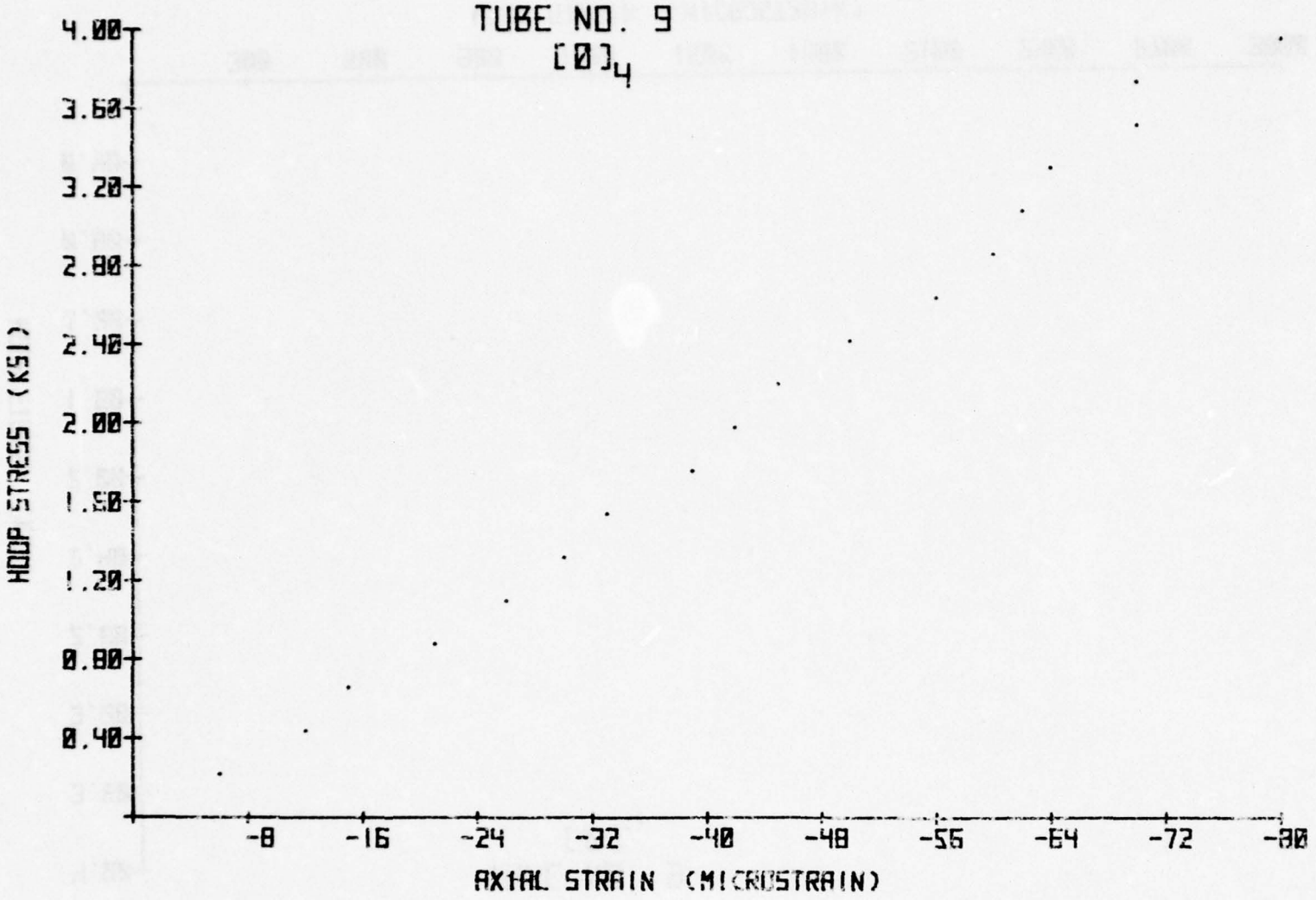
TUBE NO. 9
[0]4
4.00
3.60
3.20
2.80
2.40
2.00
1.60
1.20
0.80
0.40
HOOP STRESS (KSI)
-8
-16
-24
-32
-40
-48
-56
-64
-72
-80
AXIAL STRAIN (MICROSTRAIN)

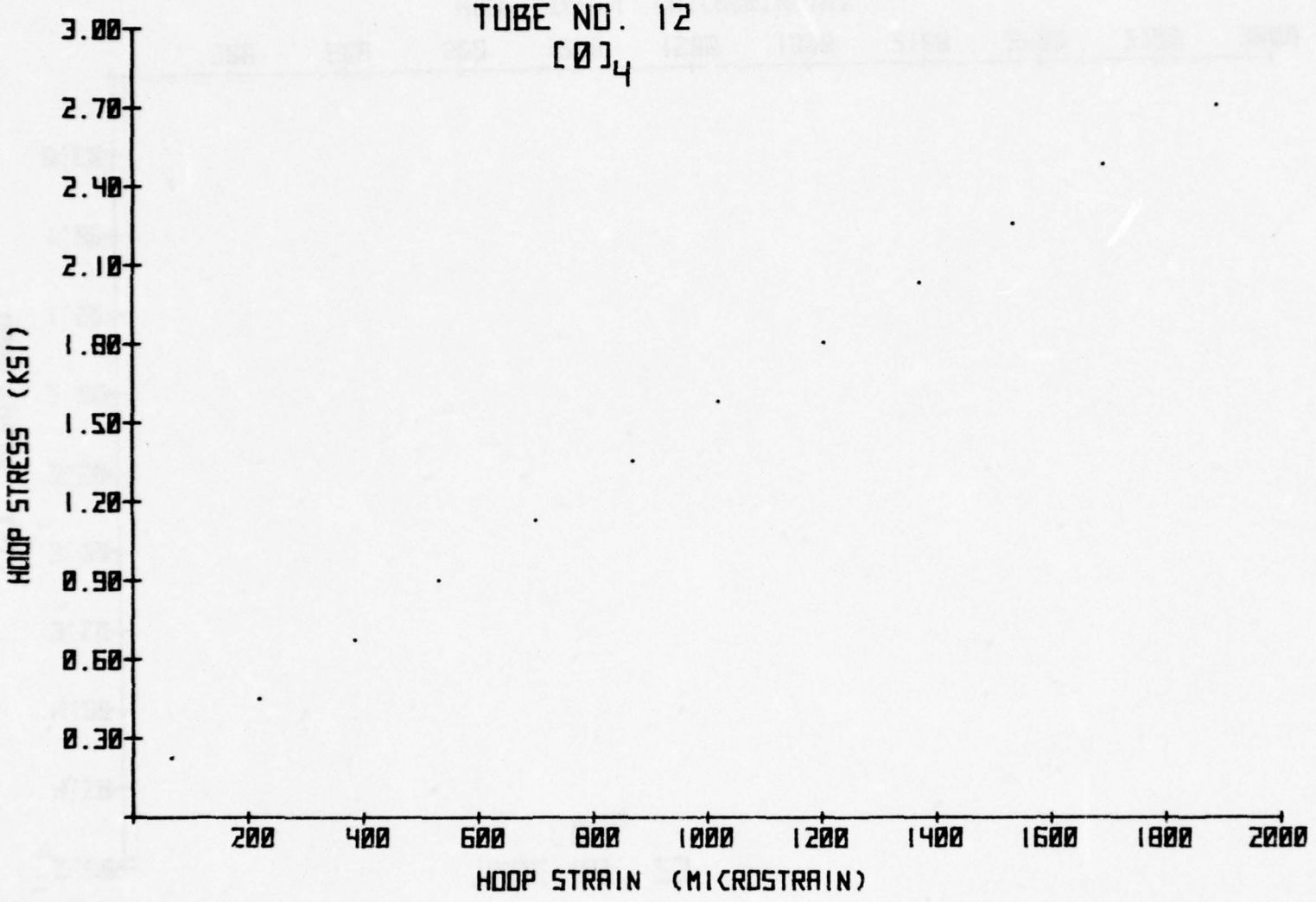
TUBE NO. 12
[0]4
3.00
2.70
2.40
2.10
1.80
1.50
1.20
0.90
0.60
0.30
HOOP STRESS (KSI)
200
400
600
800
1000
1200
1400
1600
1800
2000
HOOP STRAIN (MICROSTRAIN)

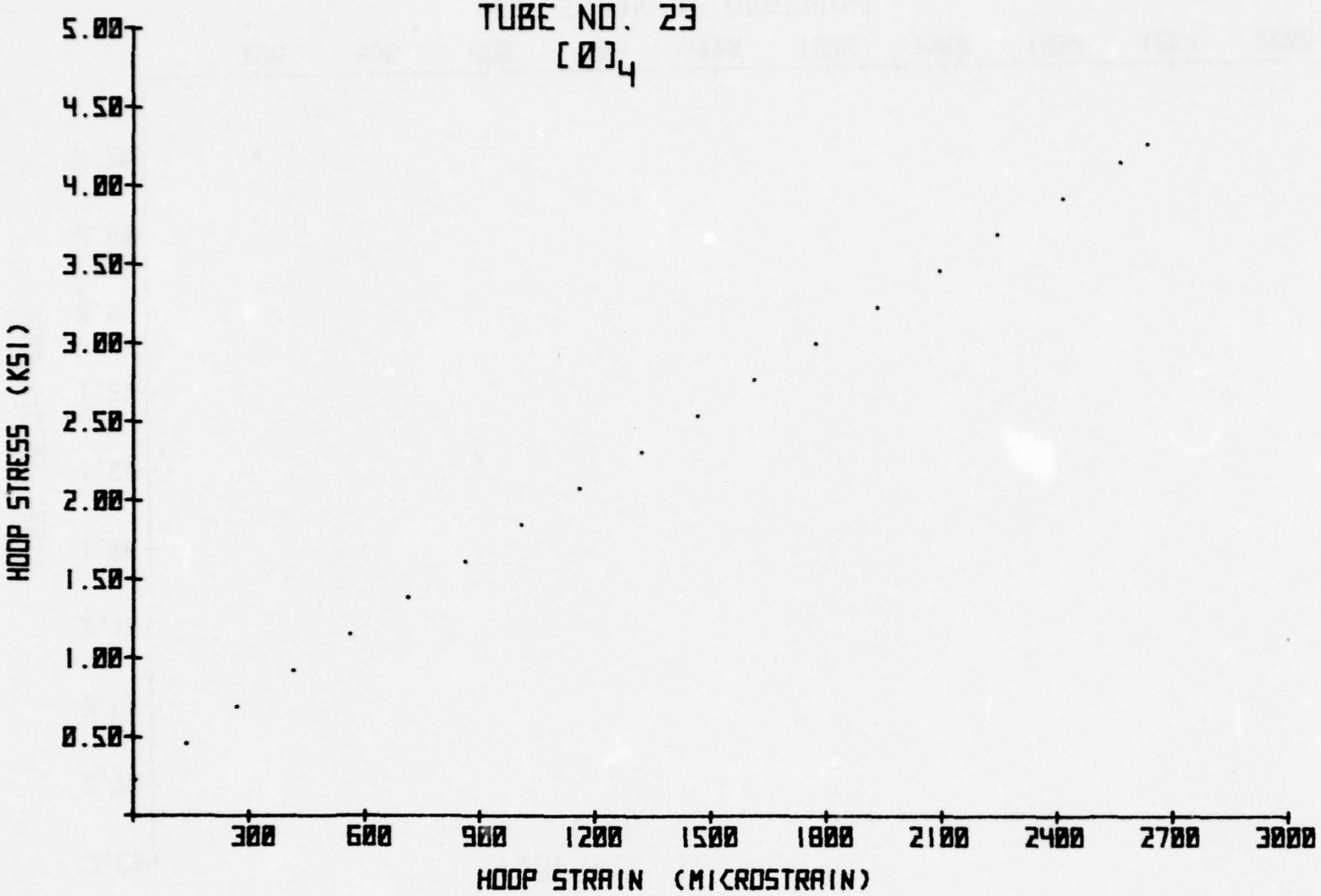
TUBE NO. 23
[0]4
HOOP STRESS (KSI)
5.00
4.50
4.00
3.50
3.00
2.50
2.00
1.50
1.00
0.50
300
600
900
1200
1500
1800
2100
2400
2700
3000
HOOP STRAIN (MICROSTRAIN)

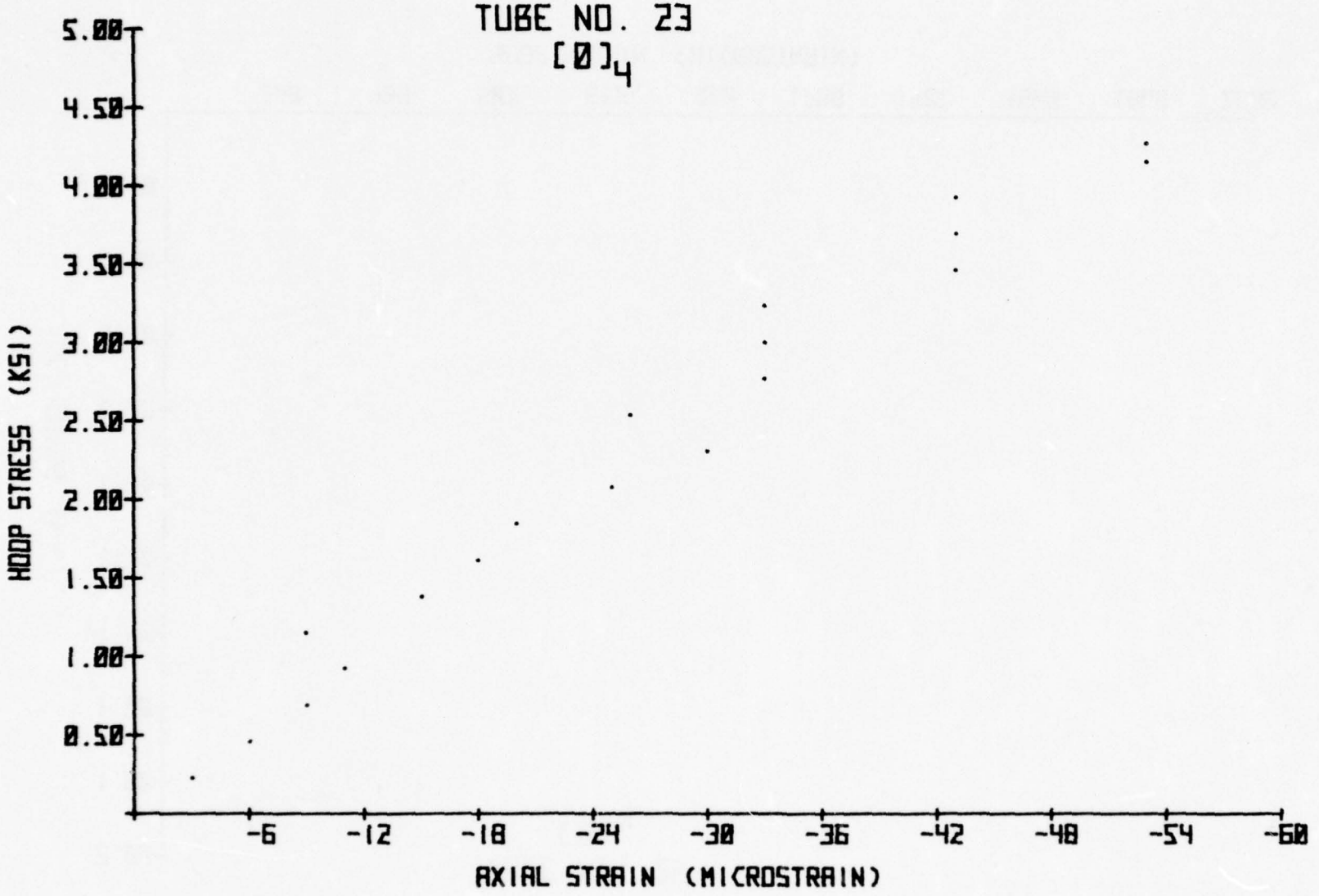
TUBE NO. 23
[0]4
5.00
4.50
4.00
3.50
3.00
2.50
2.00
1.50
1.00
0.50
HOOP STRESS (KSI)
-6
-12
-18
-24
-30
-36
-42
-48
-54
-60
AXIAL STRAIN (MICROSTRAIN)

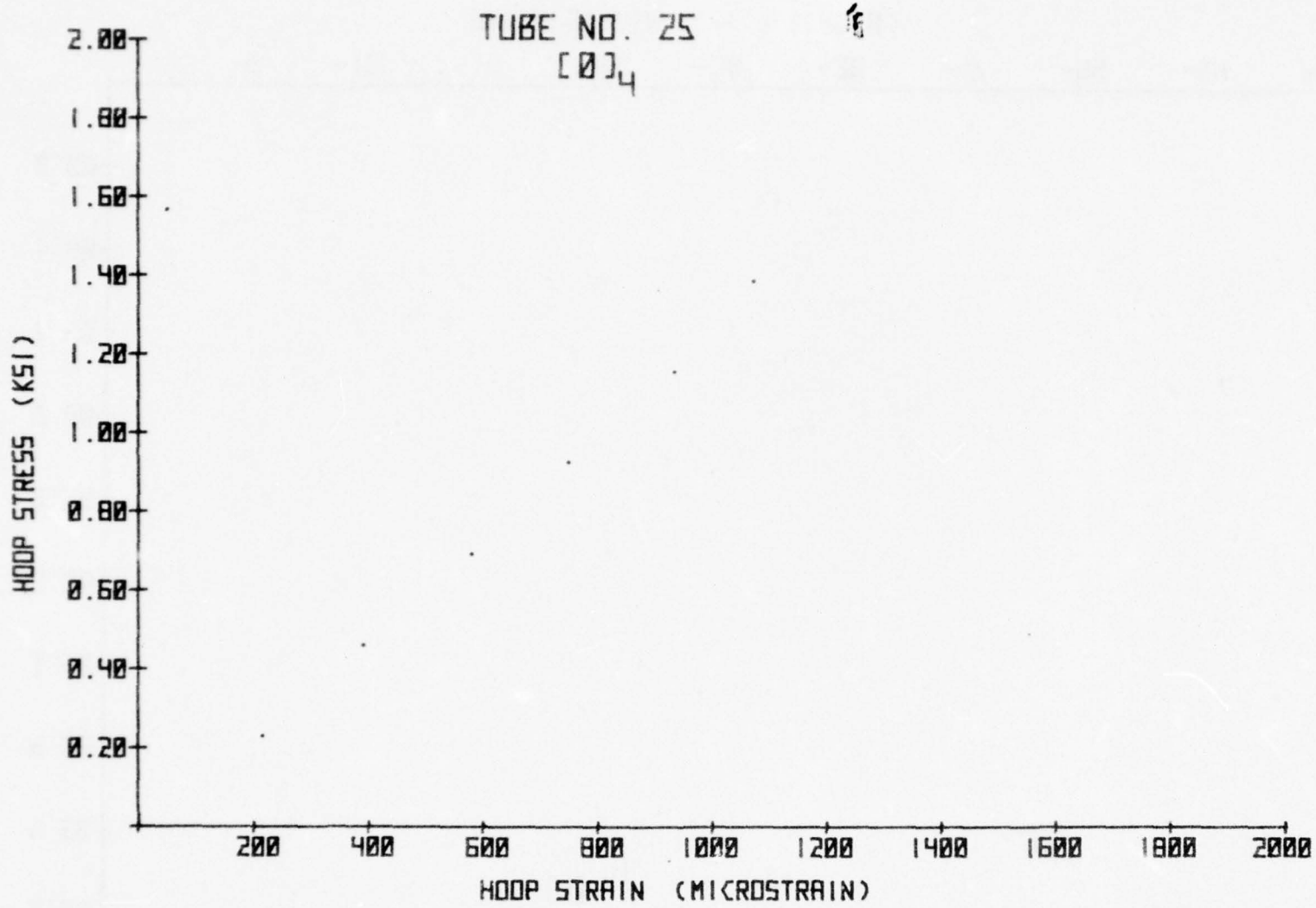
TUBE NO. 25
[0]4
HOOP STRESS (KSI)
2.00
1.80
1.60
1.40
1.20
1.00
0.80
0.60
0.40
0.20
200
400
600
800
1000
1200
1400
1600
1800
2000
HOOP STRAIN (MICROSTRAIN)

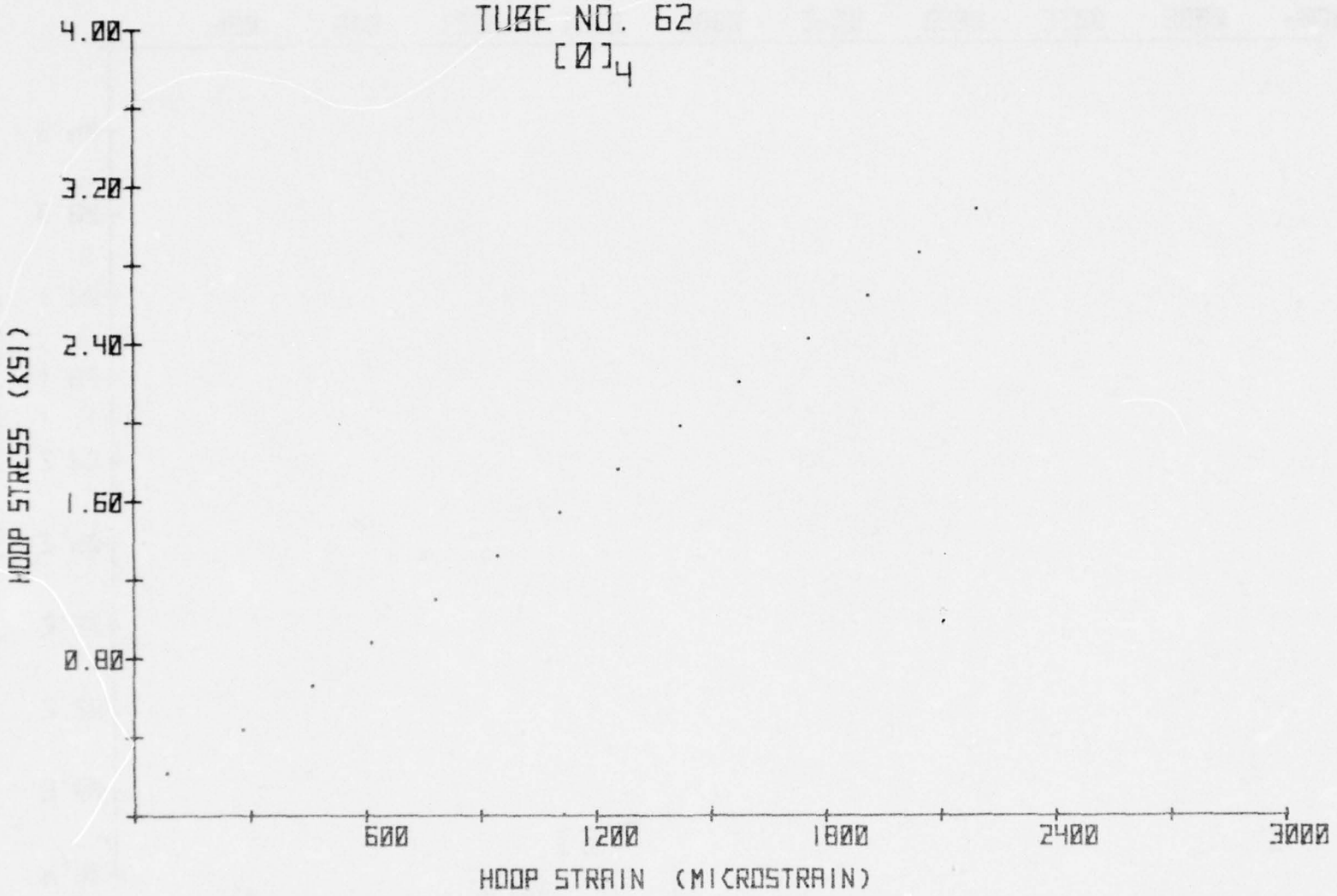
TUBE NO. 62
[0]4
4.00
3.20
2.40
1.60
0.80
HOOP STRESS (KSI)
600
1200
1800
2400
3000
HOOP STRAIN (MICROSTRAIN)

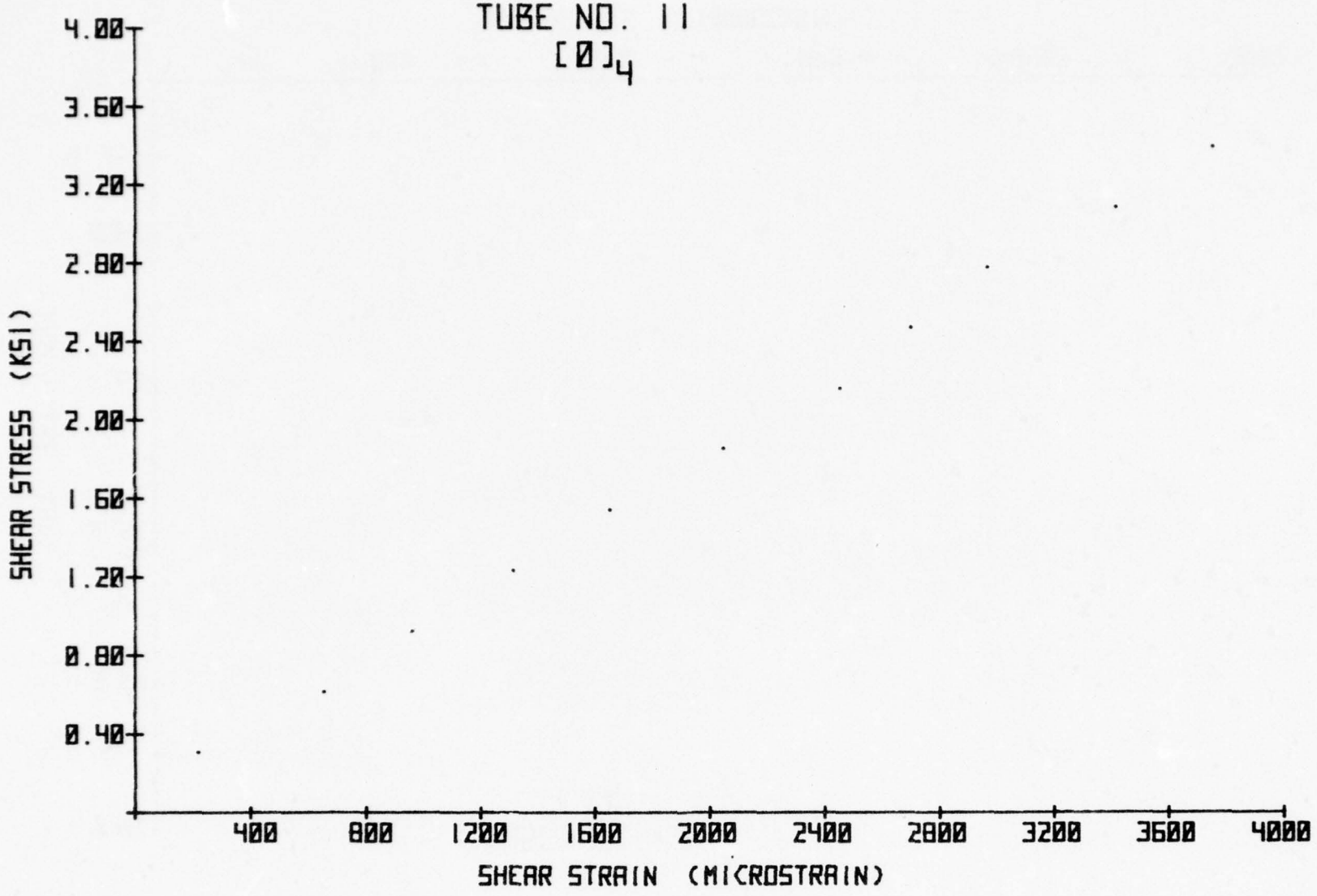
TUBE NO. 11
[0]4
4.00
3.60
3.20
2.80
2.40
2.00
1.60
1.20
0.80
0.40
SHEAR STRESS (KSI)
400
800
1200
1600
2000
2400
2800
3200
3600
4000
SHEAR STRAIN (MICROSTRAIN)

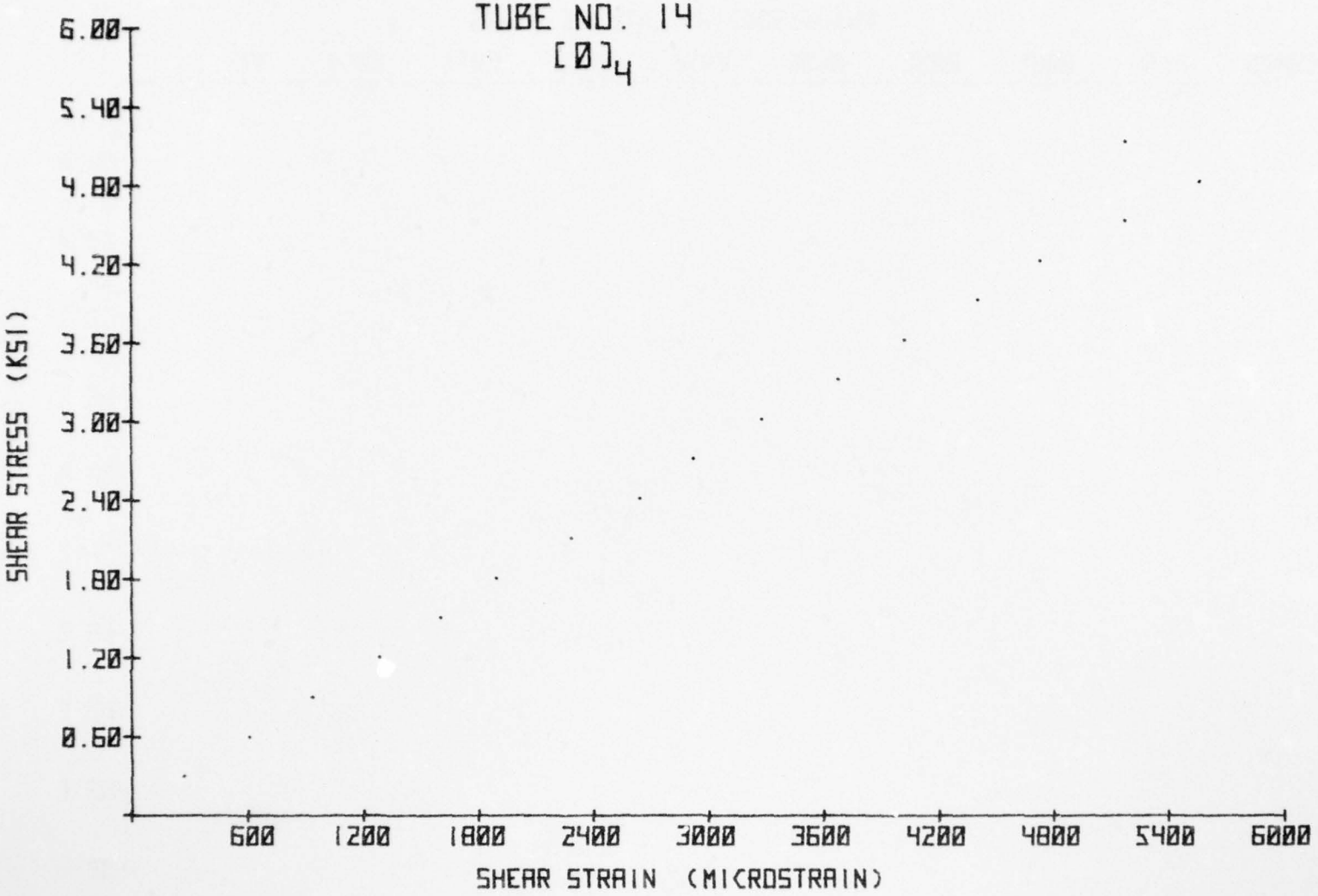
TUBE NO. 14
[0]4
6.00
5.40
4.80
4.20
3.60
3.00
2.40
1.80
1.20
0.60
SHEAR STRESS (KSI)
600
1200
1800
2400
3000
3600
4200
4800
5400
6000
SHEAR STRAIN (MICROSTRAIN)

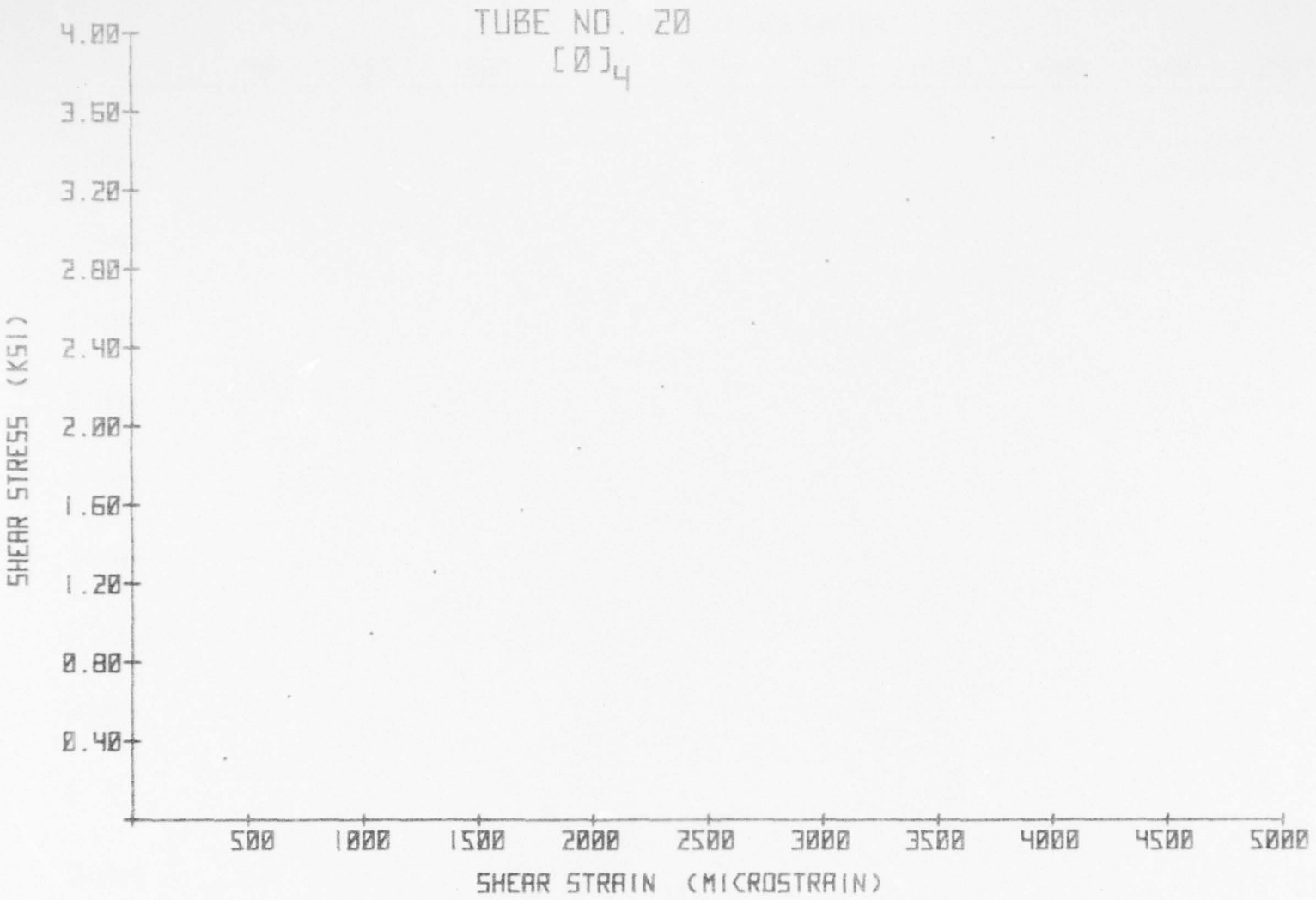
TUBE NO. 20
[0]4
4.00
3.60
3.20
2.80
2.40
2.00
1.60
1.20
0.80
0.40
SHEAR STRESS (KSI)
500
1000
1500
2000
2500
3000
3500
4000
4500
5000
SHEAR STRAIN (MICROSTRAIN)

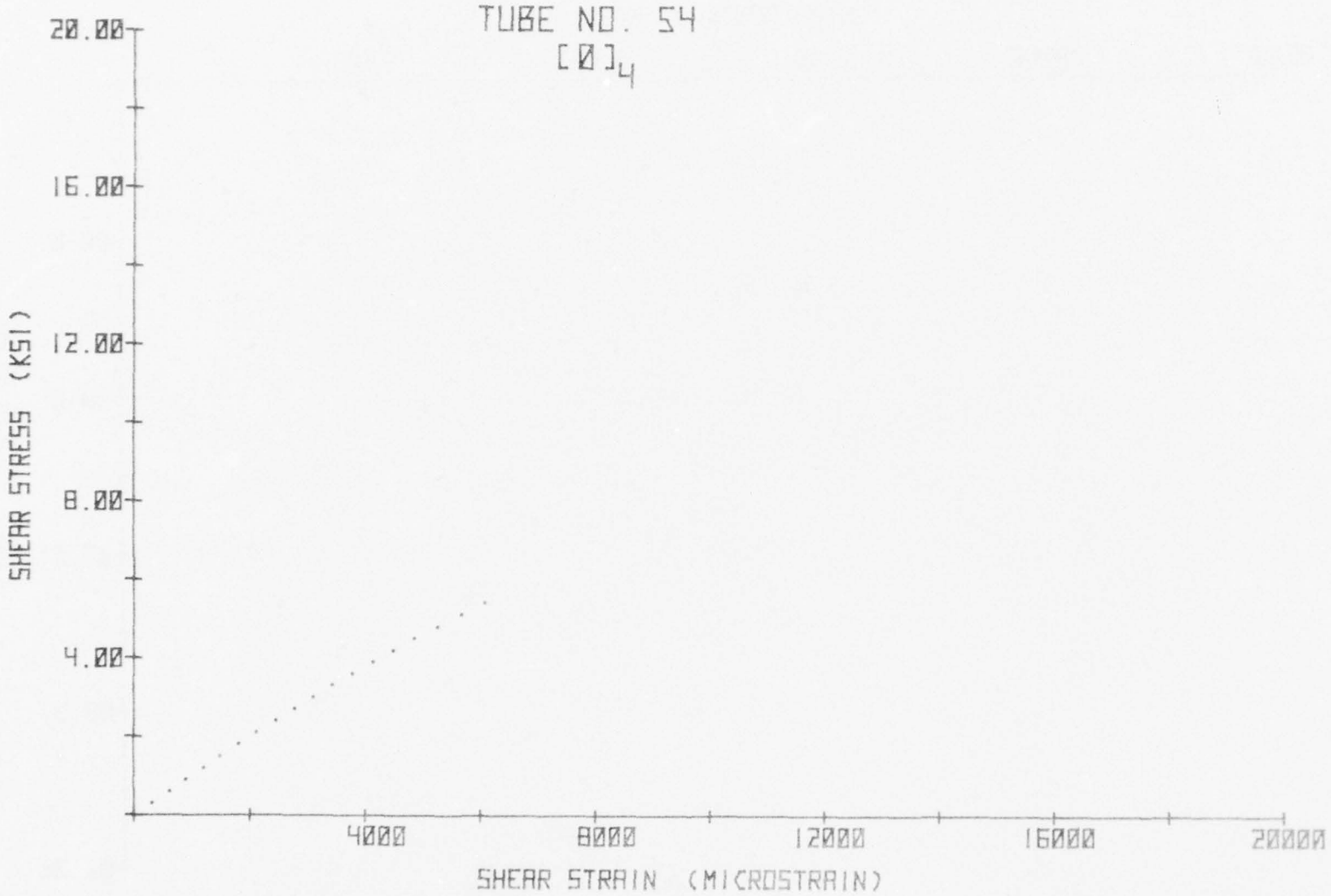
TUBE NO. 54
[0]4
20.00
16.00
12.00
8.00
4.00
SHEAR STRESS (KSI)
4000
8000
12000
16000
20000
SHEAR STRAIN (MICROSTRAIN)

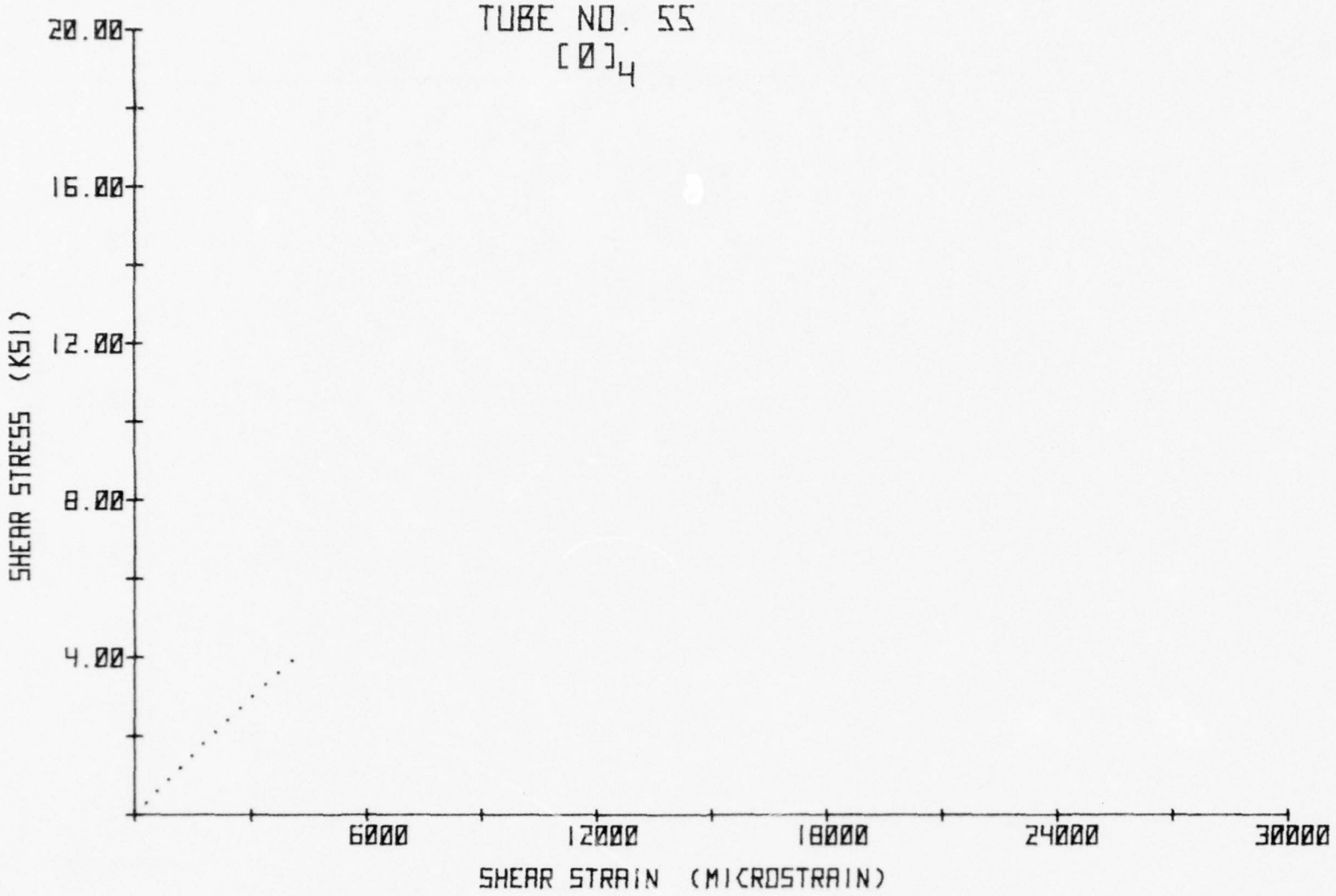
TUBE NO. 55
[0]4
20.00
16.00
12.00
8.00
4.00
SHEAR STRESS (KSI)
6000
12000
18000
24000
30000
SHEAR STRAIN (MICROSTRAIN)

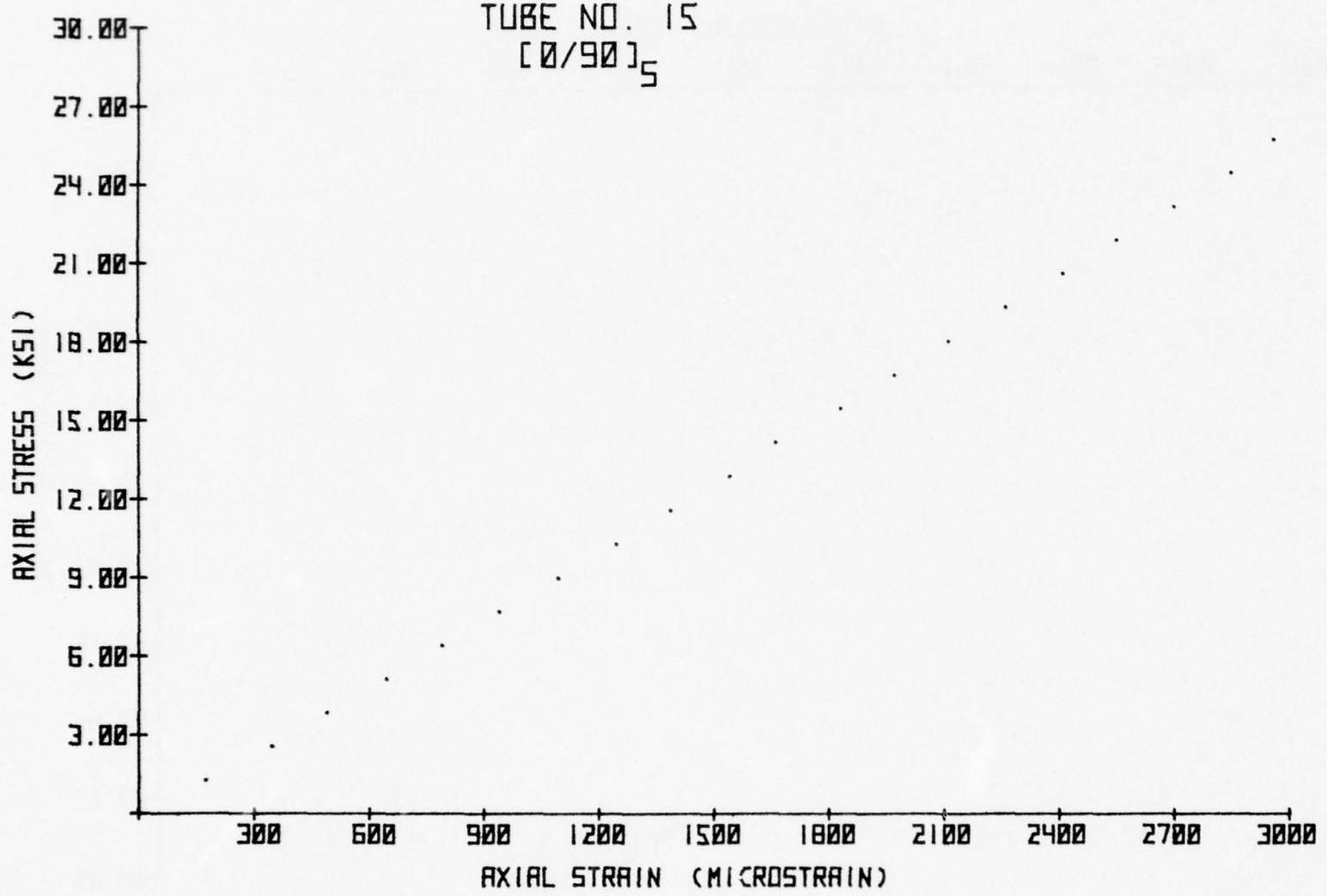
TUBE NO. 15
[0/90]5
30.00
27.00
24.00
21.00
18.00
15.00
12.00
9.00
6.00
3.00
AXIAL STRESS (KSI)
300
600
900
1200
1500
1800
2100
2400
2700
3000
AXIAL STRAIN (MICROSTRAIN)

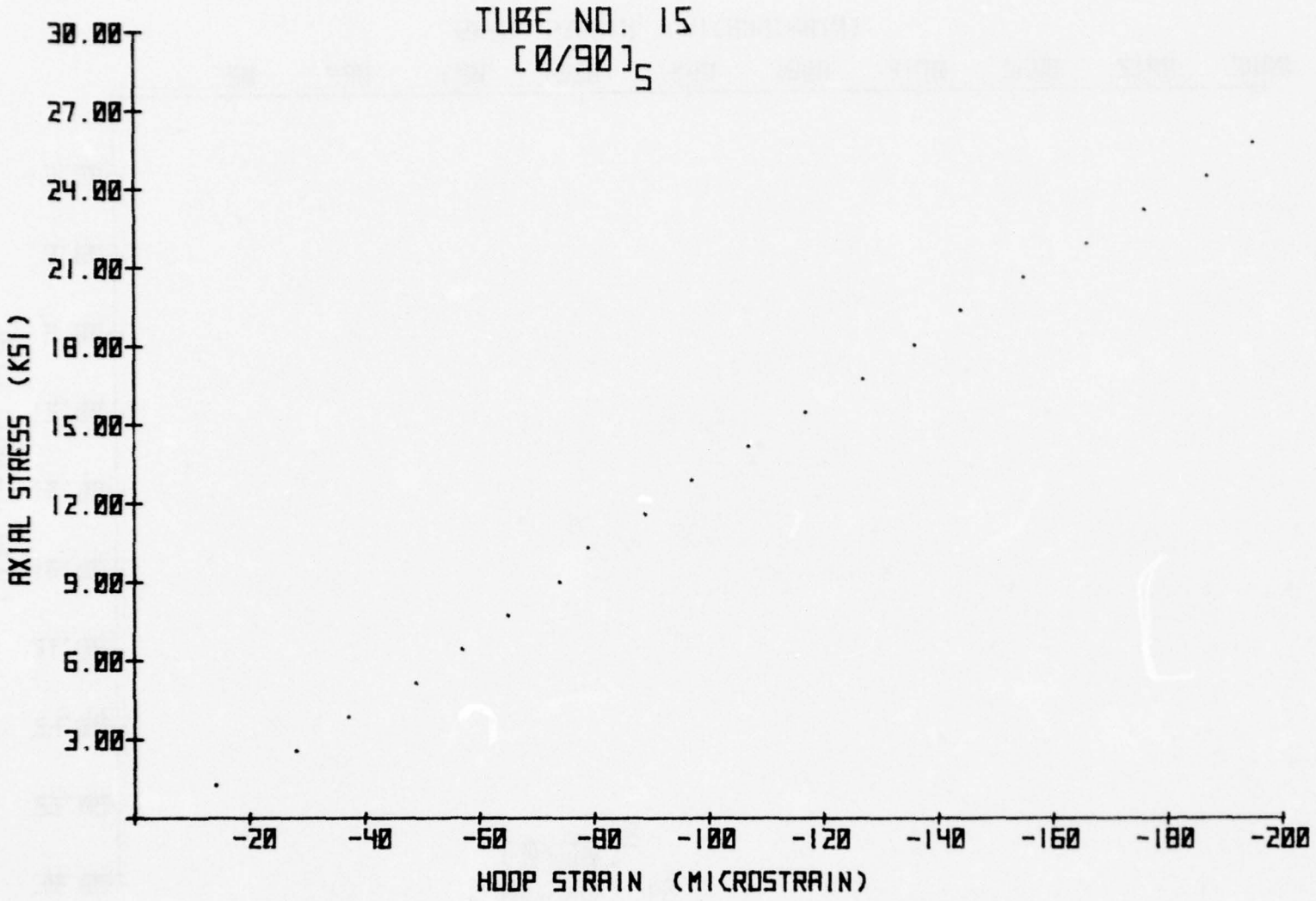
TUBE NO. 15
[0/90]5
30.00
27.00
24.00
21.00
18.00
15.00
12.00
9.00
6.00
3.00
AXIAL STRESS (KSI)
-20
-40
-60
-80
-100
-120
-140
-160
-180
-200
HOOP STRAIN (MICROSTRAIN)

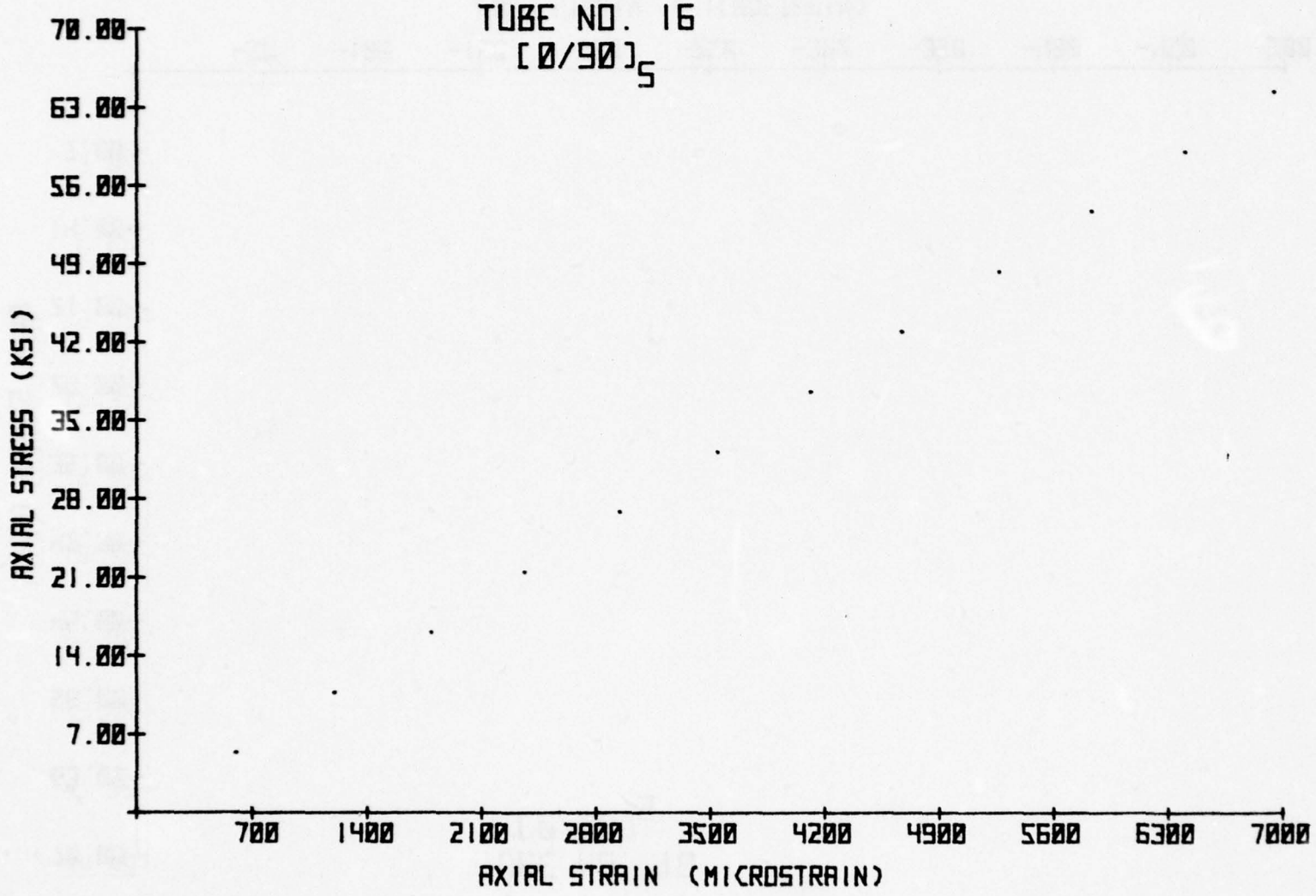
TUBE NO. 16
[0/90]S
70.00
63.00
56.00
49.00
42.00
35.00
28.00
21.00
14.00
7.00
AXIAL STRESS (KSI)
700
1400
2100
2800
3500
4200
4900
5600
6300
7000
AXIAL STRAIN (MICROSTRAIN)

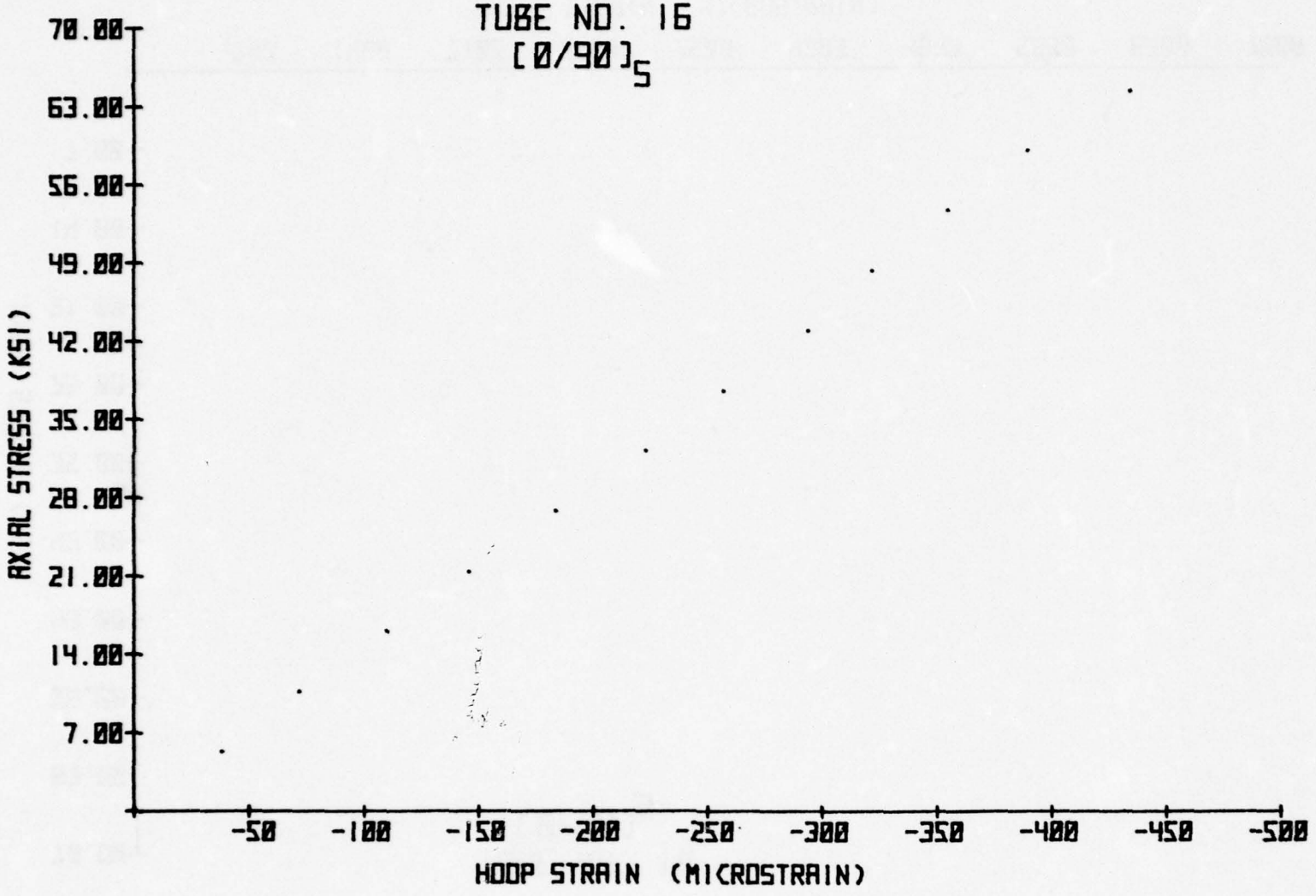
TUBE NO. 16
[0/90]5
70.00
63.00
56.00
49.00
42.00
35.00
28.00
21.00
14.00
7.00
AXIAL STRESS (KSI)
-50
-100
-150
-200
-250
-300
-350
-400
-450
-500
HOOP STRAIN (MICROSTRAIN)

LONGITUDINAL TENSILE DATA FOR COUPON SPECIMENS

COUPON NO.	LAY-UP	WIDTH (in)	THICKNESS (in)	FIBER VOLUME (%)	VOID VOLUME (%)	MODULUS (10^3 ksi)	POISSON'S RATIO	ULTIMATE STRENGTH (ksi)
	$[0]_6$			69.7	2.0			
1A		.754	.032			22.6	.33	174
1B		.755	.032			23.3	.37	231
1C		.755	.032			23.2	.31	238
	$[90]_8$			66.0	2.2			
2A		.757	.046			1.7		5.80
2B		.754	.045			1.6	.04	7.25
2C		.752	.043			1.7	.01	7.82
2D		.752	.047			1.5		
	$[0/90_2/0]_s$			70.1	2.0			
3A		.757	.047			11.4	.04	109
3B		.757	.045			11.0	.04	108
3C		.753	.045			11.3	.03	108
	$[\pm \mp 45]_s$			65.2	2.2			
4A		.753	.047			2.82	.67	21.7
4B		.757	.048			2.98	.74	21.8
4C		.753	.048			2.88	.71	21.2

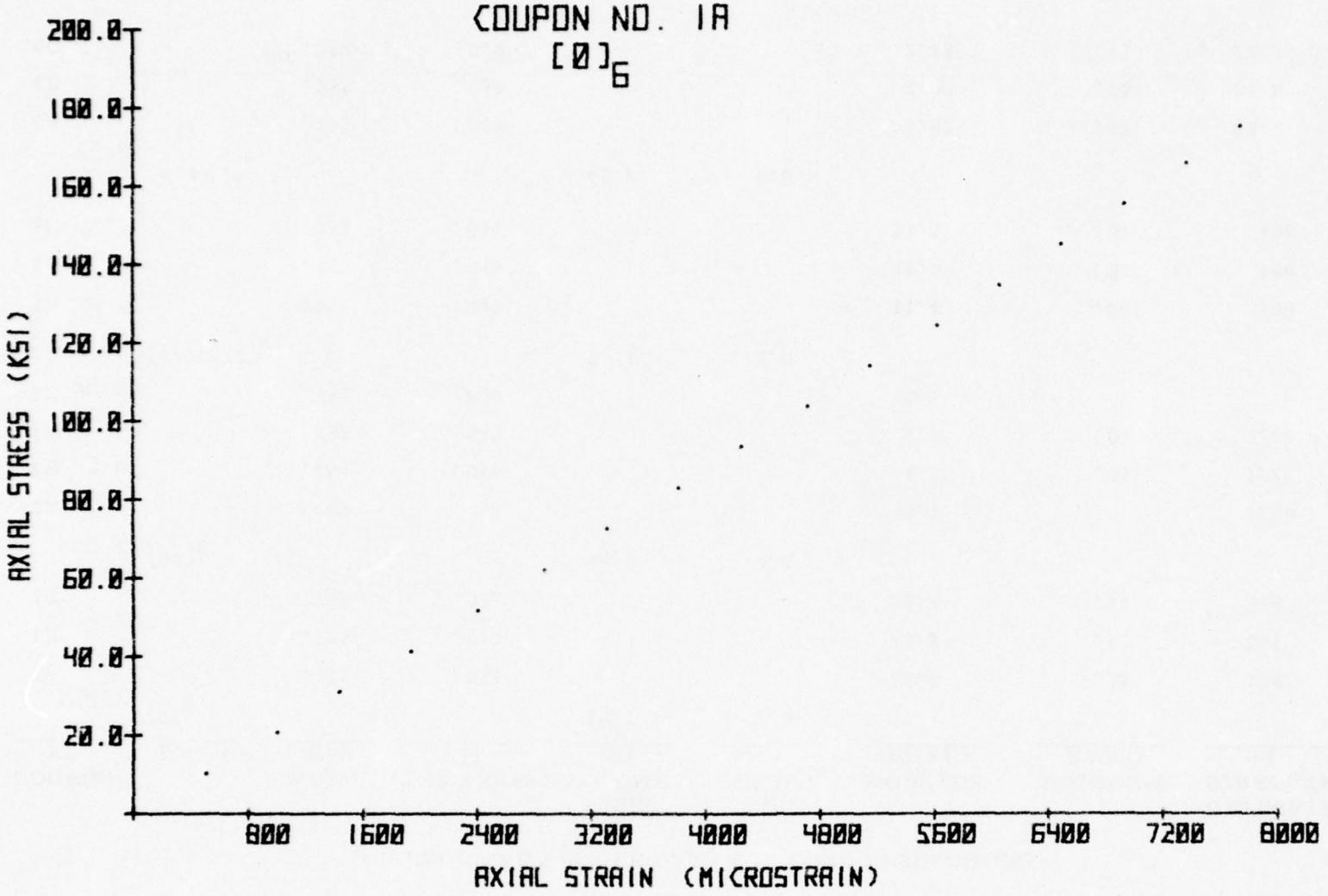
COUPON NO. 1A
[0]6
AXIAL STRESS (KSI)
200.0
180.0
160.0
140.0
120.0
100.0
80.0
60.0
40.0
20.0
800
1600
2400
3200
4000
4800
5600
6400
7200
8000
AXIAL STRAIN (MICROSTRAIN)

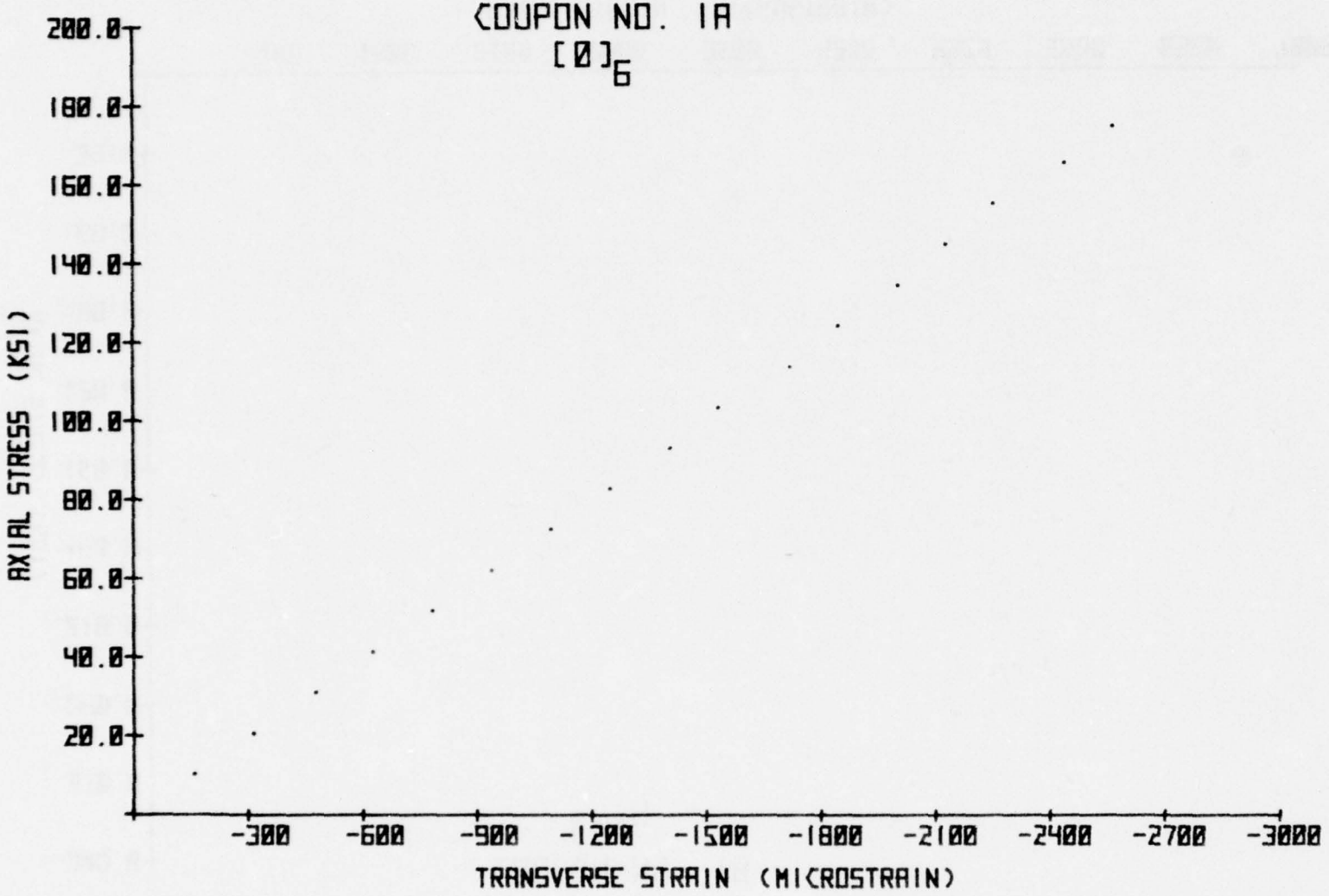
COUPON NO. 1A
[0]6
200.0
180.0
160.0
140.0
120.0
100.0
80.0
60.0
40.0
20.0
AXIAL STRESS (KSI)
-300
-600
-900
-1200
-1500
-1800
-2100
-2400
-2700
-3000
TRANSVERSE STRAIN (MICROSTRAIN)

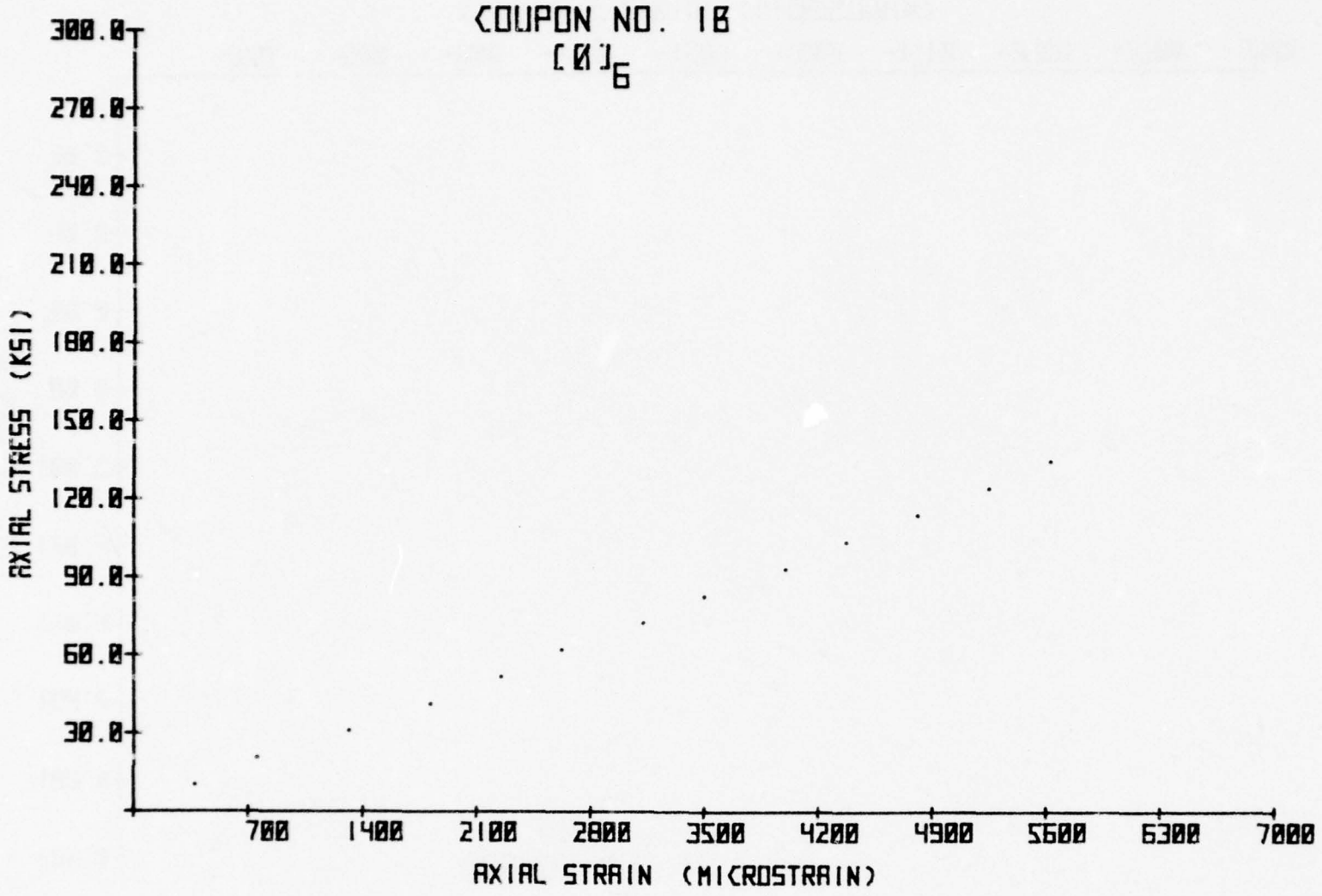
COUPON NO. 18
[0]6
300.0
270.0
240.0
210.0
180.0
150.0
120.0
90.0
60.0
30.0
AXIAL STRESS (KSI)
700
1400
2100
2800
3500
4200
4900
5600
6300
7000
AXIAL STRAIN (MICROSTRAIN)

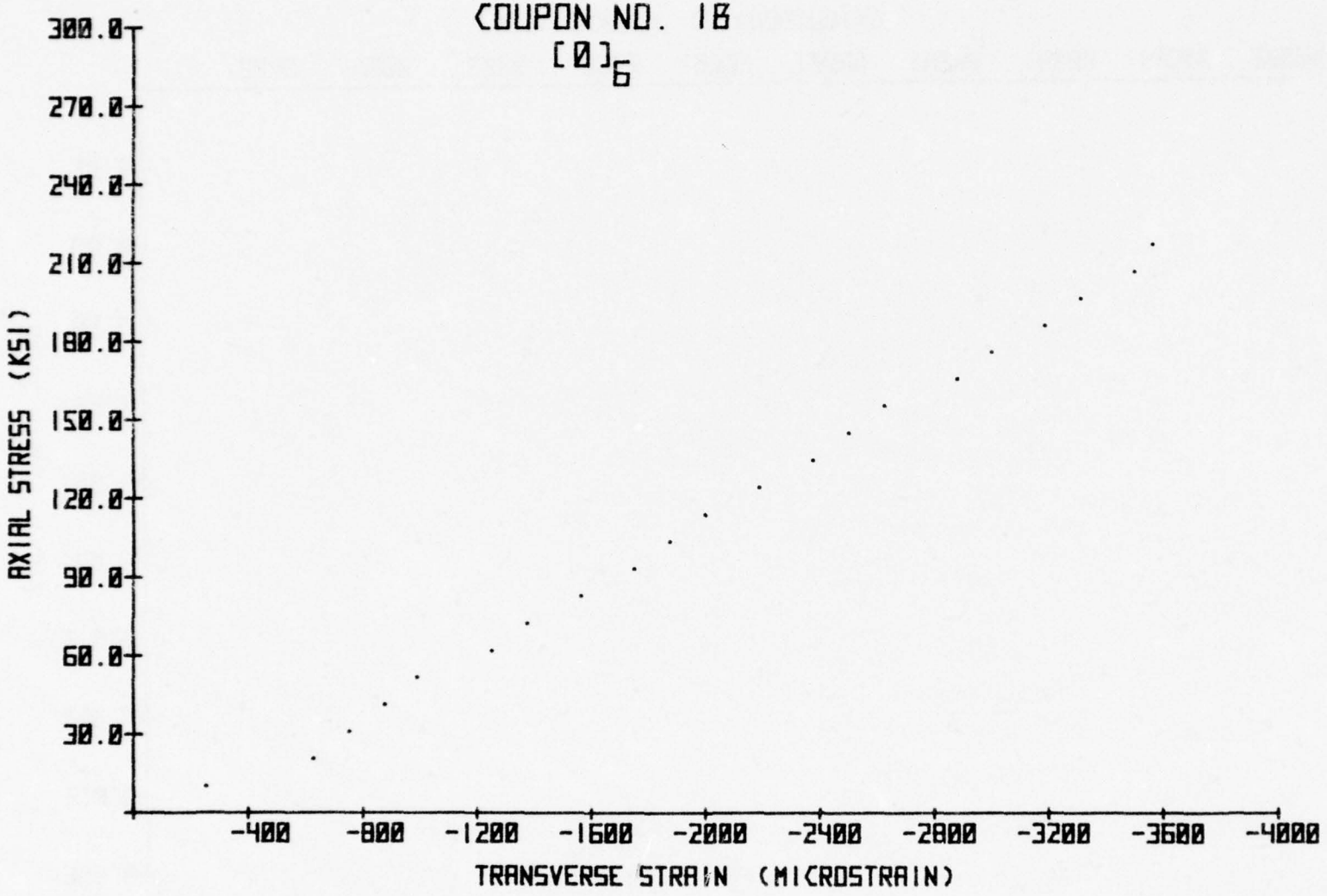
COUPON NO. 18
[0]6
300.0
270.0
240.0
210.0
180.0
150.0
120.0
90.0
60.0
30.0
AXIAL STRESS (KSI)
-400
-800
-1200
-1600
-2000
-2400
-2800
-3200
-3600
-4000
TRANSVERSE STRAIN (MICROSTRAIN)

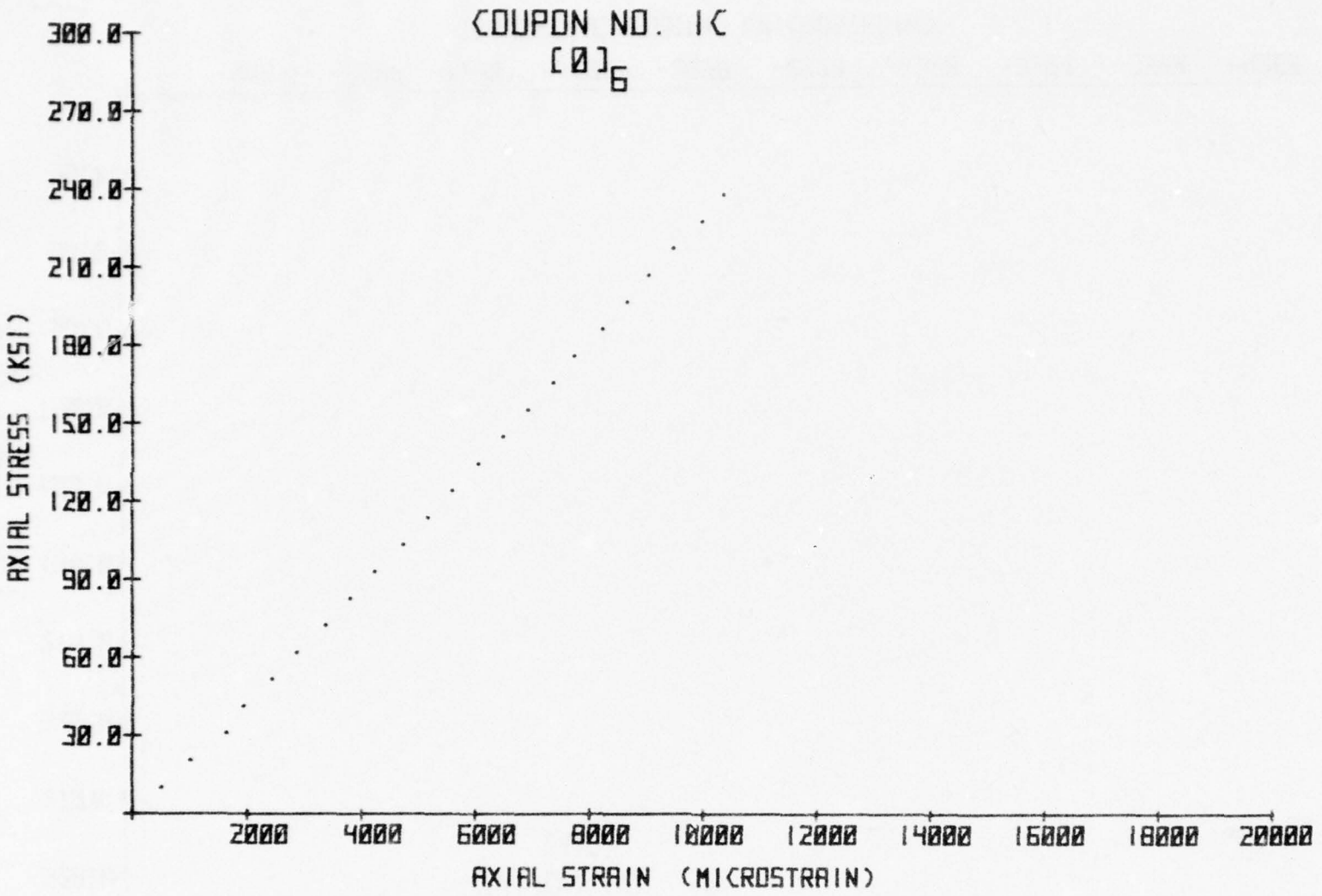
COUPON NO. 1C
[0]6
300.0
270.0
240.0
210.0
180.0
150.0
120.0
90.0
60.0
30.0
AXIAL STRESS (KSI)
2000
4000
6000
8000
10000
12000
14000
16000
18000
20000
AXIAL STRAIN (MICROSTRAIN)

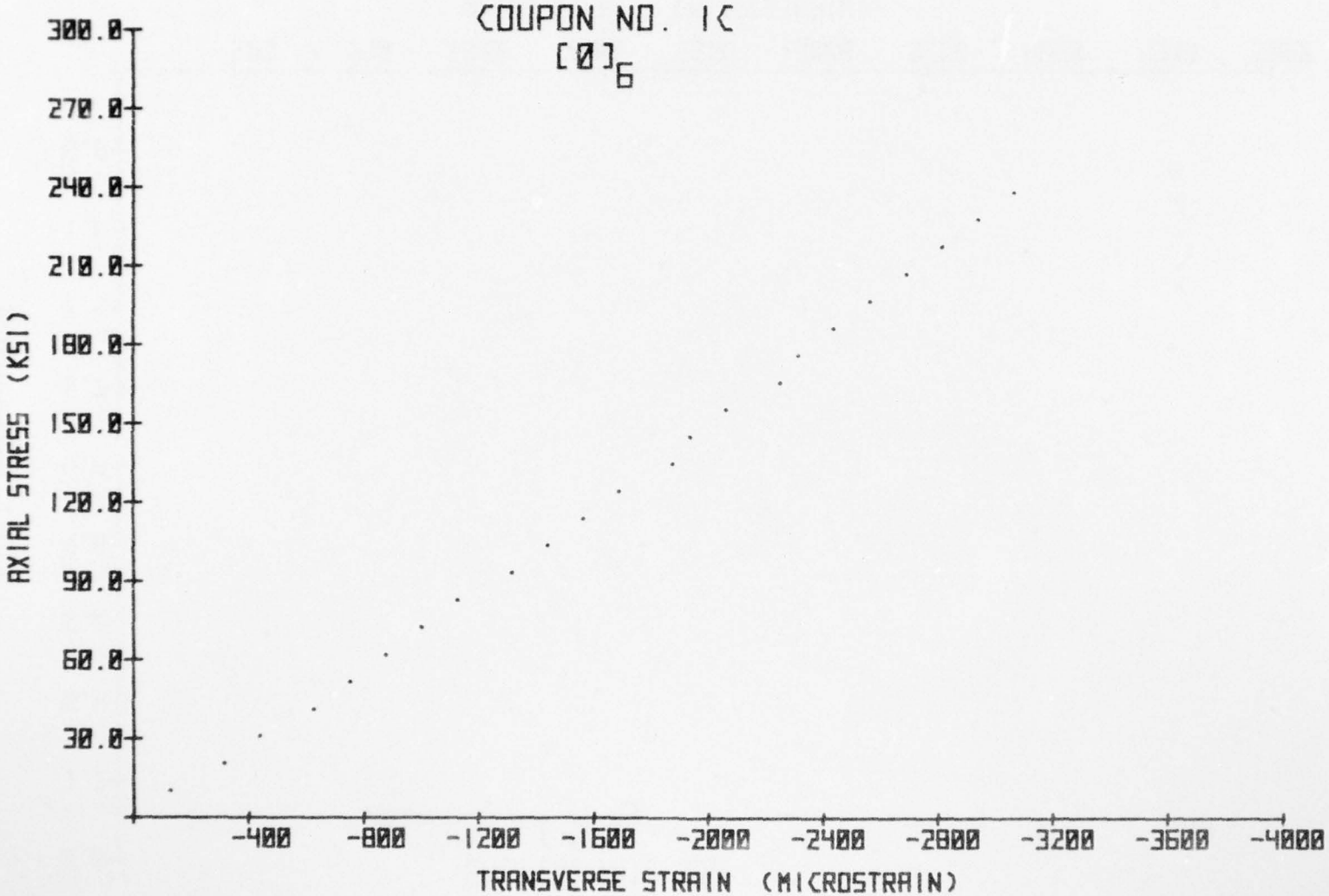
COUPON NO. 1C
[0]6
300.0
270.0
240.0
210.0
180.0
150.0
120.0
90.0
60.0
30.0
AXIAL STRESS (KSI)
-400
-800
-1200
-1600
-2000
-2400
-2800
-3200
-3600
-4000
TRANSVERSE STRAIN (MICROSTRAIN)

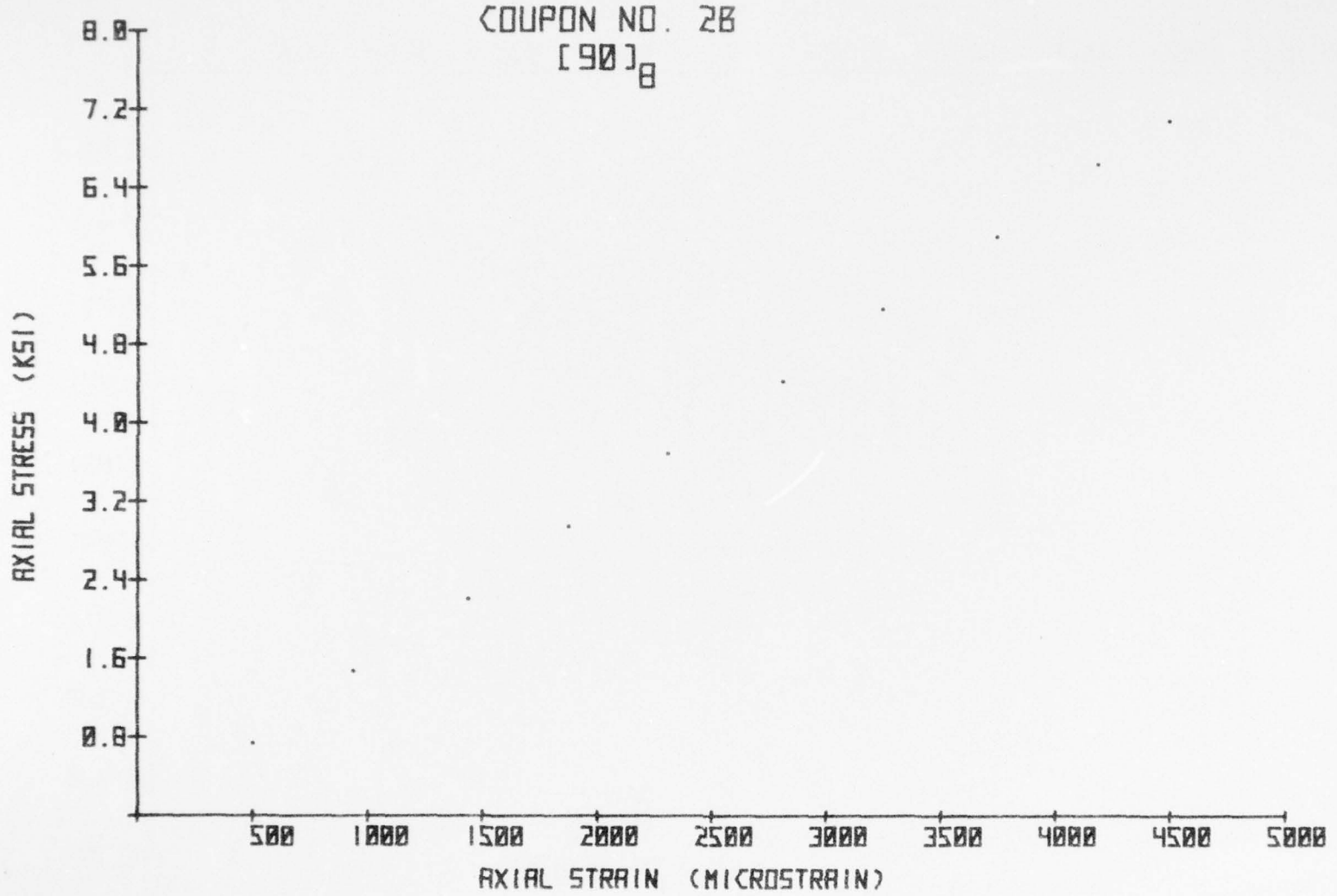
COUPON NO. 28
[90]8
8.0
7.2
6.4
5.6
4.8
4.0
3.2
2.4
1.6
0.8
AXIAL STRESS (KSI)
500
1000
1500
2000
2500
3000
3500
4000
4500
5000
AXIAL STRAIN (MICROSTRAIN)

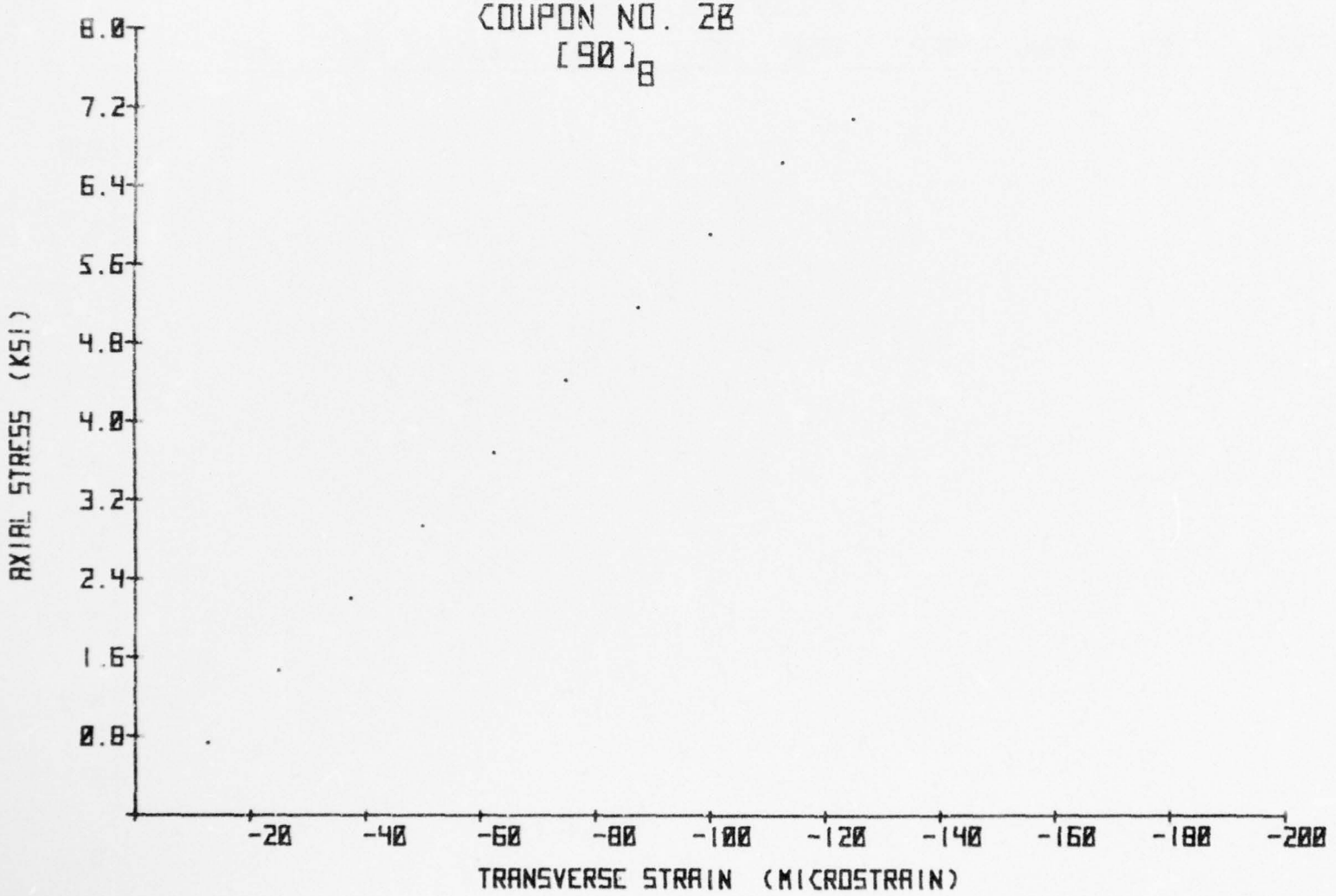
COUPON NO. 28
[90]8
8.0
7.2
6.4
5.6
4.8
4.0
3.2
2.4
1.6
0.8
AXIAL STRESS (KSI)
-20
-40
-60
-80
-100
-120
-140
-160
-180
-200
TRANSVERSE STRAIN (MICROSTRAIN)

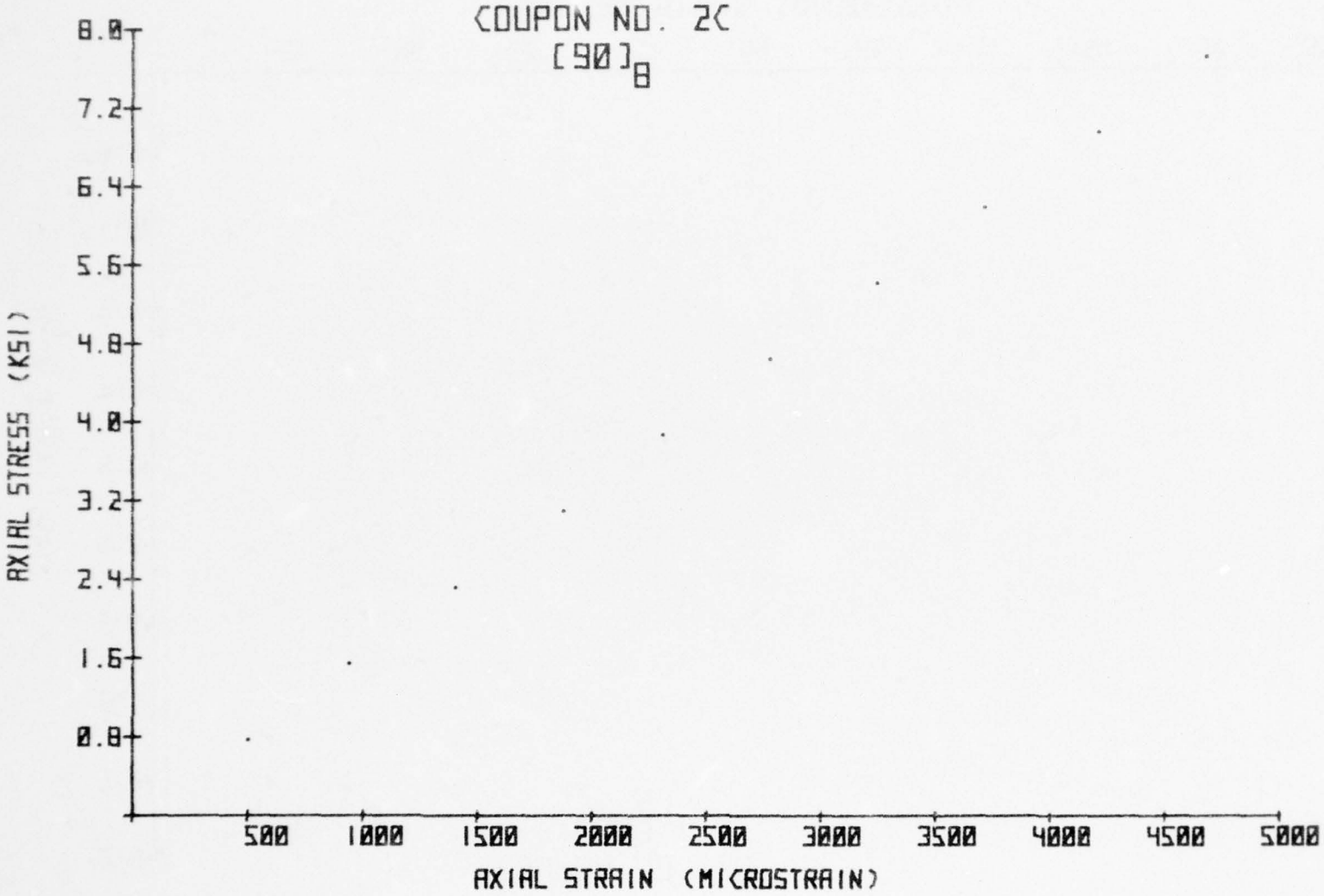
COUPON NO. 2C
[90]8
8.0
7.2
6.4
5.6
4.8
4.0
3.2
2.4
1.6
0.8
AXIAL STRESS (KSI)
500
1000
1500
2000
2500
3000
3500
4000
4500
5000
AXIAL STRAIN (MICROSTRAIN)

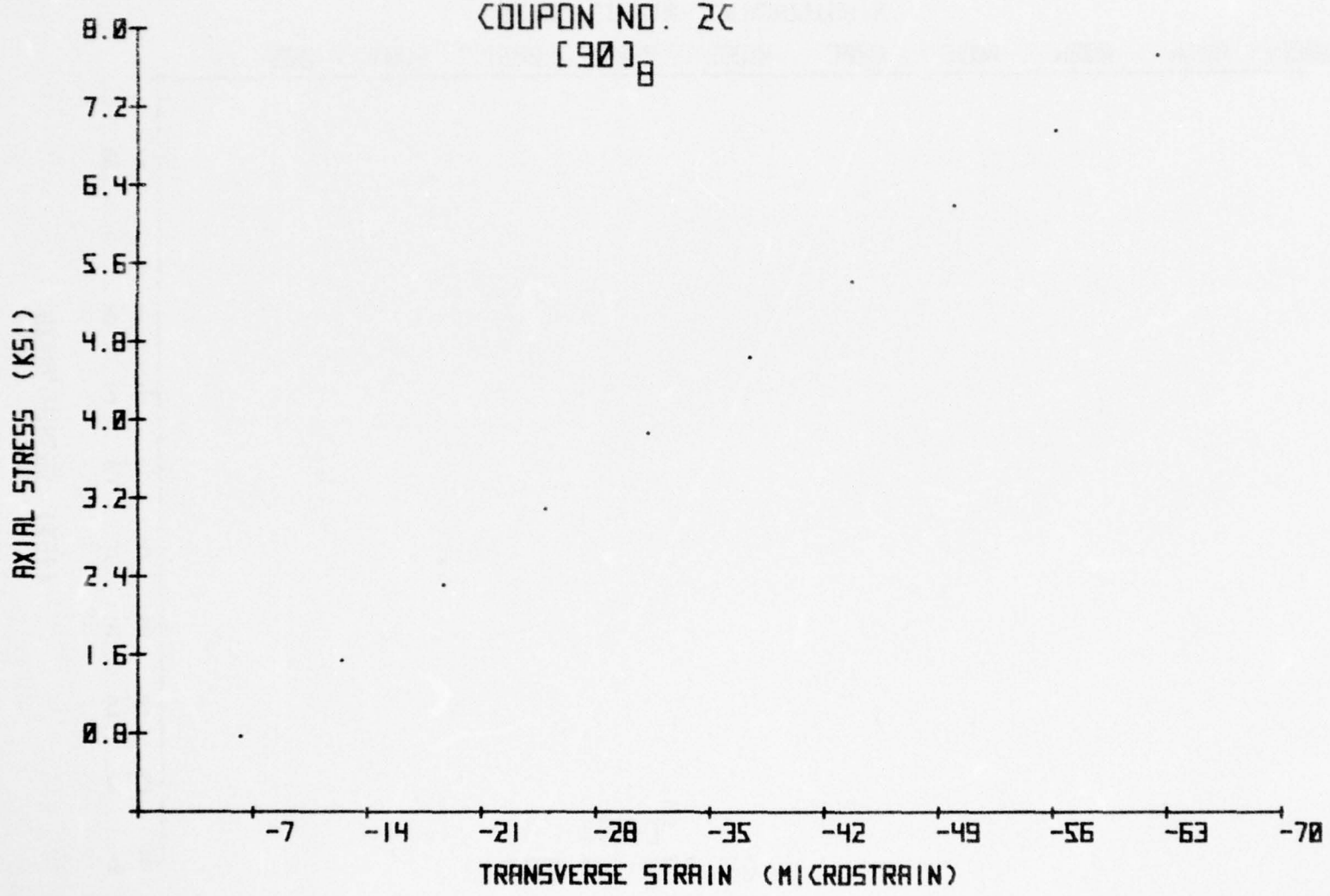
COUPON NO. 2C
[90]8
AXIAL STRESS (KSI)
8.0
7.2
6.4
5.6
4.8
4.0
3.2
2.4
1.6
0.8
-7
-14
-21
-28
-35
-42
-49
-56
-63
-70
TRANSVERSE STRAIN (MICROSTRAIN)

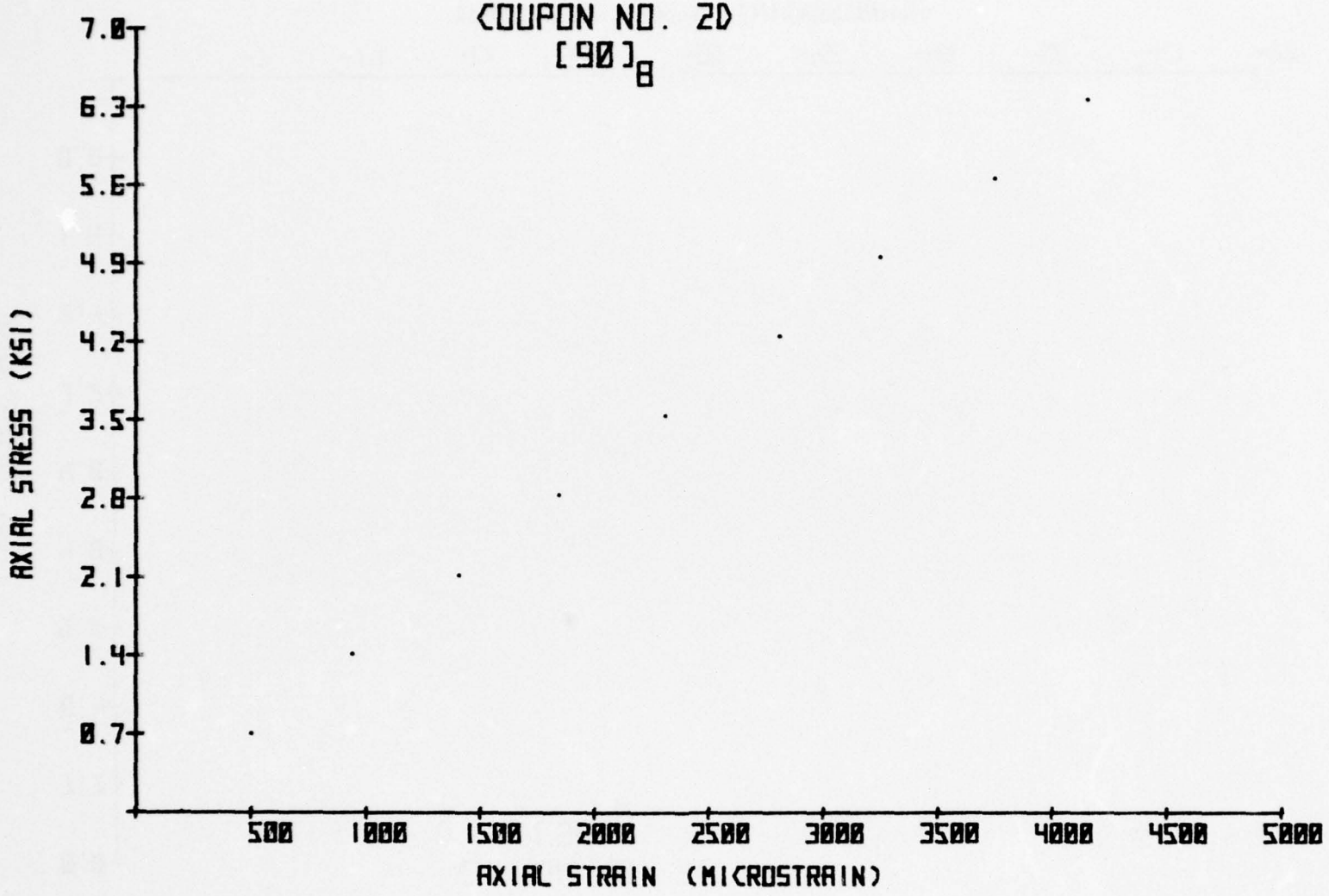
COUPON NO. 2D
[90]8
7.0
6.3
5.6
4.9
4.2
3.5
2.8
2.1
1.4
0.7
AXIAL STRESS (KSI)
500
1000
1500
2000
2500
3000
3500
4000
4500
5000
AXIAL STRAIN (MICROSTRAIN)

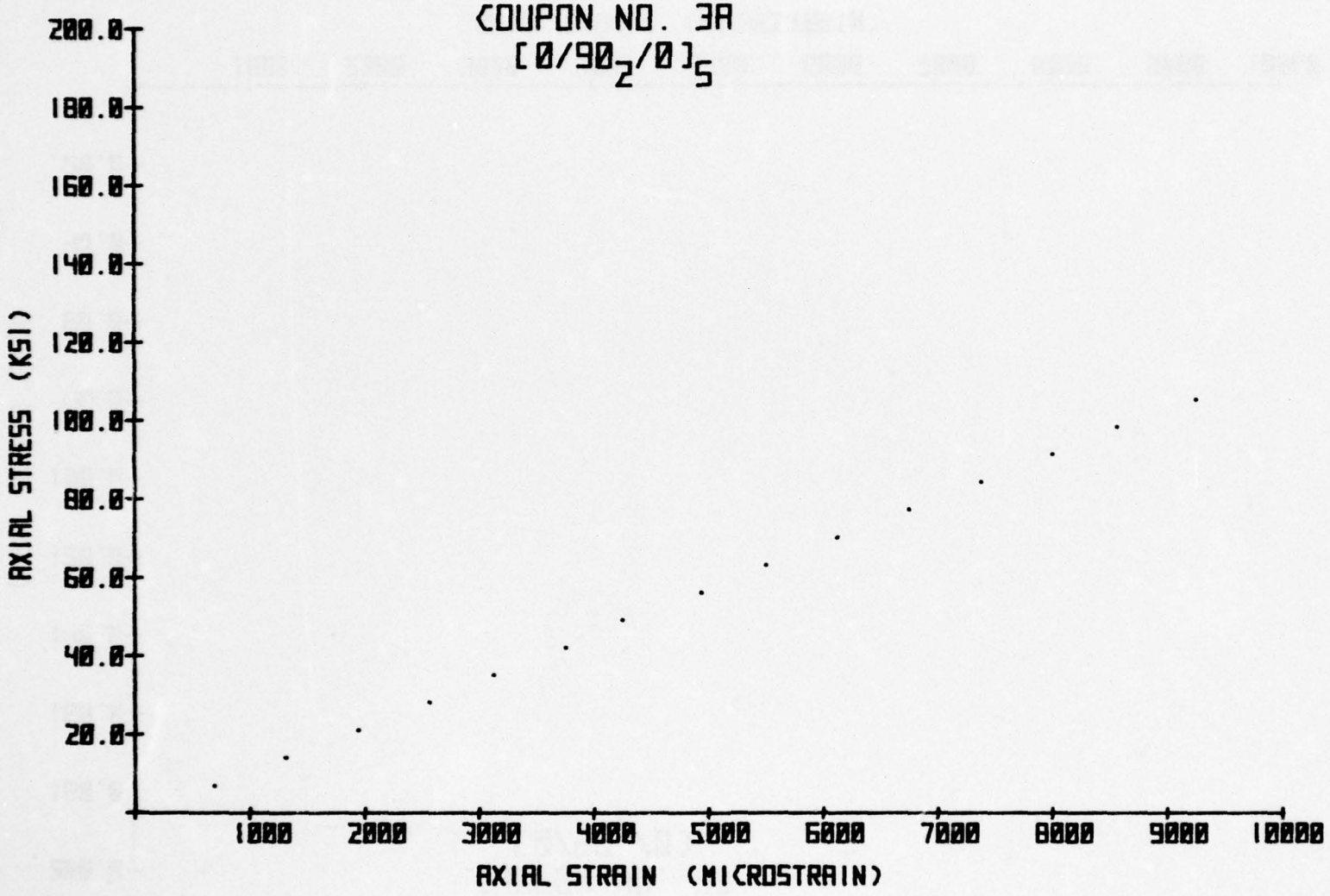
COUPON NO. 3A
[0/90$_2$/0]$_S$
AXIAL STRESS (KSI)
200.0
180.0
160.0
140.0
120.0
100.0
80.0
60.0
40.0
20.0
1000
2000
3000
4000
5000
6000
7000
8000
9000
10000
AXIAL STRAIN (MICROSTRAIN)

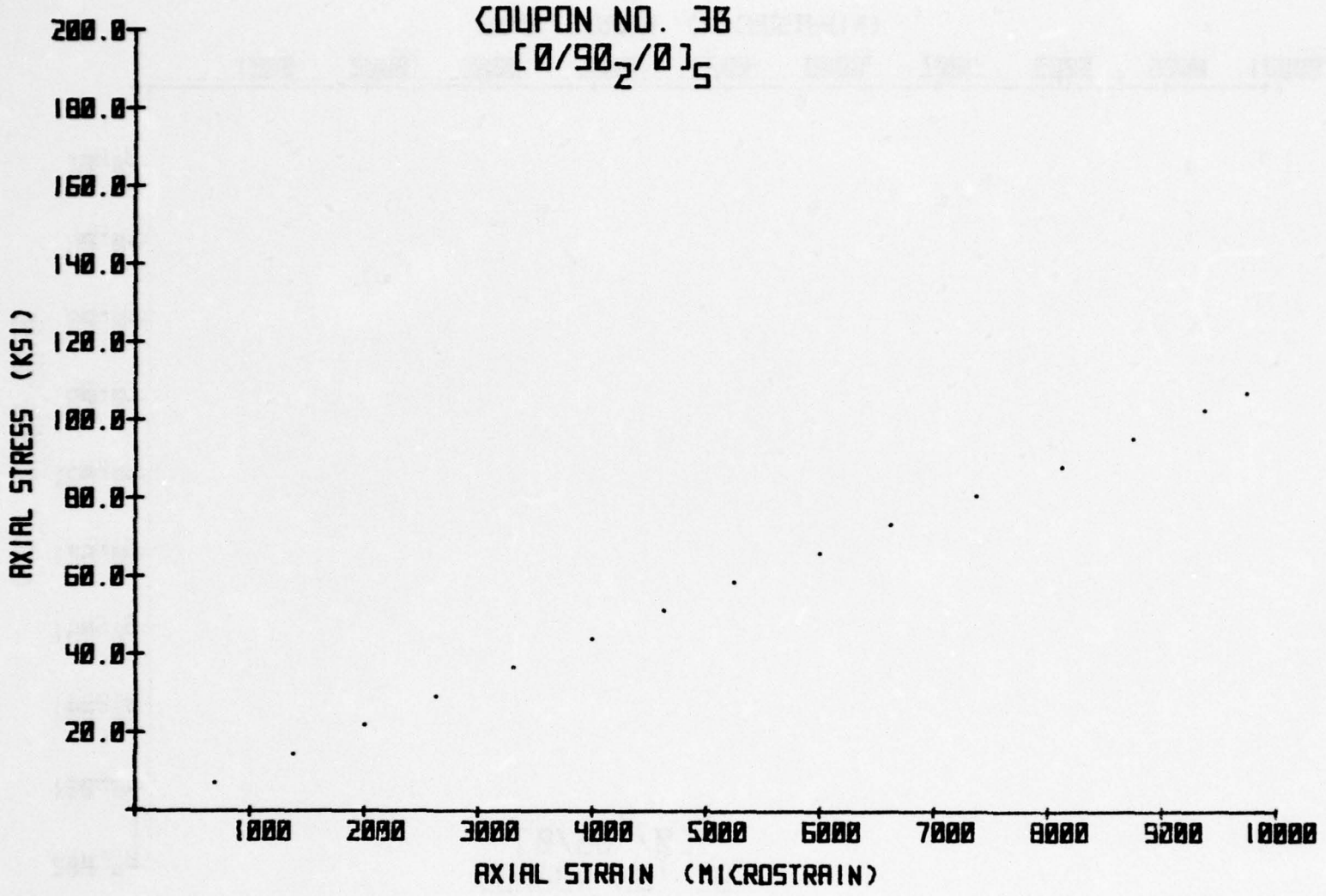
COUPON NO. 38
[0/90$_2$/0]$_S$
200.0
180.0
160.0
140.0
120.0
100.0
80.0
60.0
40.0
20.0
AXIAL STRESS (KSI)
1000
2000
3000
4000
5000
6000
7000
8000
9000
10000
AXIAL STRAIN (MICROSTRAIN)

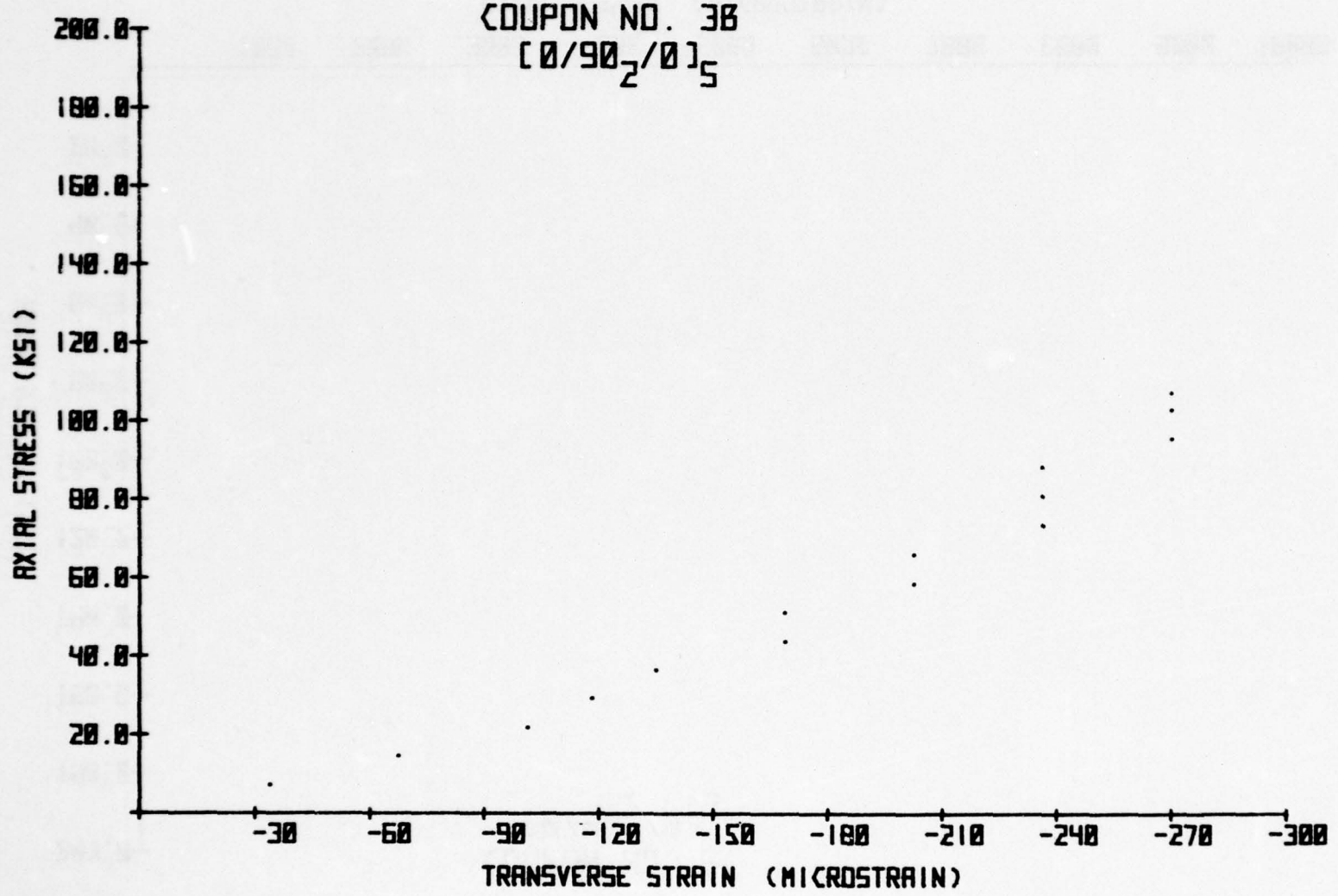
COUPON NO. 38
[0/90$_2$/0]$_S$
AXIAL STRESS (KSI)
200.0
180.0
160.0
140.0
120.0
100.0
80.0
60.0
40.0
20.0
-30
-60
-90
-120
-150
-180
-210
-240
-270
-300
TRANSVERSE STRAIN (MICROSTRAIN)

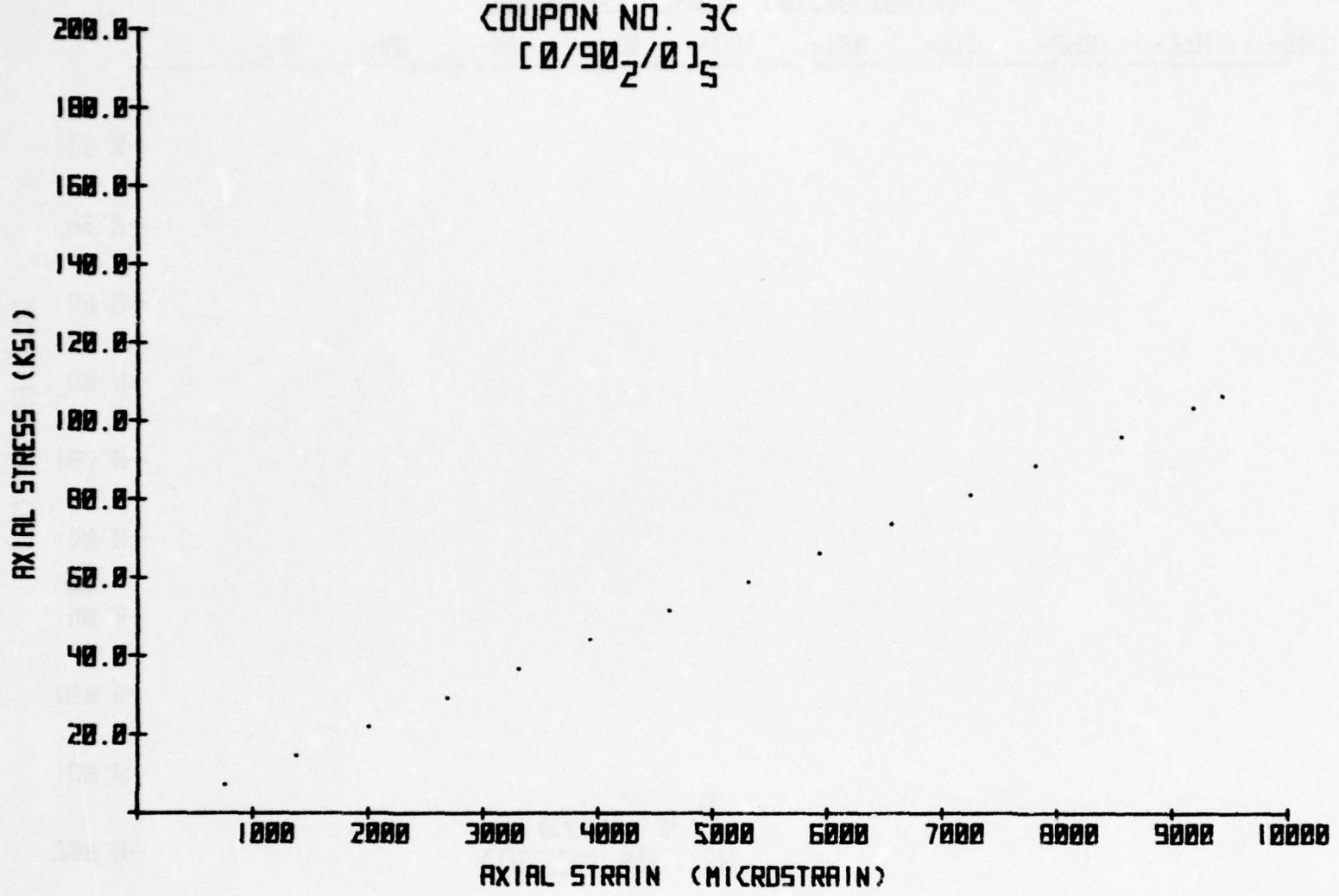
COUPON NO. 3C
[0/90$_2$/0]$_S$
AXIAL STRESS (KSI)
200.0
180.0
160.0
140.0
120.0
100.0
80.0
60.0
40.0
20.0
1000
2000
3000
4000
5000
6000
7000
8000
9000
10000
AXIAL STRAIN (MICROSTRAIN)

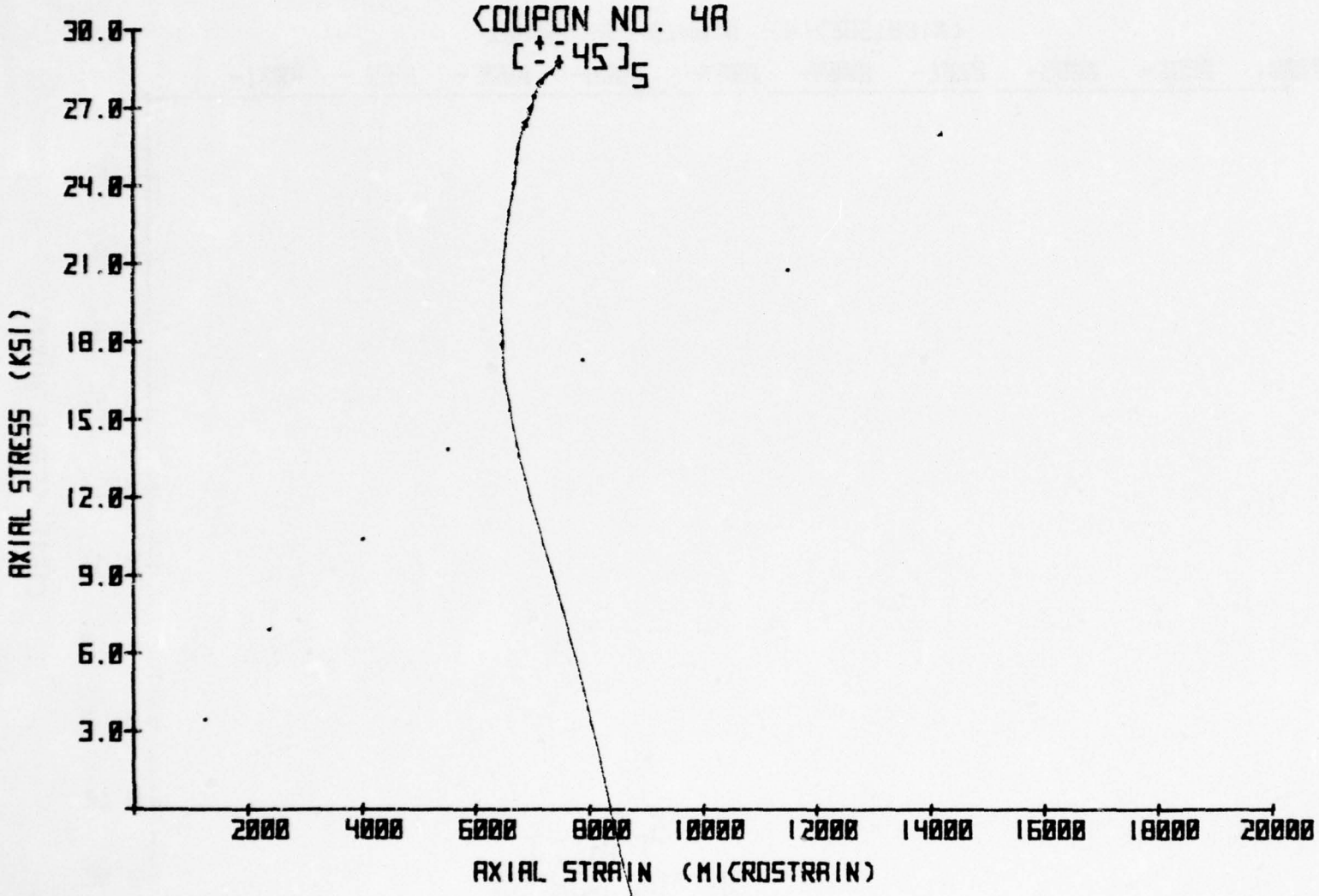
COUPON NO. 4A
[±45]5
30.0
27.0
24.0
21.0
18.0
15.0
12.0
9.0
6.0
3.0
AXIAL STRESS (KSI)
2000
4000
6000
8000
10000
12000
14000
16000
18000
20000
AXIAL STRAIN (MICROSTRAIN)

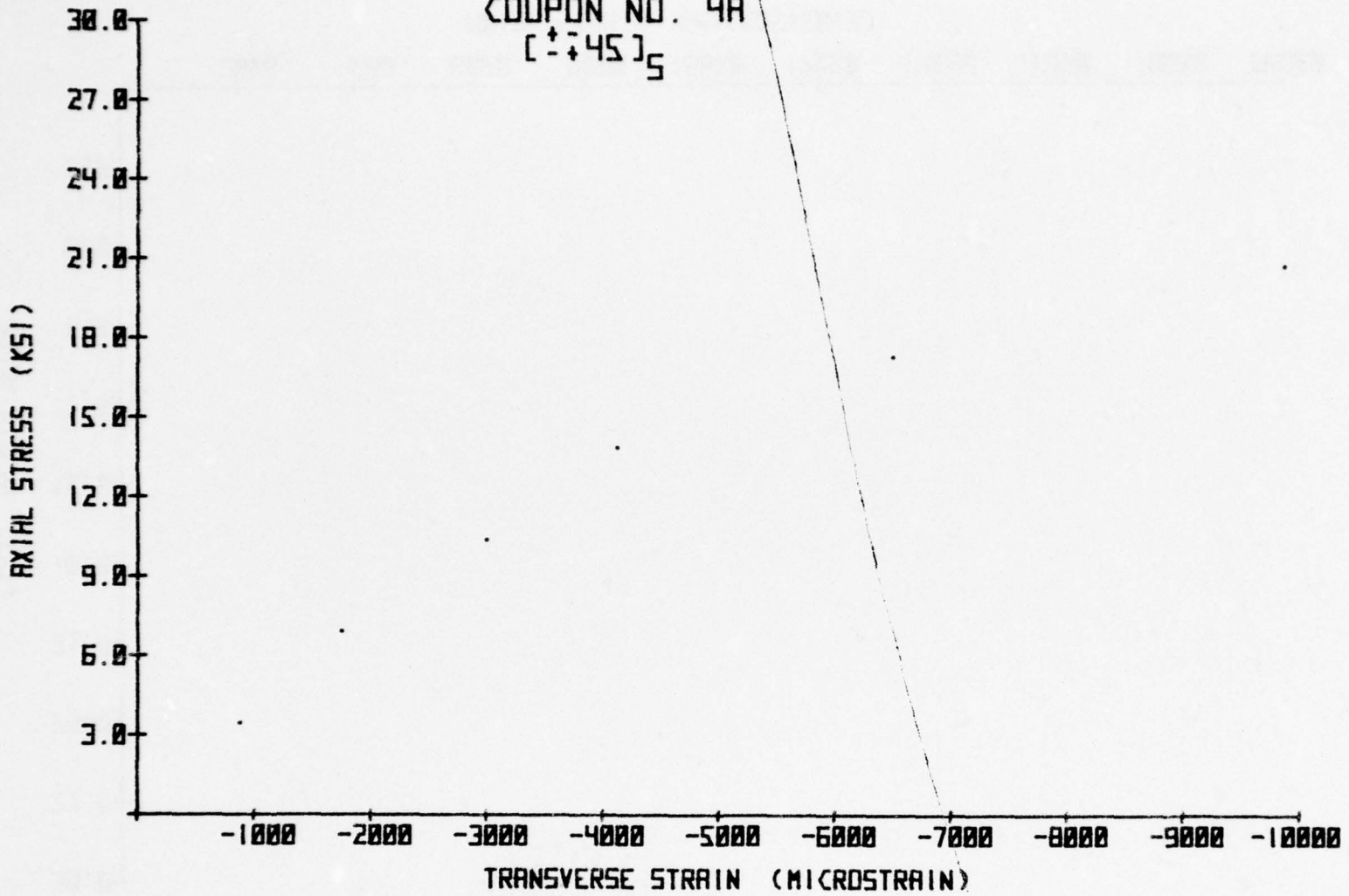
COUPON NO. 4A
[±45]S
30.0
27.0
24.0
21.0
18.0
15.0
12.0
9.0
6.0
3.0
AXIAL STRESS (KSI)
-1000
-2000
-3000
-4000
-5000
-6000
-7000
-8000
-9000
-10000
TRANSVERSE STRAIN (MICROSTRAIN)

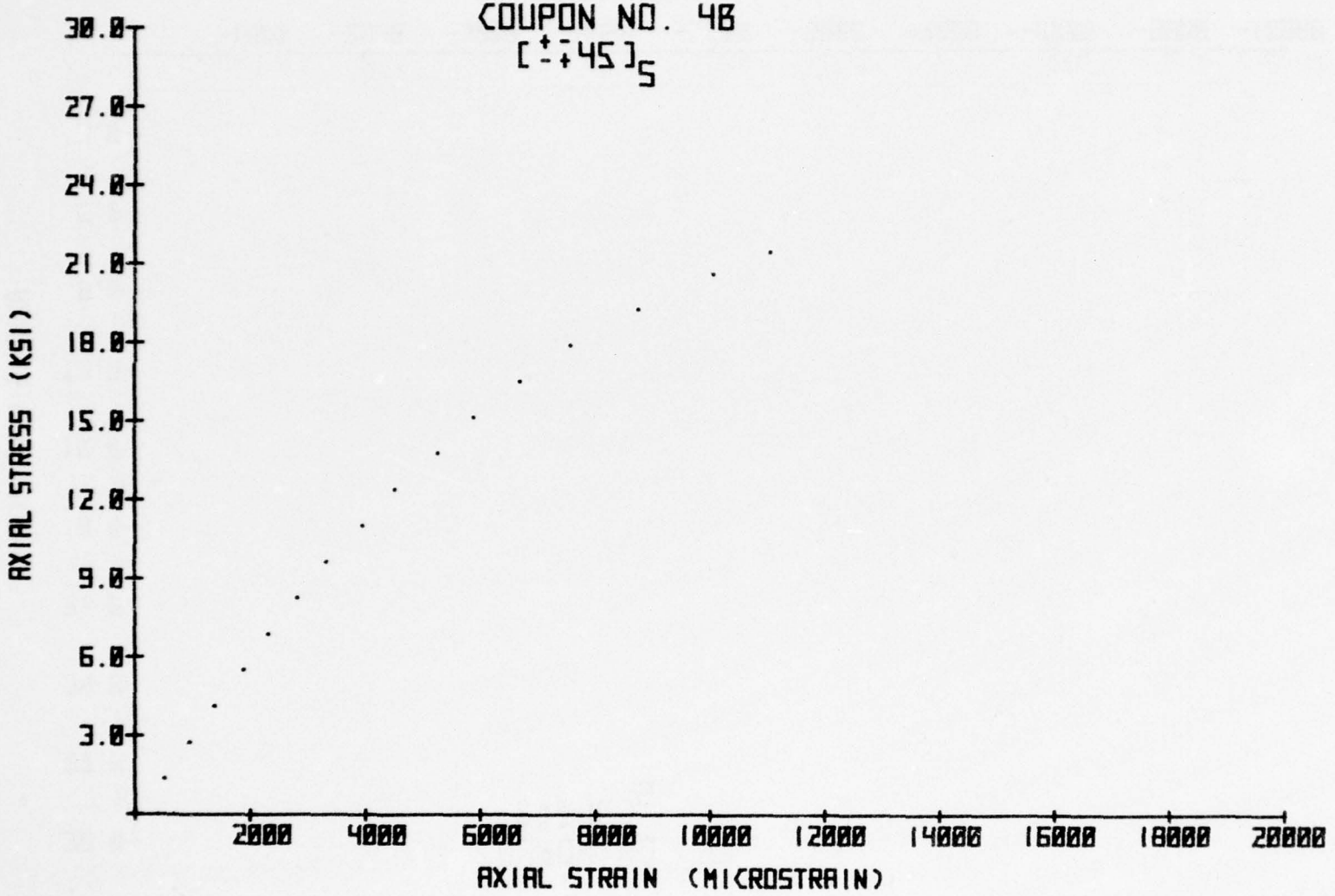
COUPON NO. 48
[±45]S
30.0
27.0
24.0
21.0
18.0
15.0
12.0
9.0
6.0
3.0
AXIAL STRESS (KSI)
2000
4000
6000
8000
10000
12000
14000
16000
18000
20000
AXIAL STRAIN (MICROSTRAIN)

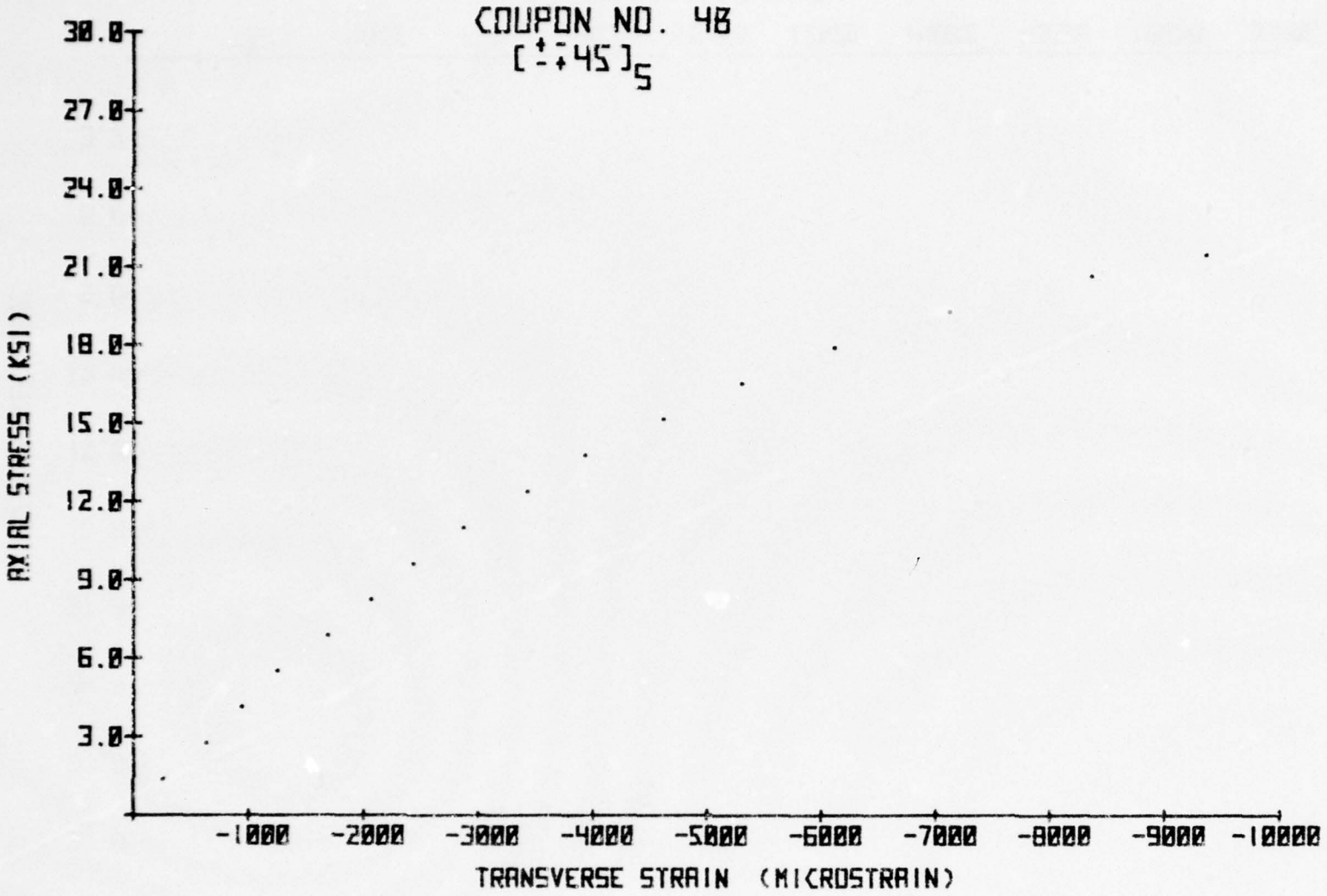
COUPON NO. 48
[±45]5
30.0
27.0
24.0
21.0
18.0
15.0
12.0
9.0
6.0
3.0
AXIAL STRESS (KSI)
-1000
-2000
-3000
-4000
-5000
-6000
-7000
-8000
-9000
-10000
TRANSVERSE STRAIN (MICROSTRAIN)

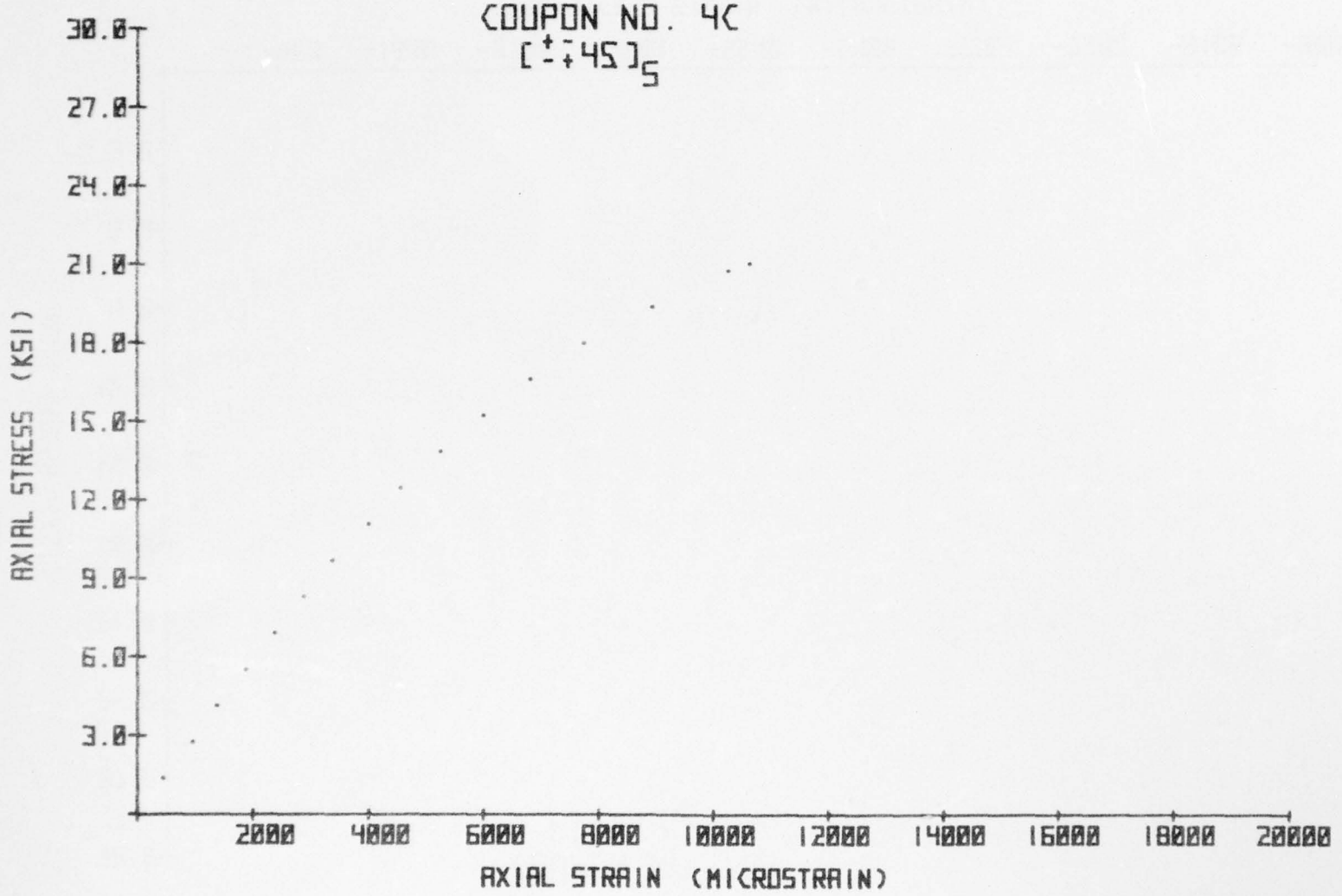
COUPON NO. 4C
[±45]S
30.0
27.0
24.0
21.0
18.0
15.0
12.0
9.0
6.0
3.0
AXIAL STRESS (KSI)
2000
4000
6000
8000
10000
12000
14000
16000
18000
20000
AXIAL STRAIN (MICROSTRAIN)

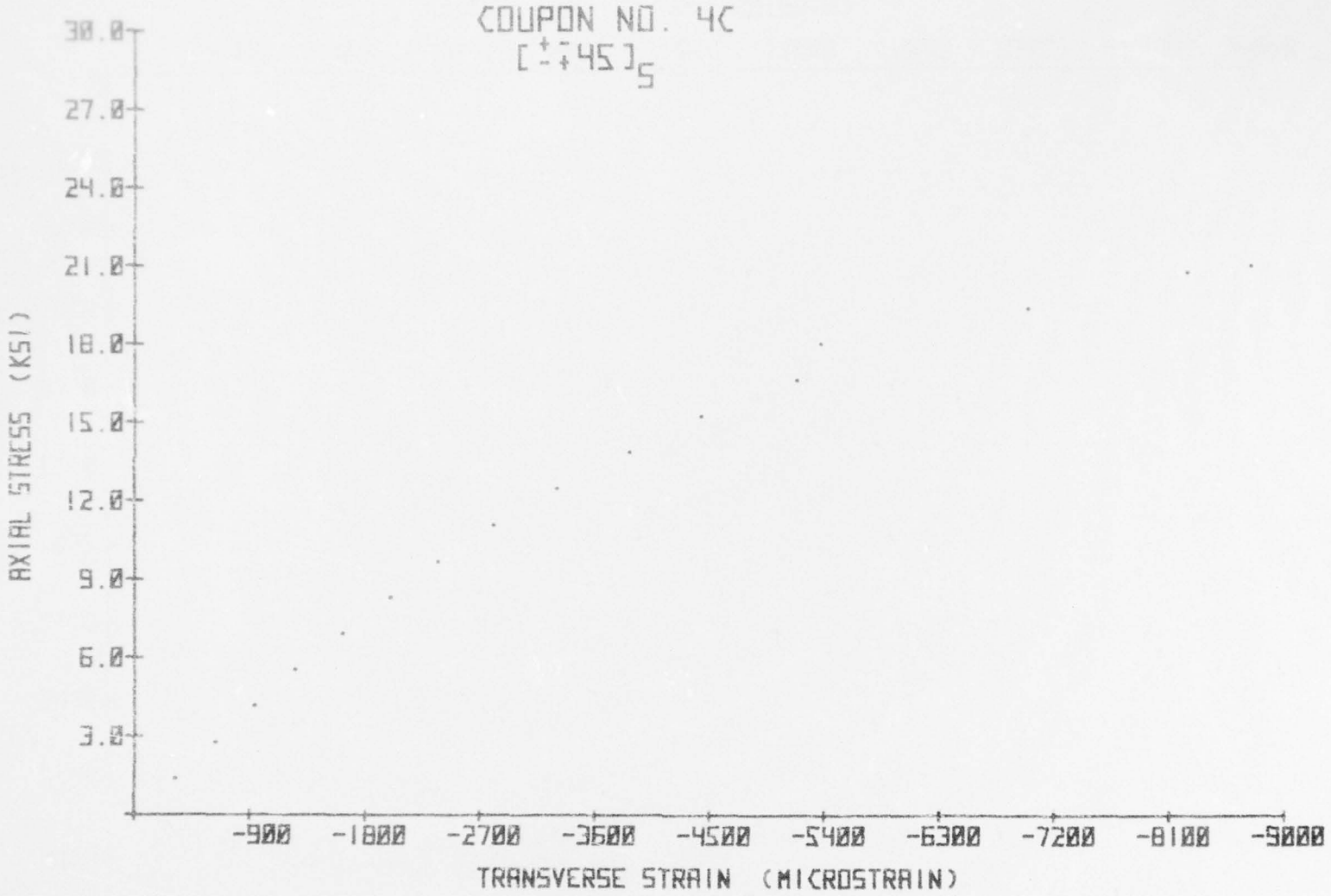
COUPON NO. 4C
[±45]S
30.0
27.0
24.0
21.0
18.0
15.0
12.0
9.0
6.0
3.0
AXIAL STRESS (KSI)
-900
-1800
-2700
-3600
-4500
-5400
-6300
-7200
-8100
-9000
TRANSVERSE STRAIN (MICROSTRAIN)